PHOTOCATALYTIC DEGRADATION OF PHENOLIC COMPOUNDS AND ALGAL METABOLITES IN WATER

EMOMOTIMI EMILY BAMUZA-PEMU

A thesis submitted in fulfilment of requirements for the degree of

PHILOSOPHIAE DOCTOR (CHEMICAL TECHNOLOGY)

in the

FACULTY OF ENGINEERING, BUILT ENVIRONMENT AND INFORMATION TECHNOLOGY

UNIVERSITY OF PRETORIA

2014

ABSTRACT

Title: Photocatalytic Degradation of Phenolic Compounds and Algal Metabolites in Water

Author: Emomotimi E. Bamuza-Pemu
Supervisor: Professor Evans M.N. Chirwa
Department: Chemical Engineering
University: University of Pretoria
Degree: Philosophiae Doctor (Chemical Technology)

Algal infestation in water bodies causes the release of soluble organic compounds that impact negatively on the taste and odour of the water. With increasing pollution in water bodies and increasing nutrient loading from agricultural activities, most water reservoirs in South Africa and around the world have become affected by this problem. In this study, an advanced oxidation process (AOP), namely, photocatalysis was evaluated for its potential to degrade aromatic compounds; and taste and odour causing bi-cyclic compounds originating from algae.

Semiconductor photocatalysis is an environmentally friendly technology requiring no chemical inputs which is capable of completely mineralising organic pollutants to CO_2 and H_2O thereby eliminating production of unwanted by-products. Although processes involved in the photo-degradation have been reported for a wide range of pollutants, the degradative pathway in this process has not been fully established. In this study, compounds including phenol, 2-chlorophenol, 4-chlorophenol and nitrophenol were successfully eliminated from simulated wastewater. Degradation of geosmin at an environmentally significant initial concentration of 220 ng/L to levels below the lowest detectable concentration was achieved with an optimum catalyst concentration of 60 mg/L at a rate of 14.78 ng/L/min. Higher catalysts loading above 60 mg/L resulted in a decrease in degradation rates. An increase in initial geosmin concentration resulted in a decrease in rates.

Ionic species commonly found in surface waters (HCO_3^-, and SO_4^{2-}) significantly reduced the efficiency of geosmin degradation. Degradation of geosmin produced acyclic intermediates from ring fission tentatively identified as 3,5-dimethylhex-1-ene, 2,4-dimethylpentan-3-one, 2-methylethylpropanoate and 2-heptanal.

The results obtained indicate that the degradation of organic pollutants in aqueous solution is as a result of synergic action from hydroxyl radicals, positive holes and direct photolysis by UV radiation, though the predominant pathway of degradation is via hydroxyl radicals in solution. Major aromatic intermediates of phenol degradation include catechol, resorcinol and hydroquinone produced in the order catechol > resorcinol > hydroquinone. All three are produced within 2 minutes of photocatalytic reaction of phenol and remain in solution until all phenol is degraded in aerated systems. Production of resorcinol in non-aerated systems is transient, further supporting the hydroxyl radical dominant reaction pathway.

DECLARATION

I Emomotimi Emily Bamuza-Pemu, declare that the thesis which I hereby submit for a Doctor of Philosophy in Chemical Technology degree at the University of Pretoria is my own work and has not been previously submitted by me for any degree at this or other institutions.

_____ _____

Emomotimi Emily Bamuza-Pemu Date

Dedicated to three generations of Pemus

Margaret Okpuma Pemu

A hardworking, loving, dedicated mother who raised such a wonderful man,

Al Pemu

my Sunshine,

and;

Okpuma, Tara and Daderhie Pemu

our three stars.

ACKNOWLEDGEMENTS

The author remains grateful for funding from the Water Research Commission (WRC) of South Africa through the WRC Project No. K5/1717 awarded to Prof Evans M.N. Chirwa of the University of Pretoria.

Sincere gratitude and appreciation is expressed to the study leader Prof Evans Chirwa for giving me the opportunity to study in his research group, for his patience and direction and for generously giving of his time.

The author is also grateful to members of the Reference Group for the WRC Project No. K5/1717 for their helpful suggestions during the course of the study. To Alette Devega, for attending to the needs around the lab beyond the call of duty; and to Prof Rohwer for giving me access to his research team and facilities and for always giving a helping hand and advice on all chromatographic related problems.

The author's gratitude also goes to colleagues from the research group at Water Utilisation and Environmental Division, of the Department of Chemical Engineering, University of Pretoria including Billy, colleagues and friends from Ambrose Alli University, Ekpoma especially Gina Ohenhen, Mercy Izomoh, Mark Azih, I.O. Asia, Larry, Uwa, Eunice and Mike Osuide for their concern and interest in my progress.

The author is eternally grateful to late Kemi Udom for her encouragement and assistance with settling into life at University of Pretoria; and to Uwem Udom and family for making SA home from the start. My gratitude also goes to the Devega family for providing a second home for me and my family in Pretoria and to Leanne De Jager and her Mum, Marion.

To darling my mother, Chief V.B. Bamuza-Mutu and my father, Chief A.E. Bamuza for the love, guidance and support through the years. My sisters Ebi Umoetuk and Pade Bamuza-Gbejewoh, thank you for always being there for me unconditionally; and to Peres Mutu for assisting with the children on the home front. To other family members especially Chief W. Pemu, Joe Penawou, Chief Broderick Bozimo and Florence Pemu – I will be forever grateful.

Al Pemu, thank you for everything, this would not have been achieved without you.

TABLE OF CONTENTS

Table of contents continued

Table of contents continued

LIST OF FIGURES

List of Figures continued

List of Figures continued

LIST OF TABLES

List of Tables continued

LIST OF ABBREVIATIONS

AOP	Advanced oxidation process
BET	Brunauer–Emmett–Teller
BTEX	Benzene, toluene, ethylbenzene and xylene
CB	Conductance Band
CIS	Cooled inlet system
CP	Chlorophenol
CPCR	Compound parabolic collecting reactor
CVD	Chemical vapour deposition
DAFF	Dissolved air floatation filters
DBBQ	2,5-Di-tert-butyl-1,4-benzoquinone
DCE	Dichloroethane
DCM	Dichloromethane
DCR	Dispersed Catalyst Reactors
DDT	Dichlorodiphenyltrichloroethane
DO	Dissolved oxygen
DOC	Dissolved organic carbon
DPB	Disinfection by-product
DSSR	Double skin sheet reactor
DWAF	Department of Water and Forestry
DWQS	Domestic water quality standards
e^-	Electron
E_{bg}	Band gap energy
EDC	Endocrine disrupting compound
EPA	Environmental Protection Agency
FW	Formula weight
GAC	Granular activated carbon
GC/MS	Gas chromatography/Mass spectrometry
HAAs	Haloaceticacids
h^+	Positive hole
$h^+ e^-$	electron-hole pair
HP	Hewlett Packard

HPLC	High performance liquid chromatography
hv	Energy of a photon
IARC	International Agency for Research on Cancer
IBMP	2-Isobutyl-3-methoxypyrazine
IPMP	2-Isopropyl-3-methoxypyrazine
MCL	Maximum contaminant level
MCLG	Maximum contaminant level goal
MDHP	2-methyl-2,2-dimethyl-1-[2-hydroxylmethyl]propylester
MDMP	2-methyl-1-[1,1-dimethyl]-2-methyl-3-propanediylester
MIB	2-methylisoborneol
MIT	Measuring Instruments Technology
MLD	Megalitres per day
NA	Not available
NCD	Not completely degraded
NHE	Normal hydrogen electrode
NIST	National Institute of Standards and Technology
NM	Not mineralised
NOM	Natural organic matter
NTU	Nephelometric turbidity unit
PAC	Powdered activated carbon
PAHs	Polycyclic aromatic hydrocarbons
PDA	Photo diode array
PE TMH	Perkin Elmer Turbo Matrix Headspace
PFTBA	Perfluorotributylamine
POP	Persistant organic pollutants
PSDVB	Polystyrenedivinylbenzene
PTC	Parabolic trough concentrators
PTR	Parabolic trough reactor
SA	South Africa
SABC	South African broadcasting corporation
SA DWQS	South African domestic water quality standards
SC	Semiconductor
SEM	Scanning electron microscopy

SHE	Standard hydrogen electrode
SIR	Single ion recording
SPE	Solid phase extraction
SPME	Solid phase microextraction
SRB	Sulphate reducing bacteria
SVOC	Semi-volatile organic compound
TBT	Tributyltin chloride
TBTO	Bis(tributyltin) oxide
TCA	2,4,6-Trichloroanisole
TCE	Trichloroethene
TDS	Total dissolved solids
TFFBR	Thin film fixed bed reactor
THM	Tetrahalomethanes
TIC	Total ion chromatogram
TOC	Total organic carbon
TPA	Terephthalic acid
t_R	Retention times
TSS	Total suspended solids
UV	Ultraviolet
VB	Valence Band
VOC	Volatile organic compound
VUV	Vacuum Ultraviolet
WHO	World Health Organisation
XRD	x-ray diffractometry

CHAPTER ONE

INTRODUCTION

1.1 Background

Shortage of freshwater supply has been a global concern for over a decade. According to the projection by the UN Environmental Program Report, two thirds of the world's population will be living under water stressed conditions by 2025 (UN Environmental Program report). The reality is that over a third of the world's population is water stressed. South Africa is a semi-arid country with unpredictable rainfall pattern having an average rainfall 52% of the global average (DWAF, 1996). Reports from sources within the Department of Water Affairs and Forestry in South Africa indicate that the current water use practices will not be sustainable beyond 2026 (DWAF, 1999). The problem is compounded by the increasing demands on freshwater sources with rapid population, industrial and agricultural growth leading to a decline in drinking water quality over the years (Jyoti and Pandit, 2001). Over the past two to three decades, growing industrial activities have caused an increase in the discharge of toxic organic pollutants into the environment.

With rapid population and industrial growth, there is increased pressure on fresh water sources with a projected global water shortage. Conventional freshwater sources are failing to meet the demand. The water industry is faced with the option of sourcing poorer quality water to supplement freshwater sources. Available alternative sources include seawater, industrial and municipal wastewater, eutrophic surface water (from dams), and filter backwash water from water treatment plants and production plants. Wastewater according to John Keys of US Bureau of Reclamation "is the last river to tap"; but to tap this river, water treatment technologies capable of producing water of quality to meet the current stringent conditions is required.

The available alternative sources are plagued by the presence of several undesirable substances, some of which are highly toxic; often refractory to microorganisms and have shown to survive conventional state-of-the-art wastewater treatment processes (Doan *et al.*, 2009, Alvarez *et al.*, 2005). Other substances render the water unpalatable and therefore not useable by consumers. The transition from availability to usability of an alternate water

source depends on the ease and effectiveness of treatment to convert water from these alternative sources to potable quality.

To meet the UN Millennium Development Target 10 of Goal 7 which aims "to half by 2015, the proportion of people without sustainable access to safe drinking water and basic sanitation" (UN, 2005), alternative treatment technologies have to be developed or adopted to handle the growing list of water pollutants in water. The search for more efficient and cleaner technologies to tackle the ever increasing threat of future water security has led to the advancement of some new methods of treatment. The most promising of these new methods in the context of pollutant abatement in water are collectively referred to as advanced oxidation processes (AOPs) (Chirwa and Bamuza-Pemu, 2010; Comninellis *et al*., 2008; Stasinakis 2008; Modrzejewska *et al*., 2007; Ljubas, 2005). Advanced oxidation processes are characterised by their catalytic, photochemical properties and oxidative degradation reactions (Maciel *et al*., 2004).

Semiconductor photocatalysis is an environmentally friendly, advanced oxidation process based on the generation of reactive electron hole pairs (h+ e-) by photoactivation of semiconductor materials acting as catalysts, utilizing low energy ultraviolet (UV) light (Simonsen *et al*., 2008; Mills and Lee, 2004). Photogenerated positive holes are powerful oxidants while the negative electrons are very good reductants. Both reactive species can either react directly with organic compounds or indirectly through the action of hydroxyl radicals generated in-situ from reduction of oxygen on the surface of the catalyst (Bahnemann, 2004; Munter, 2001), and the process often achieves complete mineralization of the organic pollutants to carbon dioxide and water (Simonsen *et al*., 2008) thereby avoiding the problem of unwanted by-products. This study employs semiconductor photocatalysis for the elimination of two common classes of water pollutants.

1.2 Aims and Objectives

The major objective of the study was to investigate the potential of photocatalysis as a treatment technology for degradation and mineralisation of recalcitrant organic pollutants in water. To achieve this objective some specific aims set out as tasks were conducted. These include:

- Chemical characterisation of natural and anthropogenic organic pollutants in source water at two treatment plants around Pretoria.
- Evaluation of the performance of a laboratory scale treatment unit employing a chemical free photocatalytic system for the degradation of environmentally significant levels of geosmin and phenolic compounds to levels below detection limits.
- Process optimisation and kinetic analysis of the photocatalytic degradation system taste and odour causing compounds to obtain process parameters for laboratory photocatalytic system.
- Evaluation of the effect of ionic species on the performance of the laboratory scale photocatalytic system during the degradation process.
- Identification of the intermediates formed during the photocatalytic degradation and determination of the fate of the formed intermediates.
- Degradative pathway analysis for the two model compounds to have a better understanding of the process.

1.3 Scope of Study

The current study investigates the feasibility of photocatalysis as a treatment technology for the removal phenol and selected mono substituted derivatives of phenol including 2-chlorophenol, 4-chlorophenol and nitrophenol; and geosmin (a taste and odour causing compound) from water to levels below environmentally acceptable limits and below human detection thresholds. Laboratory scale batch systems were employed to investigate key aspects of photocatalytic and photolytic degradation processes. Titanium dioxide was utilised as the preferred catalyst in its dispersed form.

Detailed quantitative study of the intermediates of phenol degradation was conducted and formation/disappearance profiles of the major aromatic intermediates were obtained, which gave a framework for degradative pathway analysis. For geosmin degradative pathway analysis, a qualitative analysis of intermediates was performed and a quantitative analysis was not performed mainly due to the very low levels of the compound(s).

1.4 Methodology

The feasibility of the photocatalytic process in treating organic pollutants commonly found in natural waters was examined. The methodology employed to achieve the aims and objectives of the study include:

a) A thorough literature study to evaluate a variety of advanced oxidation processes (AOPs) for treating organic compounds in water, with a relative performance efficiency analysis across the common technologies. Then a detailed literature survey of the photocatalytic process to obtain a better understanding of the technical aspects of the process,

b) An analytical survey of source water of the two major treatment plants in Pretoria. Raw water and backwash water from dissolved air flotation filters and sand/GAC filters from Rietvlei and Roodeplaat Water Treatment Works were characterised to determine common organic pollutants in the water. This was done in order to determine the compounds on which to focus during the study,

c) Families of problematic organic species identified through the literature survey and the scan of compounds (geosmin for taste and odour compounds and phenol for aromatic compounds) were investigated further in batch reactors using titanium dioxide as the photocatalyst,

d) Investigation of optimum reaction conditions for both compounds, including (1) the amount of photocatalyst added to the reactor, (2) initial concentration of the pollutant, (3) effect of aeration on pollutant removal rate, and (4) the effect of ionic species on geosmin degradation,

e) Experiments to identify the intermediates formed during the process of photocatalytic degradation for both geosmin and phenol and a degradative pathway analysis was conducted, and

f) Simple kinetic analysis using first-order reaction kinetics and a particle surface analysis to determine optimum reaction rate parameters under various pollutant concentrations.

The results were interpreted to determine the pathway of degradation and predominant reaction mechanism during the photocatalytic process.

1.5 Organisation of Thesis

This thesis consists of the following chapters and appendices:

- Chapter 1 presents an introduction to the study; it explains the motivation, main aims and objectives and scope of the study, highlighting the importance of the research. It also gives the organisational structure of the thesis.

- Chapter 2 provides a detailed report of literature relevant to the present research, with some technical information on the theoretical background of photocatalysis and some examples of applications. This chapter also provides advances in photocatalytic research and the status of the implementation of technology.

- Chapter 3 presents technical details of the laboratory reaction setup, the materials used, analytical equipment, experimental reactor-set up and reactions conditions, as well as experimental methods, data collection and analytical methods employed during the course of the study.

- Chapter 4 presents results of the preliminary studies, including the organic composition of the source water, a classification and discussion of the predominant organic compounds identified. It also gives a characterisation of the titanium dioxide catalyst and the irradiation source used for degradation studies.

- Chapter 5 discusses the results of photolytic and photocatalytic degradation of phenol, and the mono-substituted derivatives of phenol. The effects of parameters on the degradation efficiency, the profiling of the aromatic intermediates, degradative pathway analysis and some kinetic analysis of phenol degradation.

- Chapter 6 discusses the results of photolytic and photocatalytic degradation of geosmin, the effects of parameters on the degradation efficiency. It discusses the intermediates

produced and a detailed degradative pathway analysis and some kinetic analysis of geosmin degradation.

- Chapter 7 gives a summary of the key findings of the research and the conclusions drawn from the findings, also included in this chapter are a few recommendations for further studies.

- A listing of all cited reference materials is included at the end of the report.

- Appendices

CHAPTER TWO

LITERATURE REVIEW

2.1 Background

Improved analytical methods coupled with better understanding of the adverse effects of organic pollutants in water have led to the enactment of more stringent drinking water standards. The challenge that these standards place on the drinking water industry is exacerbated by the rapidly dropping quality of source water due to pollution from agricultural runoffs and wastewater from industrial and municipal sources. These pollutants have negative impacts both on the ecosystems and on humans (toxicity, carcinogenic and mutagenic properties) (Busca *et al*., 2008). Runoffs from agricultural land contains pesticides and nutrients which cause imbalances in the ecosystem and may cause algal infestation waters which leads to production of cyanobacterial toxins and taste and odour compounds (Jüttner and Watson, 2007; Sung *et al*., 2005).

Another input of organic loading is the industrial and municipal wastes which introduce a variety of chemical compounds (natural and synthetic) into the environment. Compounds from household products for example cosmetics, personal care products and detergents, and pharmaceutical products are often refractory to microorganisms and have shown to survive conventional state-of-the-art wastewater treatment processes (Doan *et al*., 2009, Alvarez *et al*., 2005). Some of these compounds inevitably find their way into surface and ground waters used as supply sources. The majority of these compounds pose potential human and animal health hazards as they are endocrine disrupting compounds (EDCs) (Watkinson *et al*., 2007), EDCs disrupt the normal functioning of the endocrine system which regulates the immune system, growth, development, reproduction and neuro system (Zala and Penn (2004). Increasing levels of organic pollutants originating from anthropogenic sources such as pesticides, aromatic compounds from industrial effluent, or pharmaceuticals; have been detected in drinking water sources lately (Malato *et al*., 2009). Current drinking water treatment technologies are inadequate to meet safety requirements with respect to this new family of pollutants (Alvarez *et al*., 2005).

In addition to the anthropogenic aromatic compounds, vegetation and phytoplankton contribute humic substances that mimic these compounds (Huang *et al*., 2006). Removal of organic pollutants in water treatment has gained even greater significance with developments establishing possible links between halogenated disinfection by-products (DBPs) and cancers (Zhou and Smith, 2002). The need for improved pollutant removal technologies to deal with the increasing complexity of pollutants and the strident standards placed have shifted research efforts to finding improved alternative treatment technologies including advanced oxidation enzymatic treatment, activated carbon adsorption and membrane separation with varying degrees of success depending on the types and concentration of EDCs and the water matrix (Kit Chan *et al.*, 2012). Advanced oxidation processes especially semiconductor photocatalysis been the subject of most active research efforts judging from the continual increase in volume of research articles produced annually.

2.2 Geosmin and 2-MIB

Taste and odour compounds, *trans*-1,10-dimethyl-*trans*-9-decalol (geosmin) and 2-methyl-isoborneol (MIB) (Figure 2.1), are volatile tertiary alcohols that are produced by secondary metabolites of actinomycetes and cyanobacteria (Tran *et al*., 2008; Zaitlina and Watson, 2006; Sung *et al.*, 2005 Watson *et al*., 2003). Geosmin and 2-MIB each exists as (+) and (-) enantiomers, and odour outbreaks are caused by biological production of the naturally occurring (-) enantiomers, which are about 10 times more potent than the (+) enantiomers (Jüttner and Watson, 2007).

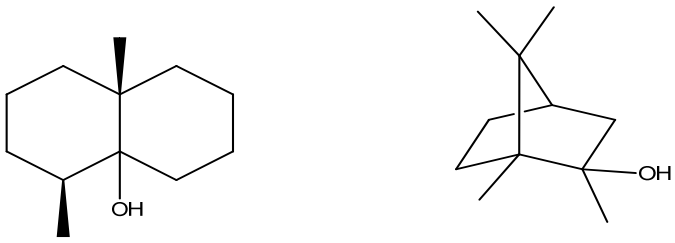

Geosmin

(a)

2-methylisoborneol

(b)

Figure 2.1: Structures of (a) geosmin and (b) MIB.

Geosmin and 2-MIB impart taste and odour in water thereby compromising the aesthetic quality of the water (Peter and von Gunten, 2007). The presence of these compounds also causes undesirable taint problems in the aquaculture industry. Geosmin is also produced by *Streptomyces* and *Myxobacteria* and is responsible for the characteristic odour of freshly turned earth (Cane *et al*., 2006) while 2-methyl-isoborneol (MIB) is produced from the blue-green alga *Oscillatoria perornata* (Meepagala *et al*., 2005). Some soil bacteria are also known to produce geosmin. The soil bacteria may be washed by rainfall runoff into nearby streams where they further increase the prevalence of odour causing compounds in surface waters. These compounds are responsible for the musty and earthy odours in drinking water even at trace concentrations in the ng/L range. The human odour threshold is at concentrations as low as 1.3 ng/L and 6.3 ng/L for geosmin and MIB, respectively (Young *et al*., 1996; Lloyd *et al*., 1998).

Although there is no proven toxicity resulting from consumption of water contaminated with geosmin and MIB, consumers judge the quality of the water primarily on the aesthetic characteristics. Water that is not appealing in appearance, taste or odour, may result in psychosomatic illnesses such as stomach upsets, headaches and stress (Lauderdale *et al*., 2004).

Lately, a variety of physico-chemical treatment technologies such as adsorption on granular activated carbon (GAC) or powder activated carbon (PAC) particles (Matsui, Y. *et al*., 2012; Srinivasan and Sorial, 2011; Zoschke *et al*., 2011; Graham *et al*., 2000), oxidation by ozonation (Schrader *et al*., 2010; Summerfelt *et al*., 2009) and biodegradation in biofilters (Hoefel *et al*., 2009; Elhadi *et al*., 2004) have been employed in treating taste and odour causing compounds. However, almost all of these technologies have been found lacking either due to poor treatment efficiency or due to high capital and operational cost. So far, adsorption on activated carbon has been used most widely in combination with sand media in filters to control odour causing compounds such as geosmin. However, filtration does not treat the contaminant as it only separates the contaminant from water with subsequent retention on the filters. There is an additional need to backwash the filters and regenerate the activated carbon. These processes generally dislodge all retained and trapped pollutants into the backwash water stream which is discharged with recovery of the pollutants. At relatively high pollutant concentrations, efficiency of adsorption drops with subsequent low

performance. As low as 69% efficiency has been reported of GAC adsorption for removal of compounds with molecular structures similar to geosmin (Pham *et al*., 2012).

Due to their complex tertiary structure, both geosmin and MIB motifs (Figure 2.1) are resistant to oxidation by ozone and other aquatic oxidants (Ho *et al*., 2002; 2006). They are resistant to chlorination even at high chlorine dosages (Lalezary *et al*., 1986). For this reason, the conventional physico-chemical processes have not been used successfully for treating these compounds. Removal of geosmin and 2-methylisoborneol from drinking water has been a matter of great interest since early 1990s especially as they are difficult to remove by conventional water treatment methods such as coagulation-sedimentation and rapid sand filtration (Saito *et al*., 1996).

2.3 Phenol and its Derivatives

Phenol (Figure 2.2a) and its derivatives are amongst the most common organic water pollutants because of their wide range of uses. Phenol is toxic even at low concentrations, and also its presence in natural waters can lead to the formation of substituted compounds during disinfection and oxidation processes (Busca *et al*., 2008). Even at low concentrations, these contaminants are a major health risk due to their genotoxicity (Ahmed *et al*., 2010).

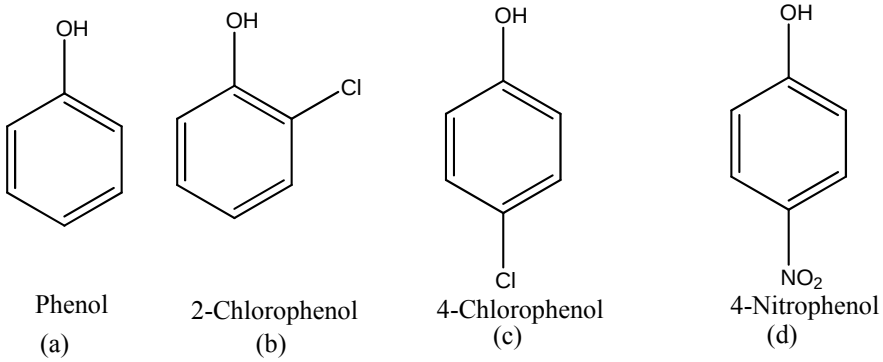

Figure 2.2 Structure of (a) Phenol (b) 2-Chlorophenol (c) 4-Chlorophenol and (d) 4-Nitrophenol.

Phenol is produced at a rate of 6 million ton/year worldwide and is a natural component of many substances (tea, wine and smoked foods), it is also emitted from the combustion of fossil fuels and tobacco (Busca *et al*., 2008).

Two of phenol's most common uses are in the production of phenolic resins, and in the preparation of bisphenol A, which is a monomer for the production of epoxy-resins. Phenol in its pure form is also used as a disinfectant and as an additive in the preparation of some creams and shaving soap for its germicidal and anaesthetic properties. Phenol is a key component in the production of several monomers for the production of nylon 6, polyphenoxy and polysulphone polymers; polyester and polyester polyols. Medicinal uses include use as an antiseptic and anaesthetic in veterinary medicine and its use in pharmaceuticals as a building block for the synthesis of aspirin. Phenol is also used as a peptizing agent in glue and as an extracting solvent in refinery and lubricant production. As a reagent in chemical synthesis, it can be converted into a variety of organic compounds including, xylenols, alkylphenols, aniline, and as an intermediate in the production of surfactants, fertilizers, explosives, paints, textiles, plastic plasticizers (Busca *et al.,* 2008) derivatives of phenol and a host of other products.

Chlorophenols (Figure 2.2b & c) are water pollutants of moderate toxicity and are suspected carcinogens. They originate from the natural degradation of chlorinated herbicides and chlorination of phenolic substances during disinfection of water with chlorine. Nitrophenols (Figure 2.2d) are water pollutants of high toxicity and they are released into the environment from the synthesis and use of organo-phosphorous pesticides, azo dyes, plasticizers, solvents (Lachheb *et al*., 2008) and some medical goods. Phenol and its derivatives (mostly the chlorinated and nitro- derivatives) are discharged regularly into the natural and wastewater streams from different process plants due to their wide use as raw materials in petrochemical, chemical, and pharmaceutical industries (Barakat *et al*., 2005). Phenol is an intermediate product in the oxidation of higher-molecular weight aromatic hydrocarbons.

Chlorophenols and phenols have been used as general purpose disinfectants and sometimes are formed as degradation products of other chlorinated xenobiotics in the environment. Biological treatment processes for the degradation of phenol and phenolic derivatives have proved to be inefficient due to their refractory nature. Activated carbon is widely used for the removal of phenolic pollutants from aqueous solutions, a process which does not actually destroy the pollutants and produces contaminated spent carbon as a waste by-product (Akbal and Onar, 2003). Due to their toxicity and genotoxicity, the degradation of these compounds in water treatment system has become a matter of high priority (Bamuza-Pemu and Chirwa 2010a).

2.4 Water Treatment Processes

Conventional drinking water treatment processes involve aeration, flocculation/sedimentation, filtration and disinfection. More recently, ion exchange and adsorption have been incorporated into some water treatment trains (EPA, 1999). The effectiveness of the conventional water treatment systems in removing volatile and semi-volatile organic compounds is very limited (Zhou and Smith, 2002). This limitation has spurred the search for more efficient and cleaner technologies to tackle the ever increasing threat to future water security. This has led to the advancement of new methods and adoption of improved methods for the removal of pollutants from water. Some promising new methods in the context of pollutant abatement in water are collectively referred to as advanced oxidation processes (AOPs) (Comninellis *et al*., 2008; Stasinakis 2008; Modrzejewska *et al*., 2007; Ljubas, 2005). Recent research has demonstrated that advanced oxidation processes are suited for the remediation of recalcitrant organic pollutants as they mineralise pollutants completely to CO_2 and H_2O (Li *et al*., 2008; Auguglisto *et al*., 2006; Klán and Vavrik, 2006; Bahnemann, 2004; von Gunten, 2003; Andreozzi *et al*., 2000; Zhou and Smith, 2002). The immense interest in AOPs can be attributed to the diversity of technologies involved, the level of success achieved by laboratory studies, and; the variety of areas of potential application and for commercialisation. Advanced oxidation processes are characterised by their catalytic, photochemical properties and oxidative degradation reactions (Maciel *et al*., 2004).

2.5 Advanced Oxidation Processes

Advanced oxidation processes encompass a wide range of methods all of which involve the utilisation of the highly reactive hydroxyl radical for the oxidation of organic and inorganic pollutants in water. A classification as presented in Figure 2.3 attempts to group these processes primarily on the principles employed for hydroxyl radical generation. These classes include: the photolytic systems (utilising only UV radiation), chemical systems, photochemical systems (combination of UV radiation and chemical oxidants); and physical systems (photocatalysis and cavitation).

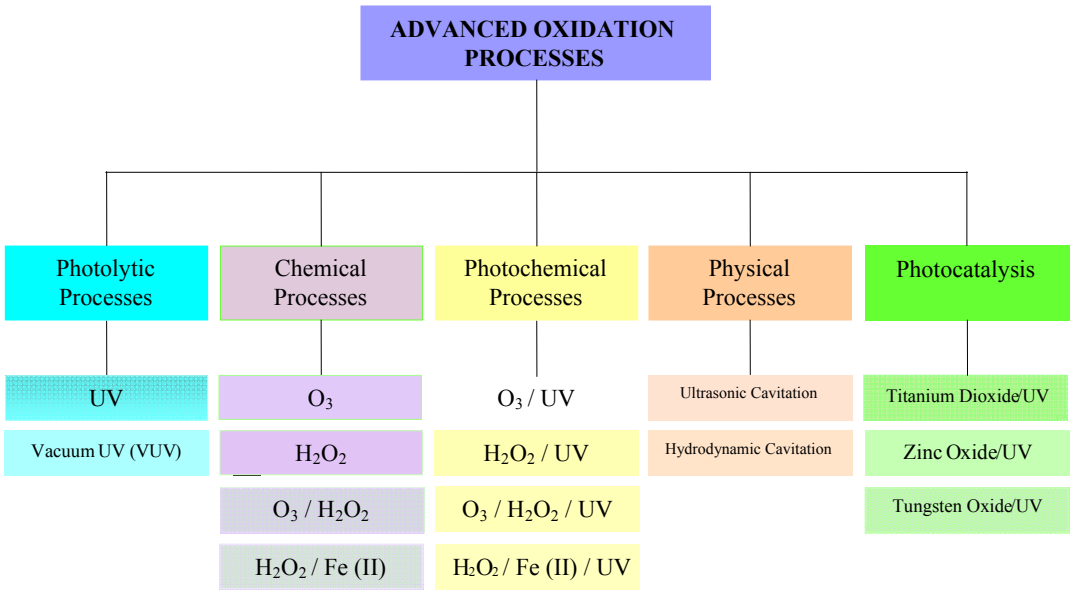

Figure 2.3: Classification of advanced oxidation processes.

The generated radicals are utilised for the degradation of organic and inorganic pollutants or for 'contact disinfection' of water by destroying potentially harmful microorganisms. The hydroxyl radical is the most powerful oxidising agent known with the exception of fluorine, with an oxidation potential of 2.80 V, exhibiting faster oxidation rates than conventional oxidants such as hydrogen peroxide (H_2O_2) and potassium permanganate ($KMnO_4$) (Gogate and Pandit, 2004; Mills and Lee, 2004). The oxidation potentials of hydroxyl radical and other commonly used oxidants are presented in Table 2.1, given in the order of decreasing potentials. Hydroxyl radicals are reactive electrophiles and are very effective in the destruction of organic compounds as they react rapidly and non-selectively with most electron rich organic compounds. Hydroxyl radicals are unstable and transient in nature, Due to their instability and are generated and used "in situ'' (Esplugas *et al*., 2002; Munter, 2001). Some advanced oxidation processes that have caught the interest of the scientific community are presented in the following paragraphs.

Photolytic systems initiate pollutant degradation directly or indirectly by the absorption of UV radiation, either from artificial sources or from solar energy. Energy supplied by

absorbed photons of light enables excitation of reactant molecules to promote degradation reactions (Parsons and Williams, 2004).

Table 2.1: Oxidation potentials of some commonly used oxidants.

Oxidant	Oxidation Potential (V)
Fluorine (F_2)	3.03
Hydroxyl Radical ($^{\bullet}OH$)	2.80
Ozone (O_3)	2.07
Hydrogen Peroxide (H_2O_2)	1.78
Potassium Permanganate ($KMnO_4$)	1.68
Chlorine (Cl_2)	1.36

Energy from absorbed photons in photolytic systems initiates pollutant degradation directly or indirectly by enabling excitation of reactant molecules to promote degradation reactions (Parsons and Williams, 2004). Direct photolysis of organic compounds by absorbed UV light occurs with dissolved organic compounds reacting with constituents of water or by induced self-decomposition. While indirect photolysis results in the photodegradation of organic compounds by photosensitizers like oxygen, hydroxyl or peroxy radicals produced by the photolysis of humic and inorganic substances (Giokas and Vlessidis, 2007). Sunlight induced photochemical reactions are considered as the most important abiotic processes that determine the fate of organic compounds in natural waters. Both direct and indirect photolytic processes occur in the surface layers of aquatic systems (Giokas and Vlessidis, 2007).

Application of photolysis as a stand-alone method for recalcitrant organic pollutant degradation has found limited application due to the lower efficiency of the photolytic systems compared to other advanced oxidation processes. Another major drawback in the use of photolysis for treating complex organic compounds is the production of intermediates that could be potentially harmful; as complete mineralisation is often not achieved. Buchanan *et al*., (2006) in their study of UV and VUV irradiation of natural organic matter; concluded that UV or vacuum UV (VUV) photolysis cannot be used as stand-alone methods. Their conclusion was based on the formation of potentially hazardous by-products due to UV

radiation. Zoh *et al*., (2009) in a separate study also concluded that UV photolysis alone was not an effective system for triclosan degradation as harmful intermediates of the dioxin type were produced. Both groups of researchers suggested the application of UV irradiation be used as a pre-treatment to biological treatment. This suggestion was based on evidence of appearance of breakdown compounds of lower molecular weight compounds (Buchanan, 2004).

Despite these short comings of the photolytic systems, the use of UV radiation for contact disinfection is a trend that is gaining popularity especially in wastewater treatment industry as it makes an excellent disinfectant especially in addition to chlorine disinfection. This has been incorporated into the water treatment trains in some water treatment plants. The Roodeplaat Water Treatment Plant, a 60 MGD plant has UV disinfection incorporated between two chlorination stages as additional disinfection and for the removal of some organics in water (Roodeplat Plant, 2007).

Ozone is a very reactive gas that is sparingly soluble in water (Zhou and Smith, 2002; Shin *et al*., 1999). Ozonation is considered a promising alternative to chlorine disinfection. Its mechanism of pollutant decontamination in water treatment involves direct reaction between ozone and the dissolved organic species; by reaction between generated hydroxyl radicals and the dissolved pollutants or by a combination of both (von Gunten, 2003, Shin *et al*., 1999; Bühler *et al*., 1984; Staehelin *et al*., 1984; and Nadezhdin 1988). Direct reaction between ozone and organic compound is selective; occurring at sites with high electron density. Ozonation systems would therefore be more effective for the degradation of highly unsaturated compounds with sites of high electron density, such as alkenes, alkynes and amines. However, organic compounds such as aliphatic carbon chains, amides, and nitroso compounds are not effectively oxidized by ozone. Oxidation of ozone-resistant compounds can be improved by irradiation of the system with UV or addition of hydrogen peroxide, which enhances $^{\bullet}OH$ production by accelerating ozone decomposition (Rosal *et al*., 2009; Lee *et al*., 2007; Beltrán *et al*., 2002).

Major drawbacks with ozone as an oxidant include its low solubility in water, cost of generation of ozone in sufficient quantities for use as an oxidant for the complete degradation of organic compounds; mass transfer limitations and the potential hazards due to the possibility of conversion of bromide ions in water to bromate (Michalski, 2003; Zhou and

Smith, 2002). The presence of bromate ions in water is as undesirable as the other disinfectant bye-products (DBPs), tetrahalomethanes (THMs) and haloaceticacids (HAAs), especially as bromate ions are not degraded by the biological filtration process (von Gunten, 2003). International Agency for Research on Cancer (IARC) classified bromate in group B-2 (as a "probable human carcinogen") and established a drinking water maximum contaminant level goal (MCLG) of zero; and MCL of 10 µg/L for bromate in drinking water (Michalski, 2003).

Engineering solutions to improve the mass transfer rates would further enhance ozone's effectiveness as an oxidant (von Gunten, 2003, Shin *et al*., 1999). Proposals to enhance the potential viability of the system include the integration of ozonation and a biological (post ozonation) system (Contreras *et al*., 2003). Research into the degradation of organic compounds by ozone is a very active field and the ozonation of several organic compounds has been studied with rate constants of over 500 compounds available in the literature (von Gunten, 2003). Ozonation is one advanced oxidation method that has been widely applied in water treatment or pre-treatment systems, and as at 2002; over 4000 ozonation plants were already in operation globally (Zhou and Smith, 2002).

Hydrogen peroxide though a moderately strong oxidant; has limited application on its own as an oxidant for the degradation of complex organic compounds. Though in the H_2O_2 process there is ready availability of the oxidant specie in solution, its use alone is not effective due to kinetic limitations at reasonable peroxide concentrations. On the other hand, aqueous hydrogen peroxide decomposes over heterogeneous catalysts including metals (i.e., Fe, Cu, Pt, Ti, and Ni) and metal oxides immobilized on various support materials such as sand, silica, zeolites, and alumina (Kitis and Kaplan, 2007). Improvement of the oxidative capacity of hydrogen peroxide can be achieved by combining hydrogen peroxide with ozone or with UV radiation or some transition metal salts. These hybrid chemical systems exhibit better oxidative properties due to the decomposition of hydrogen peroxide to release hydroxyl radicals.

The ozone/hydrogen peroxide system generates hydroxyl radicals by a radical chain mechanism resulting from interaction between ozone and hydrogen peroxide. The peroxone system is much more efficient than using either ozone or hydrogen peroxide alone for the removal of organic compounds from water, with better chances of complete mineralisation of

both target pollutant and degradation intermediates formed in solution (Rosa *et al*., 2009). The efficiency of the peroxone system can be further improved by photolysis of peroxone by incorporation of UV radiation source. The irradiation of O_3/H_2O_2 by UV from solar light or artificial light accelerates the decomposition of both ozone and hydrogen peroxide. The synergic effects of ozone, hydrogen peroxide and UV irradiation makes the photo peroxone system a very powerful method that allows fast and complete mineralization of pollutants. It is considered to be the most effective treatment for highly polluted effluents (Esplugas *et al*., 2002; Munter, 2001).

Fenton reagent is a catalytic oxidative mixture that contains an oxidant (usually hydrogen peroxide) and a catalyst (a metal salt or oxide, usually ferrous salts) and the process is increasingly used in the treatment of organics in water and soil. Decomposition of hydrogen peroxide by Fe^{2+} ions in solution spontaneously produces extremely reactive and non-selective hydroxyl radicals (Raj *et al*., 2005; Wadley and Waite, 2004; Munter, 2001). Fenton process is often modified by the use of ferric ion, which acts as a catalyst in the decomposition of H_2O_2 into H_2O and O_2; and its use could prevent accumulation of Fe (II) ions in the reaction vessel. Fe (II) in this reagent can be replaced by other metal ions and their complexes in the lower oxidation states. These metal ions have the oxidative features of the Fenton reagent and are collectively called Fenton-like reagents. They include Cu(I), Cr(II), CO(II) and Ti(III), although their application is limited due to the relative toxicity of some of these metal ions (Wadley and Waite, 2004).

The main advantages of the Fenton include: (i) the relative very low cost of the key reagents (hydrogen peroxide and iron salts). Iron is highly abundant and non-toxic and dilute solution of hydrogen peroxide is easy to handle and environmentally friendly (Momani *et al*; 2004, Wadley and Waite, 2004); and (ii) the relative simplicity of the process, requiring neither special reagents nor apparatus (Andreozzi *et al*., 1999). The use of Fenton system in water treatment is limited by its narrow pH range of efficient application (pH 2-4 best at 2.8); which is outside the pH range of natural water. There is the tendency of ferric hydroxide precipitation at pH > 3, this can be controlled by the addition of some organic ligands to complex Fe(III) to enable the process to be carried out at higher pH values (Wadley and Waite, 2004 and references therein). As discussed in the peroxone system, efficiency of the Fenton process is improved by irradiation with UV light. Photolysis of the Fenton system leads to the formation of additional hydroxyl radicals and recycling of ferrous catalyst by the

reduction of Fe(II). The increased efficiency of this process is mainly attributed to the photo reduction of ferric ion (Momani *et al*., 2004).

With the emergence of the green revolution and the collective consciousness of pollutant abatement with reduced impact; research in advanced oxidation is tending towards methods that involve the generation of the hydroxyl radicals without the addition of chemical reagents. These methods are the physical methods that include cavitation and photocatalysis.

The use of cavitation in water and wastewater treatment is a concept that is relatively new and still under investigation. Cavitation is the formation, growth and implosion of microbubbles or gaseous cavities within a liquid also called "nucleation of bubbles" (Dupree *et al*., 1998). Cavitation is accompanied by adiabatic heating of the vapour phase inside the bubbles resulting in very high local temperatures and pressures in millions of such locations within the reactor. The effective local temperature and pressure at these transient "hot spots" in water may exceed 5000K and 50 atm, respectively (Hassoon *et al*., 2004; Chen *et al*., 2006). The violent collapse of cavities results in the formation of reactive hydrogen atoms and hydroxyl radicals, which combine to form hydrogen peroxide to some extent and are responsible for promoting oxidation reactions in water (Mason and Pétrier, 2004; Gogate *et al*., 2003; Findik *et al*., 2006). Cavitation can also lead to cellular damage in microorganisms (Jyoti and Pandit; 2001). Cavitationally induced metal corrosion may be a major factor that would limit the wide application of cavitation for water treatment, as it presents an engineering challenge during reactor design (Chen *et al*., 2006). Cavitation in a liquid can be brought about by the application of ultrasonic waves or by hydrodynamic means.

Ultrasonically induced cavitation also called acoustic cavitation is the formation, growth, and collapse of gaseous or vaporous bubbles under the influence of ultrasound (Liang *et al*., 2006). High frequency sound waves, in the range of 16 kHz-100 MHz are often required to bring about cavitational inception. Alternate compression and rarefaction cycles of sound waves result in generation of the bubble cavity, bubble growth, and finally bubble collapse phases releasing large amounts of local energy. The oxidation of contaminants by acoustic cavitation is thought to progress via free radical attack and pyrolysis mechanisms (Gogate and Pandit, 2004; and references therein). During acoustic cavitation pyrolysis of water produces $^{\bullet}H$ and $^{\bullet}OH$ and in most cases, the reaction pathways observed for ultrasonic-

induced degradation of dissolved organic compounds in aqueous media involve hydroxyl radical oxidation, pyrolysis and supercritical oxidation (Song and O'shea, 2007).

Bubble creation and collapse in hydrodynamic cavitation is brought about by hydraulic devices. In such systems cavitation is generated due to pressure variations in a flowing liquid caused by changes in the geometry of the flow system (Gogate and Pandit, 2004; Jyoti and Pandit, 2001). Pressure variations are created by the passage of the liquid through a constriction such as valves and orifice plates. Intensity of cavitation generated by hydraulic devices is lower than those from acoustic cavitation. On the other hand hydrodynamic cavitation is believed to have higher efficiency and cavitational yields compared to acoustic cavitation (Gogate and Pandit, 2001).

2.6 Semiconductor Photocatalysis

While investigating the photoelectrolysis of water, the discovery by Fujishima and Honda in 1972 of the photocatalytic splitting of water on n-type rutile titanium dioxide electrodes opened the doors to numerous possibilities that the field of photocatalysis presents (Hashimoto *et al*., 2005; Zhao and Yang, 2003; Linsebigler *et al*., 1995). In recent years, research efforts in photocatalysis have been focused towards a better understanding of the underlying principles of oxidative degradation of organic pollutants in aqueous phase. Some areas that need better understanding include photodegradation pathway, as well as the identification of intermediates produced. Semiconductor photocatalysis for pollutant abatement in water and air has been the focus of immense research in the last two or three decades because it offers a unique advantage over alternative treatment methods as it presents a 'green' treatment approach, with the possibility of mineralisation, i.e., complete mineralisation of toxic organic pollutants into H_2O and CO_2 using photonic energy (Ray *et al*., 2009, Herrmann, 2005, Zhao and Yang, 2003). However, degradation of organic compounds containing heteroatoms produces mineral acids of the heteroatom in the organic pollutant.

Semiconductor photocatalysis involves the photo-excitation of electrons in solid semiconductor (SC) as a result of the absorption of electromagnetic radiation often in the near UV spectrum to produce highly reactive electronically excited states used for non-selective destruction of pollutants in air and water.

2.6.1 Photoelectronic processes on semiconductor surface

Solid materials contain a very large number of atoms in constant interaction. Corresponding energy levels are so close together that they form energy bands with each band. At the atomic levels electrons fill the energy levels from the lowest energy level upward. The highest energy band containing electrons is the valence band (VB) and the next band immediately higher in energy than the VB is the conduction band (CB). The conduction band is the lowest unoccupied energy level that is devoid of electrons.

Semiconductor materials possess a region that is void of energy bands, thereby creating an energy space between the VB and the CB. This energy difference between the VB and the CB is called the bandgap energy (E_{bg}) (Kondarides, 2005, Linsebiglier *et al.*, 1995). In semiconductor materials, unlike insulators (with much wider bandgaps); the bandgap is small enough (usually less than 4 eV) such that it can be bridged by the application of external stimuli such as heat or light. Absorption of a photon (hv) of ultra-bandgap energy results in the promotion of an electron, e^-, from the valence band into the conduction band with the generation of an electron deficient positive hole (h^+), in the valence band thus forming an electron-hole pair (h^+ e^-) (Kondarides, 2005) (Bahnemann, 2004; Mills and Lee 2004, Sumita *et al.*, 2001). The photoexcitation process and electron hole pair formation is depicted by the band diagram in Figure 2.4.

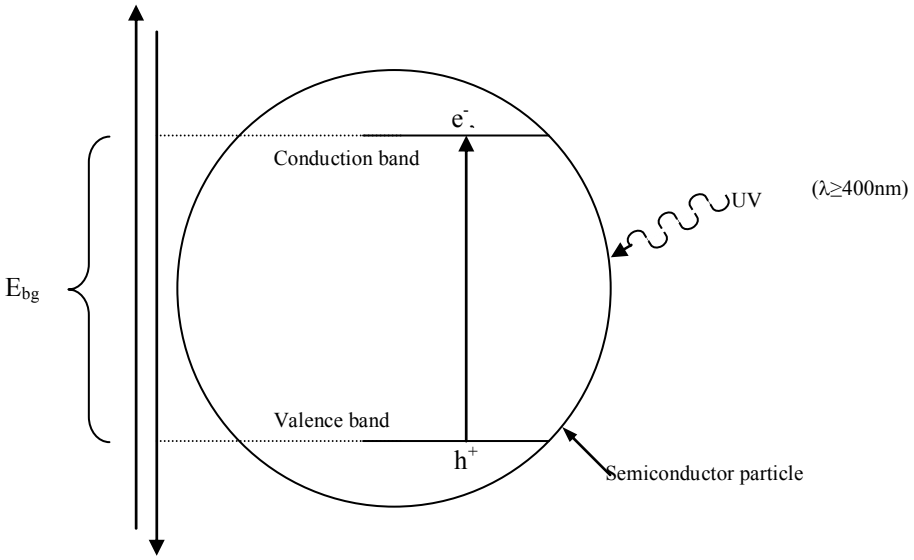

Figure 2.4: Schematic of electron-hole pair formation over a semiconductor particle.

The fate of photoelectronically excited conduction band electrons and valence band holes depends on the de-excitation electronic pathway followed by the particular species. These pathways include:

- Recombination either at the surface, or in the bulk of the semiconductor material and dissipation of the input energy to liberate heat (Δ);
- Entrapment into metastable surface states; or
- Migration separately to the surface of the semiconductor material to react directly or indirectly with electron donors and electron acceptors adsorbed on the semiconductor surface, or within the surrounding electrical double layer of the charged particles.

The various deactivation pathways and reaction processes associated with electron-hole pair formation occurring on a particular photocatalyst upon ultra-band gap photo illumination are presented in Figure 2.5.

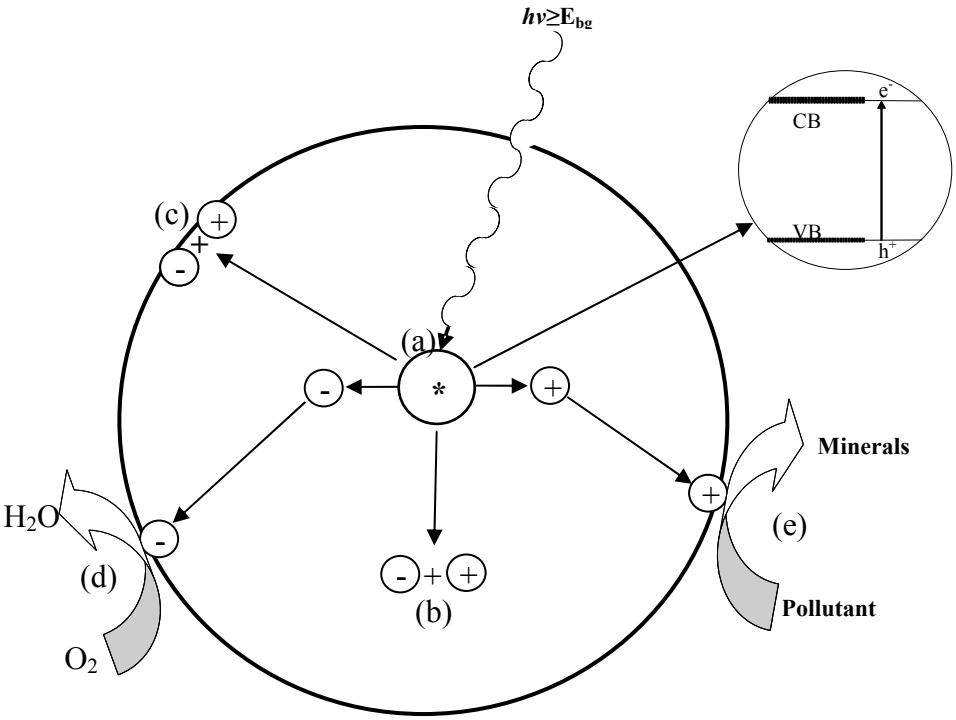

Figure 2.5: Schematics of major processes in semiconductor photocatalysis upon ultra-band gap illumination

Processes depicted by Figure 2.5 include:

(a) Formation of charged carriers (h^+ e^-) electron – hole pair by a photon with ultra-band gap energy (insert showing (h^+ e^-) pair formation);

(b) Electron-hole recombination in the bulk of the semiconductor particle;

(c) Electron – hole recombination on the surface of the particle;

(d) Direct or indirect reduction of oxygen or oxidizing intermediates by photogenerated electrons on the surface of the catalyst;

(e) Direct or indirect oxidation of pollutant, or an oxidized intermediate species by photogenerated holes at the surface of the semiconductor, leading to mineralized products (usually CO_2 and H_2O).

In the absence of suitable electron hole scavengers, the stored energy is dissipated within a few nanoseconds by recombination. Presence of suitable scavengers or surface defect states that trap the generated reactive species (electron or hole), prevents recombination and promotes the possibility of subsequent surface redox reactions (Hoffmann *et al*., 1995).

Electron hole pair recombination (processes (b) and (c)) is undesirable in the treatment process as it reduces the efficiency of the photocatalytic process by reducing the availability of reactive species (Mills and Lee, 2004; Hermann, 1999; Bauer *et al*., 1999). Efficiency of a photocatalyst is determined by different interfacial electron transfer processes such that reactions depicted by Figure 2.5 (d) and (e) involving e^-, and h^+ reacting with adsorbed species must compete effectively with the major deactivation routes of electron-hole recombination (Devilliers, 2006; Mills and Lee, 2004; Hoffmann *et al*., 1995).

Valence bond holes are powerful oxidants, with oxidation potentials of +1.0 to +3.5 V (Bahnemann, 2004; Munter, 2001; Hoffmann *et al*., 1995). Reactions of photo generated electron hole pairs on the surface of the photocatalyst occur in the presence of electron donors or electron acceptors adsorbed on the photocatalyst surface. Thus, if there is an electron acceptor, A, then the photo generated electrons can react with A (directly or indirectly) generating a reduced product A^-. Similarly the photogenerated holes that migrate to the surface can react with an electron donor, D; to form an oxidized product D^+. The

oxidation and reduction reactions on the surface are summarized in Equation 2.1 and illustrated in Figure 2.6.

$$A + D \xrightarrow{\text{semiconductor } (h\nu \geq E_{bg})} A^{-} + D^{+} \qquad (2.1)$$

where: A = electron acceptor, A^{-} = reduced product, D = electron donor and D^{+} = oxidised product.

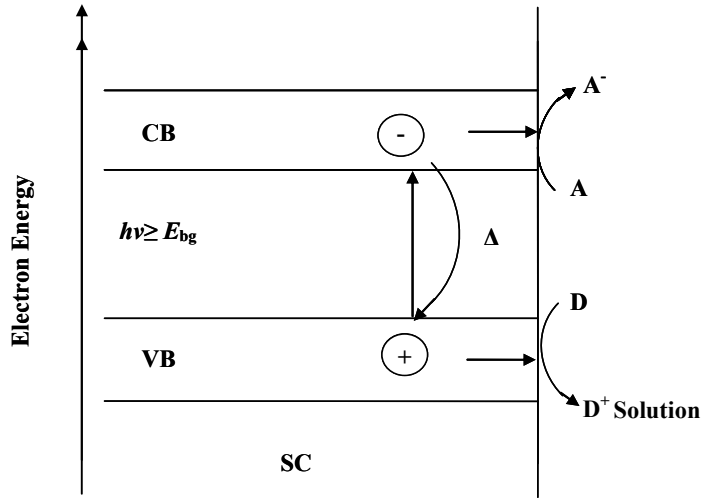

Figure 2.6: Schematic illustration of the energetics of semiconductor photocatalysis.

In water purification, the electron acceptor (A) is usually oxygen in aerated systems, and the electron donor (D) is the pollutant. The overall process is the photocatalytic oxidation of the pollutant by dissolved oxygen as represented by Equation 2.2:

$$\text{Organic pollutant} + O_2 \xrightarrow{\text{semiconductor } (h\nu \geq E_{bg})} CO_2 + H_2O + \text{Mineral acids} \qquad (2.2)$$

The presence of an external electron acceptor in a photocatalytic system leads to improvement of the system by reducing the available conduction band electrons, thereby reducing the possibility of electron–hole recombination; increasing the concentration of

reactive species in solution (hydroxyl radicals) and other oxidising species in solution (Ahmed *et al*., 2010)

2.7 Semiconductor Photocatalysts

The search for the perfect semiconductor material for photocatalysis has been a major focus in the field of photocatalysis. Various metal oxides including titanium dioxide (TiO_2), zinc oxide (ZnO), molybdenum trioxide (MoO_3), ceric dioxide (CeO_2), zirconium dioxide (ZrO_2), tungsten trioxide (WO_3), ferric oxide (Fe_2O_3), stannic dioxide (SnO_2); and metal chalcogenides including zinc sulphide (ZnS), cadmium sulphide (CdS), cadmium selenide (CdSe), tungsten disulphide (WS_2) and molybdenum disulphide (MoS_2) have been tested and used as photocatalysts (Hoffmann *et al.*, 1995; Gogate and Pandit 2004; Devilliers, 2006). Suitable photocatalyst must be:

- Chemically and biologically inert;
- Easy to produce, and use; and
- Photostable.

Sensitization of a catalyst to drive the reaction in Equation 2.2 is only possible for semiconductors with redox potentials of the photogenerated valence band hole that are sufficiently positive to generate absorbed OH radicals, which in turn can oxidize organic pollutants. In addition, the redox potential of the photogenerated conductance band electrons must be sufficiently negative to reduce absorbed oxygen to superoxide (Mills *et al*., 1993). No semiconductor available exhibits all of the above requirements. However, of all the semiconductors tested in photocatalysis, titanium dioxide (TiO_2) has proven to be the most suitable for environmental purposes. Figure 2.7 shows some of the semiconductors that have been employed for photocatalytic reactions in water and their associated band gap energies in eV.

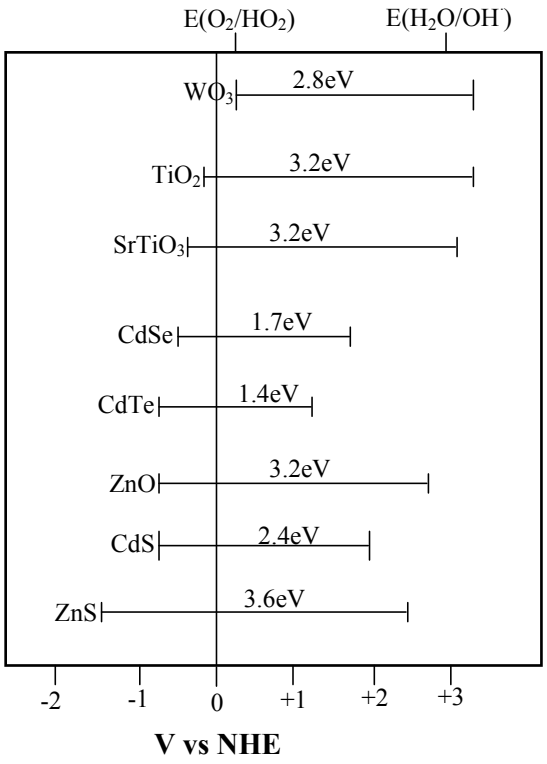

Figure 2.7: Band positions of common semiconductors used in photocatalysis and the redox potential of the $H_2O/^{\bullet}OH$ and $O_2/HO^{\bullet}_2$ redox couples at pH = 0 (Mills *et al*., 1993).

TiO_2 has suitable bandgap energy; is biologically and chemically inert; is stable with respect to photocorrosion and chemical corrosion; nontoxic, non-carcinogenic; insoluble under most conditions and it is inexpensive. TiO_2 does not present any significant fire hazards and environmental risks. It has been widely reported to give the best catalytic performances and degradation efficiencies especially in the anatase form (Malato *et al*., 2007; Hashmimoto *et al*., 2005; Mills and Lee, 2004; Gogate and Pandit, 2004; Andreozzi *et al*., 1999, Mills *et al*., 1993). Due to the above conditions TiO_2 has become the semiconductor material of choice for environmental photocatalytic processes.

Metal sulphide semiconductors are unsuitable photocatalysts as they undergo photoanodic corrosion. The iron oxide polymorphs are also not suitable semiconductors since they readily undergo photocathodic corrosion, even though they have nominally high bandgap energies and are cheap (Hoffmann *et al*., 1995).

2.7.1 Titanium dioxide (TiO_2) catalysts

Titanium dioxide exists in three crystalline forms, namely anatase, rutile and brookite, but only the anatase and rutile forms are reported to exhibit efficient photocatalytic activities with the anatase form being more efficient. The anatase form is also the easiest to produce and has therefore become the photocatalyst of choice for photocatalytic purification of water.

The threshold wavelength of radiation depends on the band gap energy. TiO_2 has large band gap energy of 3.25-3.05 eV (anatase 3.25 eV and rutile 3.05 eV). It absorbs UV light in the range of 380-405 nm, which represents a small fraction of the solar spectrum (approximately 6%). The energy input from the electromagnetic waves in this region is enough to drive the photocatalytic process (Mills and Lee, 2004). The oxidation potential of the photogenerated holes in the valence band of anatase attains a value of +2.9 eV vs Standard Hydrogen Electrode (SHE)/pH 0), which is sufficient for the complete oxidative decomposition of most of the organic molecules to carbon dioxide and water (Kluson *et al*., 2005).

Some highly efficient commercial forms of titanium dioxide are now available; the most commonly used of these is the P25 Degussa TiO_2, a non-porous 70:30% anatase to rutile mixture with a specific Brunauer–Emmett–Teller surface area (BET) of 55 ± 15 m^2/g and crystalline sizes of 30 nm in 0.1 μm diameter aggregates (Hoffmann *et al*., 1995; Doll and Frimmel, 2005). Hombikat UV100 is another commercially available form of TiO_2 frequently used in photocatalytic degradation studies (Doll and Frimmel, 2005).

2.7.2 Semiconductor surface modification

It is has been established that morphological and structural characteristics of a semiconductor material strongly affect the efficiency of its photocatalytic activity. The properties of a particular semiconductor can be altered to overcome the limitations of its use for photocatalytic activity and improve its performance. Such property alterations usually involve some form of modification of the catalyst surface. Choice of modifications depends on the expected benefit(s) which can arise from:

- Bandgap reduction increases the wavelength range of the semiconductor and extends it into the visible region of the spectrum for the beneficial use of visible light especially solar power.

- The inhibition of electron hole pair recombination by increasing the charge separation (charge carrier trapping) and thereby increasing the efficiency of the system, and
- Changing the selectivity or yield of a particular product (Linsebigler *et al*., 1995).

Modification strategies of semiconductor surface for enhanced performance include the addition to the catalyst of noble/rare earth metals in a process called metal ion doping or catalyst doping, surface sensitisation with chemisorption or physiosorption of dyes or by coupling with other semiconductor materials to obtain a composite (coupled) semiconductor. Another method employed to increase the photoefficiency of semiconductors is by the addition of inorganic co-adsorbents to the photocatalyst, such as activated carbon, silica, alumina, zeolites, clays (Matos *et al*., 2007)

2.7.3 Major reactions during photocatalysis in water

The major reactions involved in the photomineralisation of pollutants by photosensitized TiO_2 in aqueous media are presented in Equations 2.3 to 2.9:

$$TiO_2 + h\nu \rightarrow TiO_2\,(e^-_{CB} + h^+_{VB}) \quad (2.3)$$

$$TiO_2(h^+_{VB}) + H_2O_{ad} \rightarrow TiO_2 + {}^{\bullet}OH_{ad} + H^+ \quad (2.4)$$

$$TiO_2(h^+_{VB}) + OH^- \rightarrow TiO_2 + {}^{\bullet}OH_{ad} \quad (2.5)$$

$$TiO_2\,(e^-_{CB}) + O_2 \rightarrow TiO_2 + O_2^- \quad (2.6)$$

$$O_2^- + H^+ \rightarrow HO_2^{\bullet} \quad (2.7)$$

$$TiO_2(h^+_{VB}) + \text{R-H} \rightarrow TiO_2 + \text{oxidized products.} \quad (2.8)$$

$${}^{\bullet}OH + \text{R-H} \rightarrow \text{oxidized products.} \quad (2.9)$$

In the photomineralisation of organic pollutants sensitized by TiO_2 as represented by Equation 2.2, the photogenerated electrons reduce oxygen to water (Equation 2.6), and the photogenerated holes mineralize the pollutant (Equation 2.8). The mineralization process is believed to involve the initial oxidation of surface hydroxyl groups ($>Ti^{IV}OH$) on the TiO_2 to hydroxyl radicals ($>Ti^{IV}\ OH^{\bullet+}$), which oxidizes the pollutant and any intermediate(s). The final product usually is the mineral form of the pollutant, typically carbon dioxide and water. However, if there are heteroatoms present, then the mineral acid of the heteroatom is formed. Other intermediate species formed include Ti^{III} species ($Ti^{III}OH$) formed from the trapping of the photogenerated electrons by surface sites ($>Ti^{IV}OH$). $Ti^{III}OH$ reacts with dissolved

oxygen to form superoxide, O_2^{-}, which can be further reduced to hydrogen peroxide (H_2O_2). Hydrogen peroxide is also a possible source of hydroxyl radicals, which could be partly responsible for some degree of the mineralization in reaction represented in Equation 2.2. Primary processes and their associated characteristic time frames are presented in Table 2.2.

The dynamic equilibrium of Equation 2.12 represents a reversible trapping of a conduction band electron in a shallow trap below the conduction band edge, thus a finite probability of e_{tr}^- transfer back into the conduction band at room temperature exists. From Equations 2.9-2.16, two critical processes determine the overall quantum efficiency for interfacial charge transfer. These processes are the competition between charge carrier trapping (Equations 2.10-2.12) and recombination (Equations 2.14 and 2.15) – picoseconds to nanoseconds. This is followed by the competition between trapped carrier recombination and interfacial charge transfer – microseconds to milliseconds. An increase in either the recombination lifetime of charger carriers or the interfacial electron transfer rate constant is expected to result in higher quantum efficiency of the steady state photocatalysis (Hoffmann *et al*., 1995).

Table 2.2: Primary processes and the associated timeframe for TiO_2 photosensitized mineralization of organic pollutants (Hoffmann *et al*., 1995).

Primary Process	**Characteristic Times**	**Equation Number**
Charge carrier generation		
$TiO_2 + h\nu \rightarrow h_{vb}^+ + e_{cb}^-$	fs (very fast)	(2.10)
Charge carrier trapping		
$h_{vb}^+ + >Ti^{IV}OH \rightarrow \{Ti^{IV}OH^{\bullet+}\}$	10 ns (fast)	(2.11)
$e_{cb}^- + >Ti^{IV}OH \leftrightarrow \{Ti^{III}OH\}$	100 ps (shallow trap, dynamic equilibrium)	(2.12)
$e_{cb}^- + >Ti^{IV} \rightarrow >Ti^{III}$	10 ns (deep trap), irreversible.	(2.13)
Charge carrier recombination		
$e_{cb}^- + \{Ti^{IV}OH^{\bullet+}\} \rightarrow >Ti^{IV}OH$	100 ns (slow)	(2.14)
$h_{vb}^+ + >Ti^{III}OH \rightarrow >Ti^{IV}OH$	10 ns (fast)	(2.15)
Interfacial charge Transfer		
$\{Ti^{IV}OH^{\bullet+}\} + Red \rightarrow Ti^{IV}OH + Red^{\bullet+}$	100 ns (slow)	(2.16)
$e_{tr}^- + Ox \rightarrow Ti^{IV}OH + Ox^{\bullet-}$	ms (very slow)	(2.17)

where: >TiOH represents the primary hydrated surface functionality of TiO_2,
e_{cb}^- represents a conduction band electron, e_{tr}^- is a trapped conduction band electron,
h_{vb}^+ is a valence band hole,
Red is an electron donor (i.e. reductant), Ox is and electron acceptor (i.e. oxidant),
$>Ti^{III}OH$ is the surface trapped CB electron
fs is femtosecond (1 fs is 10^{-15} of a second), and
$\{Ti^{IV}OH^{\bullet+}\}$ is the surface trapped VB holes (i.e. surface bound hydroxyl radical).

2.7.4 Technological installations

A wide variety of reactor configurations have been used in photocatalytic degradation of pollutants in water. The reactor configuration is often determined by the form in which the catalyst is used and the mode of UV illumination. Reactors configurations include:

- Dispersed catalyst reactors (DCR)
- Fixed-bed reactors.

Dispersed catalyst reactors

In dispersed catalyst reactors, the semiconductor catalyst is dispersed in a powder form in the reaction solution containing the pollutant. The apparatus consist of a mixing device, reactor vessel and protected UV lamp; and may be purged with air or oxygen.

The reactor can be illuminated internally (immersion of the UV lamp in the solution) – Figure 2.8(b) or externally (irradiation of the solution from outside of the reactor, above or below the reactor) – Figure 2.8(a) and (c). Another photo-reactor for semiconductor photocatalysis is the annular system, in which the reactor solution passes along the reactor length one or more times - Figure 2.8(d).

This reactor configuration is very popular in the water disinfection industry. The annular system is a reverse of the externally illuminated system with multiple lamps arranged parallel to the main axis of flow.

The DCR reactors are easy to scale up because additional photocatalyst preparation is not required. However, a major disadvantage of these slurry reactors is the need for semiconductor particles separation from the bulk fluid phase after treatment by filtration, centrifugation or flocculation. These additional steps contribute various levels of complexity to the overall treatment process and decrease the economic viability of the slurry reactors (Hoffmann *et al*., 1995; Mills and Lee, 2004). Some simple commonly used slurry reactor designs are presented in Figure 2.8.

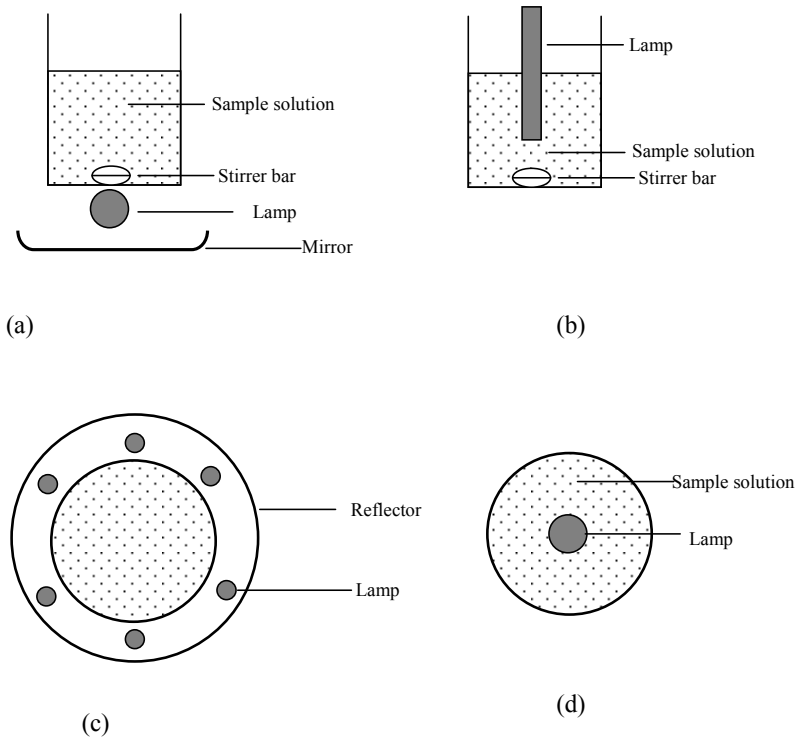

Figure 2.8: Basic photocatalytic DCR reactor designs: (a) side of reactor with external illuminator; (b) side view of reactor with immersed lamp; (c) top view of circular reactor with several lamps; and (d) annular reactor (i.e., tubular reactor with negative illumination geometry (Adapted from Mills and Lee, 2004).

Fixed-bed reactors

This is an alternative configuration which comprises a solid semiconductor coated on an inert substrate. Several inert substrates have been used as a support for coating the solid semiconductor photocatalyst, including glass walls, stainless steel (Chen and Dionysiou, 2006), and glass spiral tubes. The photocatalyst is sometimes also coated on the outer casing of the light source. A major advantage of the fixed-bed reactors is the elimination of the catalyst's recovery step. In slurry reactors, the recovery is achieved by filtration, sedimentation or other separation processes. Comparative features of dispersed and fixed-film reactors are presented in Table 2.3.

The limitations of the fixed film reactors include:

- Low surface area-to-volume ratios, as fixed bed have limited surface area of the catalyst exposed to the irradiation source;
- Reduction of reaction efficiency due to scattering of light by the reaction medium;
- Poor mixing results in inefficient exposure of pollutant to catalyst surface.

Due to the low surface area to volume ratio, the fixed-bed photoreactors are usually operated in a multipass (recycling mode) or series mode. Improvement of the surface area to reaction volume ratio can be achieved by suspended media systems. Suspended media in common use include alumina pellets, molecular sieve, glass beads, fibreglass, glass mesh or woven fibres.

Table 2.3: Comparative features of dispersed and fixed-film reactors (Mills and Lee 2004).

Feature	Dispersed semiconductor photocatalyst	Fixed film semiconductor photocatalyst
Ease of preparation of photocatalyst	Excellent. Photocatalyst easily prepared by numerous chemical routes, including hydrolysis or air oxidation of simple Ti(IV) precursors.	Can be difficult and usually involves either CVD, sol-gel, sputtering or thermal oxidation methods.
Ease of replacement of semiconductor photocatalyst	Excellent. The photocatalyst particles are simply added to the polluted water stream.	Often difficult as the usually firmly fixed film photocatalyst is often attached to the walls of the photoreactor. Photocatalyst on support materials, such as glass beads, are easier to change.
Overall ease of operation as a water purification system	Not usually very good, since a subsequent particle separation step is required, which usually brings with it the need for regular filter replacement. In addition, ideally, the filtered photocatalyst should be returned to the photoreactor, which poses another technical problem, although a recirculation system with cross-filtration appears to offer a solution. System needs constant sparging with air.	Excellent. No filtering required. In some 'close-to–ambient air' systems, oxygen sparging is really needed.

Table 2.3: Comparative features of dispersed and fixed-film reactors (continued).

Feature	Dispersed semiconductor photocatalyst	Fixed film semiconductor photocatalyst
Efficiency by m^2	High due to high photocatalyst surface area to reaction solution ratio and no mass transfer effects.	Low, thus, such systems need to be cheap per m^2.
Cost	Low initial cost, but maintenance costs can be high.	High initial cost, but maintenance costs could be low, provided the water stream does not contain any deactivating contaminants.

2.7.5 Light sources

The source of ultra-band gap illumination in photocatalysis is one of the most important factors to consider in designing the reactor. The light source is the highest contributor of capital costs of the system. UV light is required as a source of ultra-band gap illumination and is usually obtained from arc lamps in which mercury and/or xenon vapour is activated electrically. Mercury and xenon lamps are usually inefficient in terms of UV photons produced per unit of electrical energy input as a result of conversion of a great deal of electrical energy into heat or visible light. They are also expensive with limited lifetime of about 1000 h. Alternative light sources are the UV fluorescent lamps, which provide highly efficient electrical energy to UV photon conversion.

A version of the UV lamp, the black light, has high electrical energy to UV light conversion efficiencies of 10-20% and long operational lifetimes of 4000-14000 hours. A major disadvantage of black light is the emission of UVC radiation (280-100 nm, far UV) which causes cancer. Unfortunately, most black light bulbs have low light intensity of ≤150 W (Mills and Lee, 2004). Such dispersed light systems show high surface area to reaction volume ratio and even distribution of the photons on catalyst particles.

UV lamps

One of the major problems in semiconductor photocatalysis is the achievement of an even distribution of light in the photoreactor. Poor distribution of UV light in a semiconductor reactor will lead to a low overall efficiency of operation. Rate of reaction is reported to be directly proportional to the intensity of radiation (Equation 2.3). At low intensities a linear relationship exists between reaction rate and intensity. At higher intensities, rates of reaction are reported to show a square root dependence on intensity (Okimotoe *et al*., 1985; Ollis *et al*., 1991 as reported by Gogate and Pandit, 2004). A novel system for distributing ultraband gap light more evenly and efficiently has been used by Hoffstadler and co-workers. The photocatalytic material in this system is dispersed throughout the photoreactor via a series of light conductors, such as thin glass plates, rods, fibres of the hollow glass tubes (Mills and Lee, 2004).

The threshold wavelength of radiation depends on the band gap energy. TiO_2 has band gap energy of 3.2-3.0 eV and absorbs UV light of 380-405 nm. The rutile form has band gap energy of 3.05 eV, which would require 405 nm irradiation to generate an electron hole pair. Anatase has band gap energy of 3.20 eV corresponding to 380 nm of radiation. Use of lamp of the right wavelength is very important for an efficient system.

Solar source

The major component of operational cost in photocatalytic systems is associated with the artificial generation of photons required for electron-hole pair formation. This cost can be significantly reduced by the use of the "free" light source form solar energy (Esplugas *et al*., 2002; Bahdalala *et al*., 2004; Bahnemann, 2004; Gogate and Pandit, 2004; Mills and Lee 2004; Ljubas, 2005; Malato *et al*., 2007). Using solar light source would have ecological benefits as well as economic benefits. The sun has a typical UV-flux near the surface of the earth of 20-30 W/m^2; this translates to 0.2-0.4 mol photon $m^{-2}\,h^{-1}$ available in the 300-400 nm range (Bahnemann, 2004, Mills and Lee, 2004). This is estimated to be 25 times less than that from an 8 W, UV fluorescent lamp (Mills and Lee, 2004). Tapping this free source would translate into significant cost savings. Solar powered applications can only be used beneficially in the parts of the world that receive enough sunlight. Fortunately, Africa is geographically located to benefit from the use of such solar powered systems.

A number of solar powered photocatalytic systems are currently under test for various applications. They use only high-energy short-wavelength photons, which can be collected by conventional solar thermal collector designs, such as parabolic troughs and non-concentrating collectors (which utilise direct or diffuse sunlight). Non-concentrating collectors are, in principle, cheaper than parabolic trough concentrators (PTCs), as they have neither moving parts nor solar tracking devices (Malato *et al*., 2007; Rodriguez *et al*., 1996). The most commonly used solar reactor concepts are discussed in an excellent review of solar powered systems by Bahnemann (Bahnemann, 2004).

2.7.6 Application of semiconductor photocatalysis

Toxic organic compound degradation

Research into semiconductor photocatalysis has largely focused on the removal of organic pollutants from water, since a wide range of organic substrates can be completely mineralized in the presence of dissolved oxygen, photosensitized by TiO_2. One of the very attractive features of semiconductor photocatalysis is its effectiveness against a broad range of pollutants, including those that are recalcitrant to other water treatment processes. This makes it ideal for treating hazardous refractory organics such as herbicides and aromatic compounds (Mills and Lee, 2004). A non-exhaustive list of some classes of compounds mineralized by TiO_2 sensitized photocatalysis is presented in Table 2.4. Class of compounds of environmental interest in Table 2.4 include haloalkanes, such as chloroform and tetrachloromethane; halophenol; herbecides, especially dichlorodiphenyltrichloroethane (DDT) which is in the U.S.EPA's list of top priority persistant organic pollutants (POP). The haloagenated compounds are disinfection by-products (DBPs) often found in small but detectable quantities in drinking water disinfected by chlorination; and are known carcinogens.

Table 2.4: List of classes of organic compounds photomineralised by TiO_2 photocatalysis.

Class of Organics	Examples
Aliphatic alcohols	Methanol, ethanol, propanol, glucose
Aliphatic carboxylic acids	Formic, ethanoic, propanoic, oxalic, butyric, malic acids
Alkanes	Isobutane, pentane, heptane, cyclohexane, paraffins
Alkenes	Propene, cyclohexene
Amides	Benzamide
Aromatic carboxylic acids	Benzoic acid, 4-aminobenzoic, phthalic, salicylic, m- and p-hydroxybenzoic acids, chlorohydroxybenzoic and chlorobenzoic acids
Aromatics	Benzene, naphthalene
Dyes	methylene blue, rhodamine B, methyl orange and fluorescein.
Haloalkanes	Mono-, di-, tri- and tetrachloromethane, tribromoethane, 1,1,1-trifluoro-2,2,2 trichloroethane
Haloalkenes	1,2-dichloroethylene, 1,1,2-trichloroethylene
Haloaromatics	Chlorobenzene, 1,2-dichlorobenzene
Halophenols	2-, 3-, 4-chlorophenol, pentachlorophenol, 4-fluorophenol
Herbicides	atrazine, prometron, propetryne, bentazon, 2-4 D, monuron
Nitrohaloaromatics	Dichloronitrobenzene
Pesticides	DDT, parathion, lindane, tetrachlorvinphos, phenitrothion.
Phenolic compounds	Phenol, hydroquinone, catechol, methylcatechol, resorcinol, o- m-, p-cresol, nitrophenols
Polymers	Polyethylene, PVC
Surfactants	sodium dodecylsulphate, polyethylene glycol, sodium dodecyl benzene sulphonate, trimethyl phosphate, tetrabutylammmonium phosphate

Some examples of application of TiO_2 semiconductor photocatalysis in the destruction of organic pollutant and the key reaction conditions are presented in Table 2.5. The list is far from complete but careful choices of compounds have been made to include compounds from a variety of classes; under a variety of operational conditions.

Chen and Dionysiou (2006) concluded that photocatalytic activity depended largely on the structural properties and film thickness of the catalyst. On the other hand, findings by Doll and Frimmel (2005), on the effectiveness of two commercial titanium dioxide catalysts, indicate that the ultimate catalyst for photocatalysis could depend on the chemistry of the compound (Table 2.5). Combined contributions from diverse process parameters and a wide range of pollutants with different chemistries require laboratory scale kinetic studies for each pollutant type.

Table 2.5: List of some TiO_2 sensitized photodegraded compounds and key reaction conditions.

Pollutant	Catalyst Form	Radiation Source	Key Findings	Reference
4-chloroben-zoic acid	Transparent, dense TiO_2 film on stainless steel –prepared at different calcinations temperatures (400-600°C)	Four 15 W, integrally filtered low pressure mercury UV tubes.	Structural properties and film thickness affects photocatalytic activity. Reduction of calcinations temp. Improved activity significantly.	Chen and Dionysiou (2006)
Cyclopentene	Slurry (1 g/300 mL). Compared activity of eight (4 commercial, 4 prepared) TiO_2 catalyst.	250 W, vacuum Hg lamp.	Achieved above 50% degradation.	Kluson *et al.*, (2005)

Table 2.5: List of some TiO_2 sensitized photodegraded compounds and key reaction conditions - continued

Pollutant	Catalyst Form	Radiation Source	Key Findings	Reference
Pharmaceuticals	TiO_2 suspension (Hombikat UV100 and P25 Degussa)	Solar UV simulator (1000 W, Xe short arc lamp)	P25 more effective for clofibric acid, while Hombikat 100 was more effective for iomeprol degradation.	Doll and Frimmel (2005)
Formic acid	Immobilized TiO_2 (supported on glass beads) Packed bed reactor	15 W, UV lamp	Immobilization on large beads gave better degradation. Immobilized systems gave same degradation efficiency as slurry.	Dijkstra *et al.*, (2001)
4-Nitrophenol	Suspended TiO_2 catalyst. Optimum value of catalyst concentration of 4g/L with catalyst size of <70 µm	125 W high-pressure mercury lamp.	Higher degradation at pH of 3 than at 8.5.	Androzzi *et al.*, (2000)

Table 2.5: List of some TiO_2 sensitized photodegraded compounds and key reaction conditions – continued.

Pollutant	Catalyst Form	Radiation Source	Key Findings	Reference
Dyes	Suspended TiO_2 (3 g/L)	500 W super high pressure mercury lamp	Lowered pH increased degradation by about 21%. Lower concentration of acid orange dyes improved degradation rates. 75% removal achieved in about 60 min.	Tanaka *et al*., (2000)
Microcystin	Suspended TiO_2 slurry (1% m/v) of Degussa 25	280 W UVA spot 400 lamp (spectral output at 330-450 nm)	Noticed rapid destruction of microsytin to undetectable levels within 40-60 min.	Robertson *et al*., (1997)

Cleaning Effect of TiO_2 Coated Surfaces

Surfaces coated with titanium dioxide powder have been observed to have self-cleaning capacities when exposed to natural light especially when the materials are also exposed to rain as degraded substances on the surfaces can be washed away by rain. This has been observed with glass covers on highways and on tiles and is considered an additional practical application of titanium dioxide photocatalysis. Such materials are termed “photocatalytic building materials” and some have found commercial applications. One of the most notable

commercialized uses is the 20,000 m^2 exterior glass installed in the terminal building of Chubu International airport in Japan (Hashimoto *et al.*, 2005).

Degradation of toxic inorganic compounds

Due to the non-selective action of photocatalysis, it finds application beyond the degradation of organic species in water. Semiconductor photocatalysis has also found application in the degradation of toxic inorganic compounds to harmless or less toxic compounds, some examples are presented on Table 2.6. Thus semiconductor photocatalysis can be used to oxidize nitrite, sulphite and cyanide anions to form relatively harmless products, such as NO_3^-, SO_4^{2-} and CO_2 respectively as shown in Equations 2.19 – 2.21.

Table 2.6: TiO_2 sensitized photosystems for the removal of toxic inorganic compounds (Mills and Lee, 2004, Halmann 1996).

Overall Reaction	Equation Number
$A + D \xrightarrow{hv/TiO_2} A^- + D^+$	
$5O_2 + 6NH_3 \xrightarrow{hv/TiO_2} 2N_2 + N_2O + 9H_2O$	(2.18)
$O_2 + 2NO_2^- \xrightarrow{hv/TiO_2} 2NO_3^-$	(2.19)
$O_2 + 2SO_3^{2-} \xrightarrow{hv/TiO_2} 2SO_4^{2-}$	(2.20)
$2O_2 + H_2O + 2SO_3^{2-} \xrightarrow{hv/TiO_2} 2SO_4^{2-}$	(2.21)
$O_2 + 2CN^- \xrightarrow{hv/TiO_2} 2OCN^-$	(2.22)
$5O_2 + 4H^+ + 4CN^- \xrightarrow{hv/TiO_2} 2H_2O + 4CO_2 + 2N_2$	(2.23)
$2BrO_3^- \xrightarrow{hv/TiO_2} 2Br^- + 3O_2$	(2.24)
$HNO_3 + 6H^+ + 6e^- \xrightarrow{hv/TiO_2} NH_2OH + 2H_2O$	(2.25)

Bromate formation during ozonation of compounds containing bromide ions in water is a major concern with ozonation systems. With Titanium photocatalysis bromate ions in solution are decomposed to bromide and oxygen. The reactions involved are presented in Equation 2.24 (see Table 2.6). The ability to degrade bromate ions are of significant environmental advantage; due to growing concerns over its detection at environmentally significant levels in potable water that has been chlorinated (Mills and Lee, 2004).

Degradation of organo-metallic compounds

Semiconductor photocatalysis has also found application in the degradation of some organo-metallic compounds of serious environmental concern. Serious environmental hazard of spills of mercury and other heavy metals (particularly lead and cadmium) into natural waters is due to the formation of organo-metallic derivatives of the metals. Some of these organo-metallic compounds are extremely toxic. Examples of organo-metallic compounds that have been successfully degraded by semiconductor photocatalysis include mercurochrome, phenylmercury, tributyltin chloride (TBT), and bis(tributyltin) oxide (TBTO) amongst others (Halmann, 1996).

Treatment of oil spills

Oil spills are a major source of natural water pollution in oil producing regions and during transportation in high seas. Photocatalytic oxidation by sunlight of films of crude oil or of n-octane on fresh and seawater can be achieved by spreading titanium dioxide coated oleophilic glass microbubbles or beads on the polluted water surface. The possibility of a natural “self-cleaning” process has been predicted on the discovery of the photocatalytic degradation of crude oil residues in contact with beach sand on irradiation with a high-pressure mercury lamp. Photocatalytic activity of the beach sand was ascribed to the catalytic properties of magnetite and ilmenite contained in the beach sand (Halmann, 1996).

Destruction of biological species (bacteria and viruses)

In addition to the photomineralisation of organic, inorganic and organo-metallic compounds, photosensitized TiO_2 has also been effectively used for the destruction of microorganisms, such as bacteria, viruses and moulds. The photocatalytic destruction of biological material sensitized by semiconductor catalysts is generally referred to as photo-sterilization or photodisinfection (Mills and Lee, 2004).

2.7.7 Case studies

Semiconductor photocatalysis is yet to make the full transition from laboratory and pilot scale experiments to full scale application. The slow transition has limited the number of companies promoting semiconductor photocatalytic products. A limited number of case studies are available in literature compared to the volume of research that is being carried out. Most attempts at pilot scale studies have been focused on the treatment of pollutants from industrial effluents. There has been very limited application of photocatalysis in the treatment of surface water contaminants and in the drinking water treatment industry.

With recorded success of photocatalysis for the degradation of a seemingly endless list of recalcitrant organic compounds coupled with the ability to destroy microorganisms; photocatalysis could emerge in the nearest future as one stop alternative to disinfectant / treatment method in the potable water industry.

Despite its limited application outside laboratory studies, a few successes has been recorded in the area of surface and ground water remediation with photocatalysis. These include:

- Treatment of musty odour in Lake Biwa – Japan
- Contaminated surface water – Ontario, Canada
- Cleaning of groundwater contamination – Gainesville, Florida
- Oil Spill Clean-up in Japan
- Petrochemical waste site, Galveston, Texas, Texas

Treatment of musty odour in Lake Biwa – Japan

A flow through photoreactor packed with TiO_2 coated glass beads under illumination with black light at flow rates of 20-50 mL/min was developed in the laboratory to degrade 2-methyisoborneol (MIB). Concentration of MIB decreased to half of its initial value of 1 000 ng/L within a minute. The process was developed to degrade musty odour in Lake Biwa, Japan (Halmann, 1996).

Contaminated surface water – Ontario, Canada

The Photo-Cat system was installed to treat highly contaminated surface water with high levels of oil and grease which discharges into the Thames River. The system was used to treat 136.38 KL from three wells continuously on a daily basis. Contaminants include trichloroethene (TCE), dichloroethane (DCE), trichloroethane (TCE), vinylchloride, oil and grease all present in the low mg/L range in two wells and >1000 mg/L range in the third well. A low concentration of hydrogen peroxide was added as additional scavenger of photogenerated electrons to enhance overall efficiency of the system. The system is reported to have been operating since 1998 (Mills and Lee, 2004).

Cleaning of groundwater contamination – Gainesville, Florida

Clearwater Industries R2000 solar oxidation facility using a modular set of tilted flat-bed solar photoreactors, with dispersed TiO_2 photocatalyst was used to treat 500 gallons of underground water aquifer contaminated with benzene, toluene, ethyl benzene and xylene (BTEX). The R2000 system reduced BTEX to below the allowed level of 65 µg/L within 3 hours of use on a cloudy day (UV – light intensity ≅ 31 Wm^{-2}). This was compared to the use of activated carbon adsorption and trials with both systems showed that the R2000 photocatalytic system was significantly less expensive to install and operated at a fraction of the cost of the activated carbon system (Mills and Lee, 2004).

Oil spill clean-up in Japan

Degradation of a thin film of crude oil spilled on seawater was achieved by photocatalytic oxidation using TiO_2 coated microbubbles of 80 µm average diameter and 0.37 cm^{-3} density. The microbubbles stayed on the air-oil interface and promoted the initial very rapid photodegradation process of the oil with air as the oxidant. The microbubbles absorbed the oil forming oil-containing aggregates thereby leaving the water surface relatively clean. The microbubbles were reported to promote complete mineralization with destruction of intermediates at a weekly rate of about twice their weight of oil. Photoxidation eliminated both aliphatic and aromatic compounds including polycyclic aromatics. The clean-up process was reported to be accelerated by waves thereby proceeding even in high seas where skimming of oil spills is not praticable (Halmann, 1996).

Petrochemical waste site-Galveston, Texas, Texas

A 19-kW Photo-Cat system was used to reduce groundwater contaminants from 200 mg/L to 5 µg/L, in the presence of 6 000 mg/L of chloride ion. The 19-kW system was used to reduce the levels of 200 mg/L of bis(2-chloroethyl)ether to 20 µg/L. The unit was designed to operate at 15-30 L/min in fully automated mode (Mills and Lee, 2004).

With the recorded success of photocatalysis for the degradation of a seemingly endless list of recalcitrant organic compounds in the laboratory and the few reported cases for the treatment of organic compounds in surface water and groundwater, it is becoming an attractive choice for water treatment systems. The increased interest seems justified in light of enhanced awareness of the environmental implications of non-green processes; and a subsequent global shift to greener processes. This is in light of the fact that the photocatalytic process has the added advantage of being the only AOP system that can be classified as a completely green process. For the potable water industry, installation of a single system that could potentially degrade recalcitrant organic compounds and act as a disinfectant for the microbial population without the production of DBPs would be an added benefit.

CHAPTER THREE

MATERIALS AND METHODS

3.1 Chemicals and Reagents

All solvents used in this study were of either HPLC or GC grade. Acetonitrile (99.9% – BDH HiperSolv), dichloromethane (99.9% – BDH HiperSolv), phenol reagent (99.5 % – Saarchem, sodium chloride (99% – Saarchem); 2-chlorophenol (98% – Merck), 4-chlorophenol (98% – Merck), 4-nitrophenol (99% – Merck); and tertiary butanol (99.5% – Merck) were supplied by Merck, South Africa. Methanol (99.9% – HPLC grade) was purchased either from Merck, South Africa or from Waters, South Africa. Hexane (99% – Fluka) and phenol analytical standard (99.7% – Fluka) were purchased from Sigma Aldrich, Germany. Acetone (99.5% – Merck) and glacial acetic acid (100% – Merck) were purchased from Merck, Germany.

Taste and odour standards including, geosmin (99.8% – Supelco), 2-methylisoborneol (2-MIB) (99.9% – Supelco), 2,4,6-trichloroanisole (TCA) (99.1% – Supelco), 2-isopropyl-3-methoxypyrazine (IPMP) (99.9% – Supelco) and 2-isobutyl-3-methoxypyrazine (IBMP) (99.5% – Supelco); sodium azide (99.5% - Sigma), benzoquinone (99.5%), hydroquinone (99.5%), resorcinol (99.5%), and cathecol (99.6%); were purchased from Sigma Aldrich, Germany. Sodium chloride, sodium hydrogen carbonate (99% - UniVar, Saarchem), and anhydrous sodium sulphate (99% - UniVar, Saarchem) were obtained from Merck, South Africa. Taste and odour standards were purchased as 100 µg/mL solutions in methanol (1 mL). Anatase titanium dioxide powder (99.8% – Aldrich) was purchased from Sigma Aldrich, Germany. Ultra high purity helium gas (99.99%) was purchased from Afrox, South Africa.

All chemicals, with the exception of sodium chloride were used as received without further purification. Sodium chloride was dried in the oven at 105ºC for 3 hours and calcined in a muffle furnace at 540ºC for 12 hours, cooled to room temperature in a desiccator prior to use. All samples were prepared using ultrapure water from Milipore DirectQ_3 (0.05 µS/cm) (Millipore, USA; supplied by Microsep, South Africa).

3.2 Equipment

Long-arc 400 W, (Philips HOK 4/120 SE), medium pressure, and 9 W low pressure (Philips TUV PL-S 9W) UV lamps (Philips, Netherlands); were supplied by Technilamps, South Africa. Goldilux UV Smart Meters (Model GRP-1) equipped with UV-A, UV-B and UV-C probes (Goldilux, USA); were purchased from Measuring Instruments Technology (MIT), South Africa. The UV Meter and probes were calibrated at the National Metrology Institute of South Africa (NMISA). The crystallinity of anatase titanium dioxide powder was examined by XRD with a PANalytical Xpert-Pro diffractometer system equipped with an X'celerator detector (Netherlands). Surface morphology studies of titanium dioxide powders were done with Zeiss Ultra Plus SECSEM Scanning electron miscroscope (Germany).

The pH of sample solutions and variations in the pH of the reactor solutions during degradation were monitored with either an Orion3 Star portable pH Meter (Thermo Electron Corporation, USA); or an HQ11p portable pH Meter equipped with a temperature probe (HACH, USA, supplied by Aqualytic Environmental & Laboratory, South Africa). Dissolved oxygen measurements were obtained with an HACH HQ30d portable DO Meter, also equipped with a temperature probe (HACH, USA, supplied by Aqualytic Environmental & Laboratory, South Africa). Homogeneity of reactor contents was obtained by mixing with WiseStir MSH 30D magnetic stirrer (Wisd Laboratory Equipments, South Africa), equipped with a temperature probe for on line temperature monitoring. Temperatures of the reactor contents presented are average readings from the pH and DO meter readings. Air flow into the reactor for experiments that required aeration was controlled and measured with an air flow meter with capacity of 0-100 mL/min.

3.3 Properties of Experimental Reagents

Phenols are aromatic alcohols with an acidic proton. Phenol is very soluble in water making it highly mobile in surface and ground waters. Phenol is the most soluble of the four phenolic compounds under investigation and their relative decreasing order of solubility is phenol >> 4-chlorophenol (4-CP) >2-chlorophenol (2-CP) > 4-nitrophenol (4-NP). Some physical properties of phenol, the chloro- and nitro-derivatives of phenol (McMurry, 2012) are presented in Table 3.1

Table 3.1: Physicochemical properties of phenol, 2-chlorophenol, 4-chlorophenol and 4-nitrophenol.

Compound	Formula	FW	Melting Point (ºC)	Boiling Point (ºC)	pKa	*Solubility (g/100g)
Phenol	C_6H_5OH	94.11	43	182	10.00	9.48
2-chlorophenol	C_6H_4OHCl	128.56	8	175	-	2.04
4-chlorophenol	C_6H_4OHCl	128.56	43	220	9.38	2.77
4-nitrophenol	$C_6H_4OHNO_2$	139.11	115	279	7.16	1.34

Table 3.2: Physicochemical properties of taste and odour compounds.

Compound	Formula	FW	Melting Point (ºC)	Boiling Point (ºC)	Flash Point (ºC)
Geosmin	$C_{12}H_{22}O$	182.30	43	270	104
IBMP	$C_9H_{14}N_2O$	166.22	-	210.8	66.7 (80)
IPMP	$C_8H_{12}N_2O$	152.19	-	120-125	73
2-MIB	$C_{11}H_{20}O$	168.28	-	208.7	83.5
TCA	$C_7H_5Cl_3O$	211.47	60-62	132	-

3.4 Batch Experimental Setup

Photocatalytic degradation experiments were conducted in either of the two Pyrex® glass (Corning, NY) reactors. Reactor one consisted of 1000 mL capacity open double jacket reactor; with inner diameter of 95 cm, outer diameter of 130 cm and depth of 185 cm. The schematic of the reactor setup is presented in Figure 3.1 as configuration A. UV irradiation was provided by the 400 W medium pressure or 9 W low pressure UV lamps encased in quartz sleeves. Circulation of cooling water through the outer jacket of the reactor was not effective for cooling the reactor contents and reactor temperature sometimes rose above 30ºC which necessitated modification of the reactor configuration.

The setup of the modified reactor consisted of 2 L glass reactor (Pyrex® glass (Corning, NY); with the UV lamp enclosed in a double walled quartz sleeve. Temperature in the reactor was better controlled by circulating cooling water through the outer jacket of the double walled quartz sleeve. Schematic of the modified reactor is presented in Figure 3.1 as

configuration B. The reactor configuration was modified to improve temperature control in the reactor. The reactor contents were continually aerated at a flow rate of 10 mL/min with an air Flow Meter and a perforated quartz disc or a quartz rod. Dissolved oxygen (DO) was measured with an HQ30d DO Meter. Mixing of reactor contents was achieved with a WisD magnetic stirrer, stirring speed for all batches was set at 300 rpm.

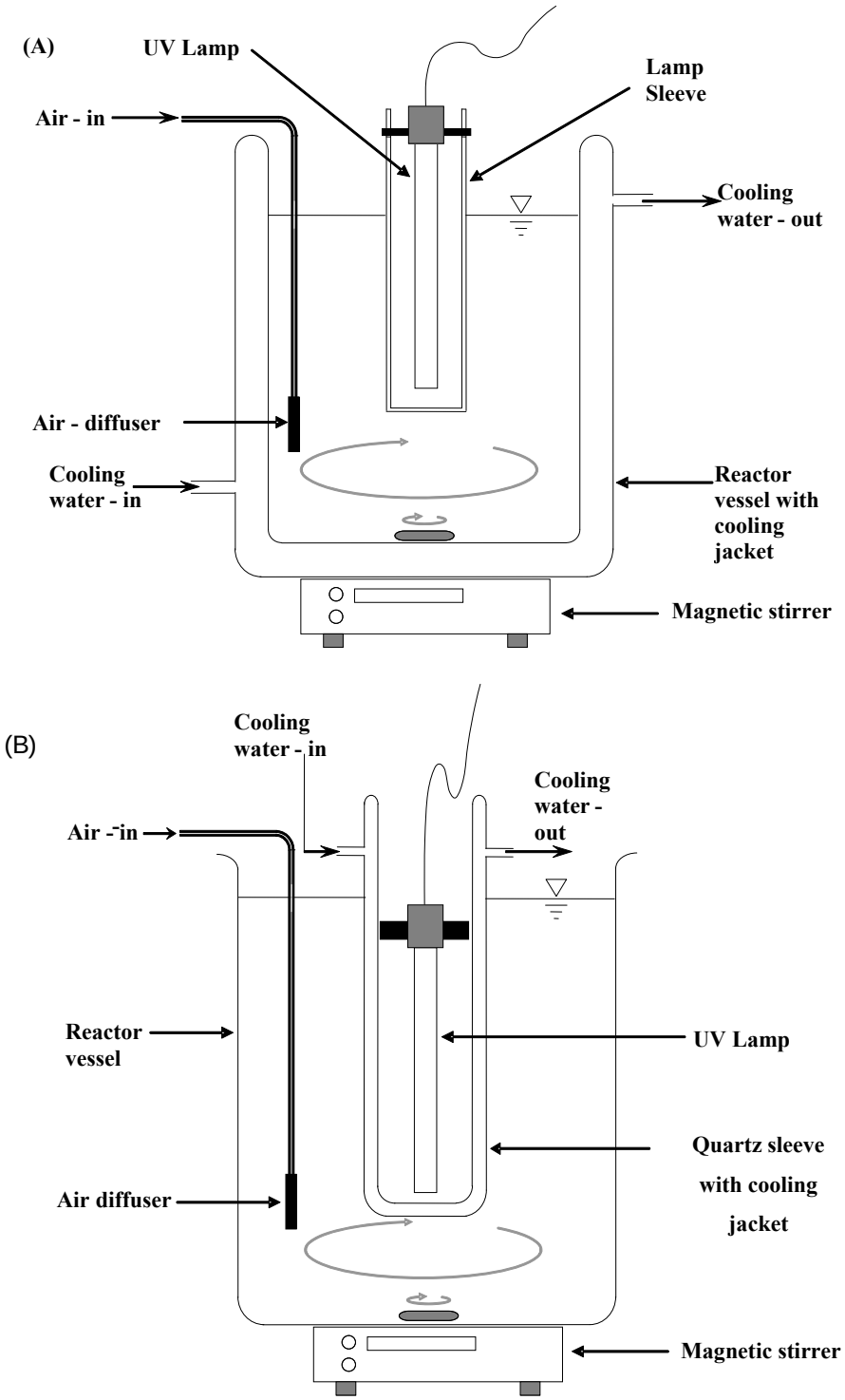

Figure 3.1: Schematics of experimental reactor setup - Configuration A and configuration B.

3.5 Reactor Startup

The reactor contents are loaded into the reactor usually starting with the catalyst (for batches containing the catalyst) and the pollutant solution. Air into the reactor is switched on after the addition of 1000 mL pollutant solution in the required concentrations, the circulation pump for the cooling water and the stirrer are switched on. The UV light and the timer are switched on simultaneously, as the time for the switching on of the UV light is recorded as the start time (time at zero minutes – T_o) of the each experimental batch. Some sets of reactions in each group were conducted in duplicate to assess the reproducibility of the experiments.

3.6 Collection of Water Samples

Water samples were collected from the Water Treatment plant at Rietvlei. Duplicate samples were collected at three sampling points, which are:

1. The inlet to the reservoir for source water from the dam;
2. The collection tank for filter backwash water from the DAFF filters and;
3. The collection tank for filter backwash water from the GAC filters.

Sampling was carried out between 12:30 and 13:00, immediately after the filters were backwashed and the backwash water drained into the collection tanks. Water samples were collected into 1 L Duran Schott short bottles that were filled without air space. Samples were pre-treated on site with 0.02 mg/L sodium azide and 20 mL/L methanol. Addition of sodium azide was to prevent microbial degradation of water samples during transportation to the laboratory and during storage of samples. Temperature, pH and the turbidity of the water were measured at the sampling site immediately after sample collection. Samples were transported to the laboratory in a cooler box packed with ice for chromatographic analysis.

Raw water samples were collected at Roodeplaat Treatment plant at the raw water inlet; and filter backwash water was collected at the outlet (point of discharge) of the filter backwash from the rapid sand filters. Sampling was carried out immediately after the filters were backwashed. On site pre-treatment with sodium azide and methanol as described earlier was

also done and samples were transported in ice cooled cooler boxes to the laboratory for chromatographic analysis. Samples were analysed as described in Section 3.7.

3.7 Analytical Methods

Characterisation/identification of organic compounds of dam water and monitoring of progress of degradation for goesmin was carried out by gas chromatographic analysis on a Perkin Elmer Clarus 600T gas chromatogram/mass spectrometer equipped with headspace sampler. The GC/MS comprised of Clarus 600T GC, Clarus 600T Mass spectrometer; and Turbomatrix 40 trap headspace sampler equipped with a trap for on line extraction and concentration of sample constituents.

Progress of degradation of phenol, 2-chlorophenol, 4-chlorophenol, 4-nitrophenol and the degradation intermediates obtained from the degradation of phenol was monitored on a Waters 2695Alliance high performance liquid chromatograph (HPLC). The Waters HPLC system is equipped with an autosampler with a capacity for 120 samples. Mobile phase system consists of a pump connected by four switching valves to four solvent reservoirs enabling the simultaneous use of four solvents in isocratic or gradient mode. Chromatographic separation of peaks was achieved on either Symmetry C_{18}, 150 mm x 3.9 mm, 5 µm column (supplied by Separations Scientific, South Africa) or Synergi 4U-Fusion RP Column. Separated peaks were detected on a photo diode array (Waters 2998 PDA) detector and Empower software (Waters, USA) was used for data acquisition and analysis.

3.7.1 Analysis of phenolics

HPLC analysis of the synthetic polluted water containing phenol, 2-chlorophenol, 4-chlorophenol or 4-nitrophenol as single pollutants in solution or as a mixture of pollutants; and their degradation products in solution were performed using EPA Method 604 with a Symmetry C_{18}, 150 mm x 3.9 mm, 5 µm column. Sample constituent separation and elution was achieved with a binary gradient mobile phase consisting of 1% acetic acid in water (Solvent A) and 1% acetic acid in acetonitrile (Solvent B) at a constant flow rate of 1.2 mL/min.

The mobile phase gradient was from 70% of Solvent A, 30% Solvent B at time zero; to 0% of Solvent A and 100% of Solvent B at 20 mins. Injection volume was 20 µL. Concentrations

of phenol and derivatives of phenol were obtained at 280 nm from calibration curves of standard solutions performed for each compound in solution. The list of phenolic compounds, the retention times in the HPLC chromatogram and their individual detection limits are presented in Table 3.3

Table 3.3: Detection limits for phenolic compounds.

Compound	Chemical Formula	Retention Time (min)	Detection Limit (µg/L)
Phenol	C_6H_5OH	4.445	3.50
Catechol	$C_6H_4(OH)_2$	2.869	4.50
Resorcinol	$C_6H_4(OH)_2$	2.268	3.70
Hydroquinone	$C_6H_4(OH)_2$	2.001	1.50
Benzoquinone	$C_6H_4O_2$	3.037	5.20
2-chlorophenol	$C_6H_4(OH)Cl$	6.316	6.20
4-chlorophenol	$C_6H_4(OH)Cl$	6.740	6.80
4-nitrophenol	$C_6H_4(OH)NO_2$	6.452	9.80

3.7.2 Trace analysis of organic compounds in water

The taste and odour causing compounds, geosmin and 2-MIB (target compounds) occur in the environment at very low levels and since some people can smell these compounds at concentrations as low as 10 ng/L (Sung *et al.*, 2005) it is imperative to identify these compounds at levels as low as 5 ng/L or lower. Analyses of taste and odour compounds were conducted at levels between 0.5 and 1000 ng/L with the Perkin Elmer turbo matrix headspace without pre-sample preparation. Analysis for taste and odour compounds including geosmin, 2-MIB, IBMP, IPMP and TCA were conducted with standards at 100 ppm. Trace analysis for geosmin and MIB were conducted with headspace at concentrations of 10-1000 ng/L in full scan (TIC) and single ion recording (SIR). Other volatile organic compounds (VOCs) and semi volatile organic compounds (SVOCs) in the water sample were obtained from the total ion chromatograms (TIC) of the water samples and the compounds in the chromatogram were tentatively identified by matching the electron impact spectra of the peaks with those in the NIST chemical database.

3.7.3 Analyses of taste and odour compounds

Gas chromatographic analysis for the identification of taste and odour compounds in water samples from Rietvlei and Roodeplaat Plants was carried out on the Clarus 600T GC/MS

from Perkin Elmer with modifications to methods reported by Sung and co-workers (Sung *et al.*, 2005); and Ikai and co-workers (Ikai *et al.*, 2003).

Analysis of Standards

Taste and odour standard solutions (geosmin, 2-MIB, IPMP, IBMP and TCA) were injected directly into the GC/MS as received without dilution or further treatment to obtain the retention times and mass spectra of the individual standards as a guide to the development of single ion recording (SIR) methods for subsequent trace analysis.

1 µL of each standard was introduced into the gas chromatograph by direct injection with the auto sampler with injector temperature of 250°C, and separated on a Perkin Elmer Elite-5MS capillary column (30 m x 0.25 mm, 0.5 µm film thickness). The oven was programmed at 40°C (3 min), 6°C /min to 150 (0 min), then 15°C/min to 250°C (0 min) with equilibration time of 0.5 min using helium as carrier gas at a flow rate of 1 mL/min, split injection was performed with a split ratio of 20:1.

A mass scan was performed in the mass range 35-350 amu, with PerkinElmer Clarus 600T mass spectrometer with multiplier voltage of 1350 V, transfer line temperature was set at 250°C and source temperature at 180°C, and solvent delay at 3.5 min. Scans were acquired at a scan time of 0.28 sec and inter-scan delay time of 0.02 sec, with an electron (trap) current of 75 µA. Data acquisition and interpretation was performed with TurboMass 5.0 software. The mass spectra of peaks of the standards were compared with the spectra of the compounds in the mass spectral data of NIST library database in the software.

3.7.4 Method development for headspace extraction and GC/MS analysis

Low concentration of taste and odour compounds in water always necessitates extraction and pre-concentration steps prior to gas chromatographic analysis. Extraction and pre-concentration of taste and odour compounds at trace levels has been either by the use of solid phase micro extraction (SPME) (Sung *et al*., 2005; Lawton *et al.*, 2003; Bao *et al*., 1997); or by solid phase extraction (SPE) (Ikai *et al*., 2003); prior to GC/MS analysis. In this study, analyses of taste and odour compounds were conducted at levels between 0.5 and 1000 ng/L with the Perkin Elmer Turbo Matrix Headspace (PE TMH) without SPE or SPME. The trap in the PE TMH equipped with a purging device allows on-line extraction and concentration

of organic constituents thereby eliminating the need for offline SPME or SPE processes. Trace analyses for geosmin and 2-MIB, were conducted with headspace at concentrations of 10-1000 ng/L in full scan mode; and 0.50-1000 ng/L, in single ion recording (SIR) mode.

Headspace extraction and sample introduction

Principles of Headspace Extraction

Dynamic headspace technique is a continuous method of extraction of volatile and semi volatile organic components from a sample matrix by continuous flow of an inert gas, which is coupled to a GC for automatic on line injection of extracted components onto the GC column. The sample (gas, solid or liquid) is placed in a sealed airtight headspace vial (Perkin Elmer, 2008) with sufficient gas volume above the sample matrix for equilibration of analyte components between the two phases. Analyte extraction in headspace involves thermostatting the sample matrix at a constant temperature until equilibrium of the two phases is achieved. The purged volatiles in the gas phase are then adsorbed on a trap for subsequent desorption onto a GC column (Kolb and Ettre, 2006). The Perkin Elmer HS 40/110 headspace sampler allows for 1 – 4 repeat extraction steps (called trap repeat cycles) for maximised analyte extraction onto the trap packing before desorption onto a GC column. Conditions during the extraction and concentration processes have to be the same throughout for all samples during a particular analysis for reproducibility of results especially for quantitative trace analysis.

Extraction Process

Sodium chloride was dried in the oven at 105°C for 3 hours, then baked in the furnace at 540°C for 12 hours; and cooled in a desiccator prior to use in head space vials to ensure complete elimination of moisture and trace organic contaminants from the sodium chloride salt. Solutions of the standards (0.5-1000 ng/L) were prepared in ultrapure water from the 100 mg/L standard of the taste and odour compounds. Ten millilitres (10 mL) of standard solution of the required concentration was transferred into a headspace vial, 3 g of sodium chloride was dissolved in the standard solution in the headspace vial; and the vials were sealed. The sealed vials were placed into the headspace autosampler for on line extraction as described below.

Key factors that affect the extraction efficiency of organic compounds in solution include:

- Thermostat time
- Oven temperature
- Trap temperature.

The trap temperature was set at a temperature range of 40-280°C for all samples. Samples were extracted at three different thermostat times with all other headspace conditions held at a constant. Thermostat times were varied from 20-60 minutes (20, 40, and 60 minutes). The effect of oven temperature on extraction efficiency was determined by extracting the sample solutions under varied oven temperatures at constant thermostat time and pressure settings. Oven temperature was set at 40, 60, 80 and 90°C.

Organic compounds in sealed headspace vials were extracted on the headspace with the optimum conditions obtained and introduced into the GC/MS for analysis through a 0.32 mm id. fused silica transfer line. Details of the optimum conditions obtained for headspace extraction of the analytes in the compounds under analysis are presented in Table 3.4 and details of the GC and MS conditions used for analysis are presented in Table 3.5.

Table 3.4: Headspace operating conditions for analysis of taste and odour compounds with the Clarus 600T GC/MS system.

Head Space Conditions	
Head Space Transfer Line	0.32 mm ID fused silica tube.
Temperature Settings	
Headspace Oven Temperature	80°C
Trap Temperature Gradient	40-280°C
Needle Temperature	95°C
Transfer Line Temperature	150°C
Pressure Settings	
Column Pressure	20 psi
Desorb Pressure	15 psi
Vial Pressure	30 psi
Timing	
Vial Pressurized Time	2 min
Trap Load Time	1 min
Dry Purge Time	5 min
Trap Hold Time	6 min
Trap Repeat Cycles	4 Cycles

Table 3.5: GC and MS operating conditions for analysis of taste and odour compounds with the Clarus 600T GC/MS system.

GC Conditions	
GC Column	Perkin Elmer Elite – 5MS capillary column
Column Dimensions	30 m x 0.25 mm (0.5 µm)
GC Oven Conditions	
Initial Oven temp.	40°C (3 min)
Ramp 1	6°C/min to 150°C
Ramp 2	15°C/min to 250°C
Carrier Gas	Helium
Flow Rate	1 mL/min
Split Ratio	20:1 (Direct injection)
MS Conditions	
Transfer Line Temperature	250°C
Source Temperature	180°C
Ionisation Mode	Electron impact (EI^+)
Electron Energy	70 eV
Mass Scan	35-350 amu
Scan Time	0.28 sec
Inter Scan delay	0.02 sec
Solvent Delay (Direct Injection)	3.5 min
Electron multiplier Voltage	1350 V (Direct injection – standards)
Electron multiplier Voltage	1500 V (Head space – trace analysis)
Database Library	NIST

The MS method for trace analysis of taste and odour compounds included five individual functions for SIR scans for each the five compounds. This was done to obtain scans for each compound in its own window without interference of peaks from other compounds. This serves to improve the sensitivity for identification of trace amounts of the compounds. The base peak and the next most prominent peak were chosen as qualifier ions for each compound, which were used as identification ions in the SIR scans. SIR scan functions, parameters and detection limits for each of the five taste and odour compounds are presented in Table 3.6a.

Table 3.6a: Parameters for SIR scan functions in the MS for target analytes.

Compound	**Function Number**	**Scan Time Window**	**Quantifier Ion**	**Qualifier Ions**	**Detection Limit (ng/L)**
IPMP	2	12.0-14.0	137	124, 152	0.55
IBMP	3	14.0-16.0	124	94, 151	0.35
2-MIB	4	15.0-18.5	95	108, 110	0.30
TCA	5	18.5-20.5	195	169, 210	0.40
Geosmin	6	20.5-24	112	55, 125 (or 150)	0.15

Table 3.6b: Parameters for SIR scan functions in the MS for target analytes for degradation studies of field samples.

Compound	Function Number	Scan Time Window	Quantifier Ion	Qualifier Ions
2-MIB	2	14.5-17.0	95	108, 110
Geosmin	3	20.0-21.5	112	55, 125 (or 150)
Geosmin	4	20.0-21.5	112	111, 149

3.8 Identification and Quantification of Taste and Odour Compounds

Current data on the prevailing levels of taste and odour compounds in raw water sources in Gauteng were not readily available. Screening of raw water sources to two major water treatment plants (Rietvlei and Roodeplaat Plants) around Pretoria was conducted to obtain the concentrations of geosmin and 2-MIB in the water sources. Screening was also conducted on the filter backwash water from the treatment plants to determine the extent to which these two compounds are retained by the filters. This would be a key factor in determining the suitability of these secondary water sources for recycle purposes. Detailed quantitative analysis of the taste and odour compounds gave an indication of the extent of retention of target organic compounds by the different filter types in the Treatment Plants. Maximum concentration of geosmin obtained from quantitative analyses was used as environmentally significant concentration for subsequent laboratory photocatalytic degradation studies.

3.8.1 Quantification of geosmin and 2-MIB

Taste and odour compounds, geosmin and 2-MIB were positively identified and quantified with analytic standards. Geosmin and 2-MIB were quantified by single ion recording (SIR) scans from linear calibration curves of the individual environmental standards. The values obtained for the geosmin and 2-MIB in the water samples from Rietvlei and Roodeplaat treatment plants are presented in Tables 4.2 and 4.3 respectively.

3.9 Characterisation of Anatase Titanium Dioxide Powder

Anatase titanium dioxide powder used for photocatalytic degradation studies was characterised by x-ray diffractometry (XRD) analysis; and by high resolution scanning electron microscopy (SEM)

3.9.1 X-ray diffractometry analysis of anatase titanium dioxide powder

Crystallinity of anatase titanium dioxide powdered was examined by XRD with a PANalytical Xpert-Pro diffractometer system equipped with an X'celerator detector; and variable divergence and receiving slits with Fe filtered Co-Kα radiation. Anatase titanium dioxide powder was prepared for XRD analysis using the back loading preparation method. XRD analysis was performed with the detector in continuous scan mode operating at 35 kV and 50 mA; and 2θ in the range of 5°-90°. The phases were identified using X'Pert Highscore

plus software. The semi quantitative phase amounts (as percentages by weight) were estimated using the Reference Intensity Method in the X'Pert Highscore plus software. Amorphous phases, if present, were not taken into account in the quantification. The x-ray diffraction pattern of anatase titanium dioxide used for the study is presented in Figure 3.2. X-ray diffraction patterns from Figure 3.2 show that the TiO_2 powder has predominantly 94% anatase phase and 6% rutile phase with no brookite present.

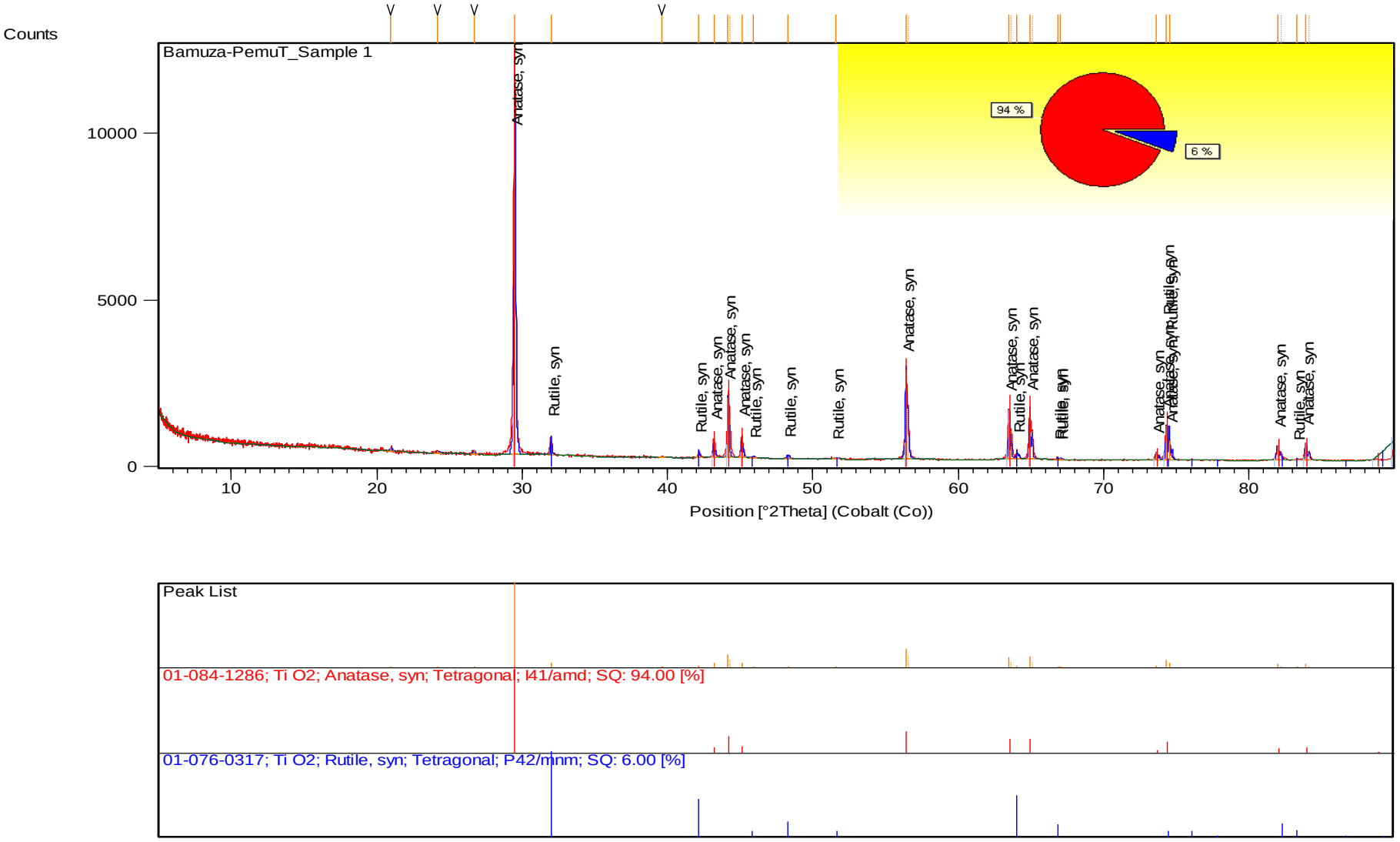

Figure 3.2: X-ray diffraction pattern of anatase titanium dioxide powder.

3.9.2 Surface morphology of anatase titanium dioxide powder

High resolution SEM images of the anatase titanium dioxide powder were obtained with Zeiss Ultra Plus SECSEM electron microscope operated at 0.5 kV. Images were taken at low and high resolution of 10,000 and 30,000 magnifications respectively. Titanium dioxide sample was prepared for SEM by first coating the powder on a carbon tape; the coated tapes were dried in the oven at 60°C for 8 minutes and finally a carbon coat was applied over the titanium dioxide powder. The SEM images are presented in Figure 3.3

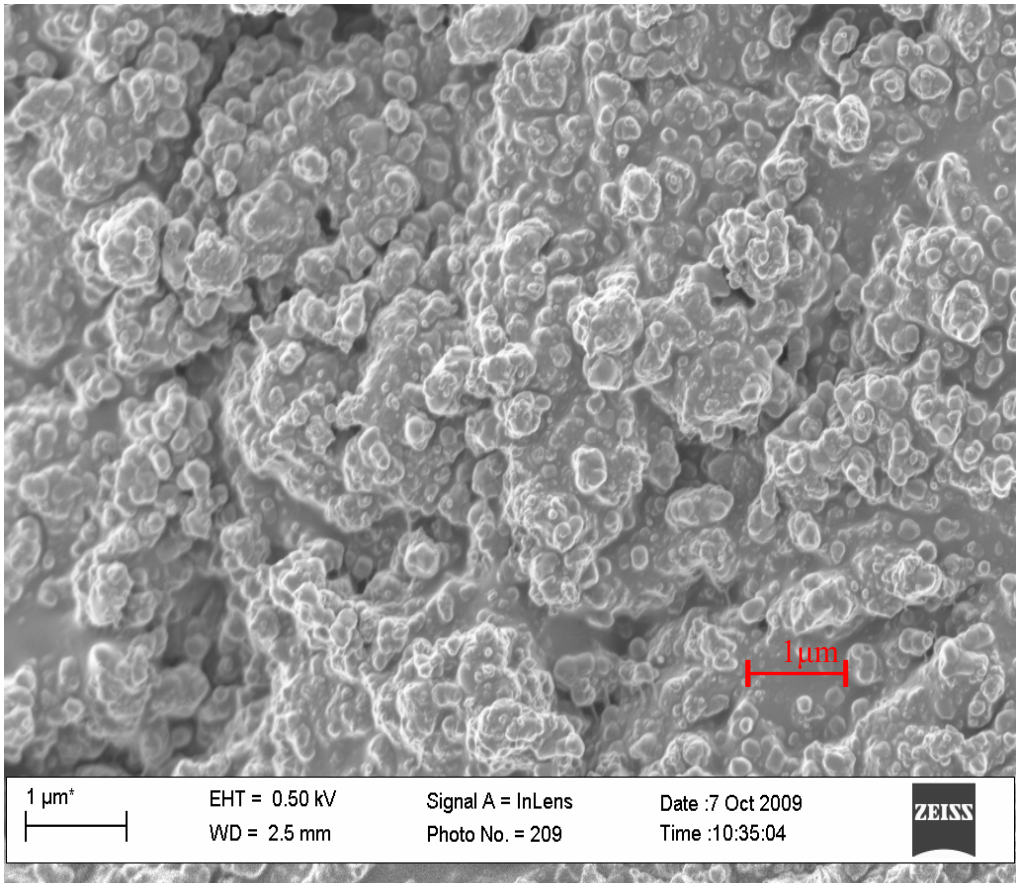

Figure 3.3: SEM image of anatase TiO_2 showing particle size distribution.

Titanium dioxide powder used for the photocatalytic degradation studies has mainly tetragonal crystal structure with 94% anatase and 6% rutile as shown by x-ray diffraction pattern (Figure 3.2), with non-uniform particle sizes less than 0.5 µm (Figure 3.3).

3.9.3 Actinometric measurements

The UV radiance emitted in the reactor system and transferred to pollutant components in solution is a key component which provides a measure of the efficiency of a photocatalytic system. The amount of radiation emitted by the UV lamps (UVA, UVB and UVC) and transferred into the reactant solution was determined for the both UV lamps with a Goldilux UV Smart Meter (Model GRP-1), with UVA, UVB and UVC probes used for each of the three regions (UVA, UVB and UVC). Measurements were obtained with the UV lamp placed in the centre of the reactor; in a closed metal box for maximization of photons produced. UV radiation was measured with the UV probes placed on the outside of the reactor wall**:**

- With an empty reactor and UV sleeve (Reactor configuration A)
- Empty reactor and UV sleeve with water circulating through outer jacket of the sleeve (Reactor configuration B).

The properties of the two UV lamps used for the study are presented in Table 3.7 and 3.8. The lamp wattage and voltage as presented in Table 3.7 are values supplied by the manufactures. UV radiation values obtained from laboratory measurements during the course of the study are presented in Table 3.8

Table 3.7: Physical and electrical properties of radiation sources.

Lamp Type	Length (mm)	Width (mm)	Lamp Wattage (W)				Voltage (V)
			Elect	UVA	UVB	UVC	
400 W	110	16	400	31	32	52	125
9 W	167	28	9	1.90	0.75	2.40	60

Table 3.8: Radiation properties of light sources.

Lamp Type	UV Radiation (n = 5)		
	UVA (mW/cm^2)	UVB(mW/cm^2)	UVC ($\mu W/cm^2$)
(a) With Empty Sleeve			
400 W	34.81 ± 0.50	13.98 ± 0.06	599.24 ± 0.38
9 W**	1650 ± 2.55	14.35 ± 0.03	15.20 ± 0.02
(b) With Water Circulating Through the UV Lamp Sleeve			
400 W	33.65 ± 0.07	11.59 ± 0.01	431.28 ±0.16
9 W**	1326.14 ± 3.83	9.82 ± 0.06	9.61 ± 0.02

** Values for 9 W lamp are in $\mu W/cm^2$

Organic compounds identified by chromatographic analyses of source waters are listed in Table 4.1 and the classes of compounds are discussed. The properties and morphology of the catalyst used are presented in Chapter 4. The properties of the UV lamps as supplied by the producers and obtained from the actinometry measurements are presented in Table 3.8

CHAPTER FOUR

ASSESSING THE IMPACT OF ALGAL INFESTATION ON THE ORGANIC COMPOUND MATRIX OF SOURCE WATER

4.1 Evaluation of Natural Organic Matters in Source Waters

Suitability of a water source for potable use is usually judged based on its tactile quality (i.e., clarity, smell and taste). A common problem that has emerged in most water resources is the increase in aromatic and polar organic compounds in source waters (Sproul and Ryckman, 1961; Sibali *et al*., 2010). This comes as a result of increasing pollution loading to water bodies from industrial and agricultural sources (Griffini *et al*., 1999). Furthermore, large nutrient inputs have been linked to algal infestation in natural water bodies resulting in high incidence of offensive algal metabolites and humic substances. On the backdrop of the level of algal infestation in dams in South Africa, an evaluation of source waters from Rietvlei and Roodeplaat water treatment plants near Pretoria, South Africa; was conducted to qualitatively characterise the organic compound matrix of the source waters and the filter backwash waters from the treatment plants. Detailed gas chromatographic analysis was performed as described in Sections 3.7.2 – 3.7.4 to identify the constituent organic pollutants in the water.

4.2 Predominant Organic Compounds Identified in Water Samples

Forty-two VOCs and SVOCs belonging to ten different classes of compounds were qualitatively identified during GC/MS analysis of the water samples from filter backwash water and source waters Rietvlei and Roodeplaat Water Treatment Works. The list of organic compounds of environmental significance that were identified during the chromatographic analysis is presented in Table 4.1; other organic compounds also identified are listed in Table A1in Appendix A. Organic compounds in water samples were qualitatively identified by mass spectral comparison with compounds in the spectral database in the Turbomass software from the inbuilt library of chemical compounds. This was achieved by comparing the peak distribution in the mass spectra of the unknown compounds in the water samples with the peaks in the spectra of similar compounds in the NIST Library.

Table 4.1: List of environmentally significant organic compounds tentatively identified in water samples from Rietvlei and Roodeplaat dams.

S / No.	t_R (min)	Name of Compound (Formula)	Fit	Reverse Fit
A		Taste and Odour Compounds		
1**	22.69	Geosmin ($C_{12}H_{20}O$)	662	778
2**	16.93	2-Methylisoborneol (MIB) ($C_{11}H_{20}O$)	636	654
B		Phenols		
1	21.29	2-(1,1-dimethylethyl)-5-methylPhenol ($C_{11}H_{16}O$)	481	607
2	23.65	2,6-bis[1,1-dimethylethyl]-4-methylphenol also known as Butylated hydroxytoluene ($C_{15}H_{24}O$)	879	886
		Polycyclic Aromatic Compounds		
1	17.42	Naphthalene ($C_{10}H_8$)	675	810
2	22.05	2-ethenylnaphthalene	794	838
3	23.20	2-(1,-methylethyl)naphthalene ($C_{13}H_{14}$)	441	681
		Quinones		
1	23.20	2,5-di-tert-butyl-1,4-benzoquinone ($C_{14}H_{20}O_2$)	695	722
		Carbonyl compounds – Aldehydes and Ketones		
1	15.07	Nonanal ($C_9H_{18}O$)	693	829
2	12.06	2-octanone ($C_8H_{16}O$)	883	889
3***	14.31	Acetophenone	718	891
4	16.94	3,4,5,6,7,8-hexahydro-4a,8a-dimethyl-1 H-Naphthalen-2-one ($C_{12}H_{20}O$)	700	725
		s-Triazine Herbicides		
1	32.36	Atrazine		

** Positively identified with standards (Fit parameters from TIC of standards) and retention times.

*** Detected in DAFF and GAC backwash water only

The peak fitting by the software was conducted to obtain forward and reverse fit values (in a scale of 1 to 1000). The most probable compound for each peak was chosen from the generated list of likely compounds using both peak fit and reverse fit parameter of 500 and above. The compounds, the individual retention times (t_R) in the TIC and the NIST library match parameters are presented in Table 4.1. The mass spectra of the analytes in the water samples and the spectrum of the corresponding compounds from the NIST library match of some selected compounds are presented as head to tail spectra in Appendix A. The identified compounds are discussed grouped into the different classes of compounds and by known applications.

4.3 Classes of Compounds

Compounds in Tables 4.1 and A1 are listed according to their different classes of organic compounds into ten different types as follows:

- Taste and odour compounds (Geosmin and 2-MIB)
- Phenolic compounds (Phenols)
- Polycyclic aromatic hydrocarbons (PAHs)
- Quinones
- Carbonyl compounds – ketones and aldehydes
- s-triazine-ring herbicide
- Acid esters
- Indene
- Alcohols
- Hydrocarbons – alkanes and alkenes

4.3.1 Taste and odour compounds (geosmin and 2-MIB)

Taste and odour causing compounds when present in water even in very low concentrations are considered offensive to the senses due to the low human threshold and are a source of concern to the water industry. Five taste and odour causing compounds including geosmin, 2-MIB, TCA, IBMP and IPMP; were tested for in the water samples as described in Section 3.7.4 with SIR scans using parameters listed in Table 3.5A. Only geosmin and 2-MIB of the five taste and odour compounds tested were detected in the source water samples from

Rietvlei and Roodeplaat water treatment plants. Quantification of geosmin and 2-MIB from the source water and filter backwash water samples as described in Section 3.8.1revealed that both compounds occur at concentrations above the human detection threshold of below 6 ng/L (Young *et al*., 1996; Lloyd *et al*., 1998). Other taste and odour causing compounds IPMP, IBMP and TCA were not detected in any of the water samples tested during the period of analysis. Geosmin concentrations of 125 ng/L and 74 ng/L were identified in Roodeplaat and Rietvlei source waters respectively (Table 4.2).

Higher values of geosmin were recorded in the filter backwash samples than those from the source waters. Geosmin concentrations of 221 ng/L and 88 ng/L were obtained from backwash water from the DAFF and GAC filters respectively (Table 4.2). Higher values of geosmin in the filter backwash water samples indicate that organic compounds are filtered out of the water and retained on the filters during the filtration process. The compounds retained on the filters are subsequently dislodged from the filters during the backwash process. Retention of organic compounds on the filters was calculated using Equation 4.1:

$$\text{Retention (\%)} = \left(\frac{[C_b]-[C_i]}{[C_i]}\right)\times 100 \quad \text{..... (4.1)}$$

Where:

$[C_i]$ is the concentration of the organic compound in the inlet water
$[C_b]$ is the concentration of the organic compound in the filter backwash water

Retention was most prominent in the DAFF filters both for geosmin recording 276%. Backwash water from GAC filters showed lower retention for geosmin (14-167%). This is an indication that DAFF filters are more efficient in filtering off taste and odour compounds. Records of length of use of activated carbon media and regeneration times were not collected at the time of sample collection, so the length of time the GAC filter materials have been in use was not available. This can impact on the performance of GAC filters as the efficiency of filtration will depend directly on available surface area of filter media. Retention of geosmin in the sand filters of the Roodeplaat treatment plant was not observed in the samples analysed during this study, as the geosmin concentrations were either the same in both inlet and backwash water (November 2009), or lower in the backwash water (August 2009).

Table 4.2: Geosmin concentration in water samples from Rietvlei and Roodeplaat water treatment plants.

Sample	Geosmin Concentration (ng/L)			
	Jan 2009	May 2009	Aug 2009	Nov 2009
Rietvlei Raw	71	74 ± 3	NA	3 ± 0
Rietvlei DAFF	89	221 ± 2	30 ± 1	10 ± 3
Rietvlei GAC	81	88 ± 36	29 ± 1	8 ± 1
Roodeplaat Raw	NA	125	28 ± 1	NA
Roodeplaat Backwash	NA	111	28 ± 0	NA

Concentrations of 2-MIB obtained from water samples from both sources was also above the human detection threshold of below 10 ng/L (Young *et al*., 1996; Lloyd *et al*., 1998). MIB concentrations of 151 ng/L and 91 ng/L were obtained from the source waters of Roodeplaat and Rietvlei respectively (Table 4.3). No retention of MIB was observed with the GAC filters as the concentration of MIB remained unchanged from 91 ng/L as in Rietvlei source water but an increase to 182 ng/L was observed from DAFF filters. MIB concentration increased from 151 ng/L in Roodeplaat source waters to 194 ng/L in filter backwash water from the sand filters.

Table 4.3: 2-MIB concentration in water samples from Rietvlei and Roodeplaat water treatment plants.

Sample	2-MIB Concentration (ng/L)			
	Jan 2009	May 2009	Aug 2009	Nov 2009
Rietvlei Raw	NA	91 ± 6	NA	5 ± 0
Rietvlei DAFF	NA	182 ± 59	NA	26 ± 2
Rietvlei GAC	NA	91 ± 1	NA	0.50 ± 0
Roodeplaat Raw	NA	151	NA	NA
Roodeplaat Backwash	NA	194	NA	NA

NA – Not available

South Africa has no clear sensory quality standards with regards to taste and odour; instead the term "not objectionable" has been previously used (Pieterse, 1989; Le Roux, 1988). Although South Africa has no clear sensory quality standards for taste and odour in potable water, consumer complaints resulted in a survey of water bodies in South Africa in the early 1990's. The survey conducted by Wnorowski (1992) on South African water bodies revealed that 30% of the water bodies examined had odour problems and 50% of these problems were attributed to geosmin. Odour problems in water in South Africa have not been completely eliminated since the survey with recurring incidences especially in summer months. The situation has grown worse over the years with one of the worst cases in recent years experienced by Rand Water between September and November 2005, where high cyanobacteria concentrations in the source water resulted in high concentrations of geosmin in drinking water with a resultant consumer rejection (Swanepoel and Preez, 2006).

Various municipalities have on different occasions found the need to educate and placate the consumers on the occurrence of taste and odour in their drinking water. The City of Tshwane in its Water Quality document explained to the Residents of Pretoria North suburbs that taste and odour problems in their tap water are due to the presence of geosmin formed due to an increase in algal biomass in the Roodeplaat Dam. The water treatment plant has included a treatment step to remove these odours and the levels are being continuously monitored. The City of Cape Town had a widely reported (SABC News) case of taste and odour in the drinking water during the weeks of February, 2012 due to blue-green algal bloom in both the Theewaterskloof and Voëlvlei Dams. The City on its part sent out a detailed press release to re-instil consumer confidence. Both the City of Cape Town and the City of Tshwane have been reported to comply with the Blue Drop standards and are very highly rated.

4.3.2 Phenols

Two phenol derivatives; 2-(1,1-dimethylethyl)-5-methylphenol and 2,6-bis[1,1-dimethylethyl]-4-methylphenol (butylated hydroxyltoluene) commonly used as preservatives and antioxidants (Eriksson *et al*., 2003) were identified in water samples from the raw water inlet and filter backwash water from both sources**.** Phenols are classified as water pollutants with MCL of 0.5 µg/L set by the European Community Directive (1980), and a U.S.EPA limit of 1 mg/L (U.S.EPA, 2009, Steiner *et al*., 2008) in drinking water. The ingestion of a concentrated solution of phenol could cause severe pain and shock leading to renal damage,

circulatory collapse and eventual death. The fatal dose is of the order of 1500 mg (DWAF, 1996). Though specific limits are not stated in the South African domestic water quality standards (SA DWQS), the range 0-1 mg/L is listed as suitable for long term intake (DWAF, 1996). Notably, the SA DWQS gives reference to the toxic concentration of 3 mg/L as assigned for phenol by the World Health Organisation (WHO) in 1984.

The SA DWQS suggests oxidation for the treatment of phenols as they are not effectively removed from water using conventional water treatment techniques, and discourages the use of chlorine in treating water polluted with phenol due to the strong tendency of formation of chlorophenols as disinfection by-products (DWAF, 1996). Additionally, phenols are prone to partial degradation resulting in the formation of acetates and other short-chain fatty acids that readily combine with chlorine to form haloacetic acids (HAAs) in water (Chirwa and Bamuza-Pemu, 2010).

Butylated hydroxyltoluene can be classified as a phenol and a toluene. Potential health effects from toluene ingestion include nervous system, kidney or liver problems and the U.S.EPA has set the MCL and MCLG for toluene at 1 mg/L (U.S.EPA, 2009).

4.3.3 Polycyclic aromatic hydrocarbons

The data from source water samples from both Rietvlei and Roodeplaat show the presence of at least three PAH compounds, i.e, naphthalene, 2-ethenylnaphthalene and 2-(1-methylethyl) naphthalene. Potential health risks associated with PAHs include reproductive difficulties and carcinogenity (U.S.EPA, 2009). PAHs are of serious environmental concern because they are microbially recalcitrant and have high bioaccumulation potential (Martens and Frankenberger, 1995); and are toxic, having mutagenic and carcinogenic properties (Maila and Cloete 2002). PAHs are resistant to conventional oxidation and biodegrade slowly; requiring 60 days for complete degradation of naphthalene under natural conditions. Up to 120 days may be required to achieve 5-87% degradation for higher molecular weight PAHs (Ashok *et al*., 1995). Photocatalytic degradation is suggested as faster process for treatment of such compounds to enhance their removal from water and reduce the chances of their build up in the treatment train. Presence of PAHs in source waters could also result in the formation DBPs from breakdown products on chlorination.

PAHs pollution is usually related to industrial sources and especially the petroleum and the petrochemical industries and from vehicle exhaust fumes (Bacaloni *et al.*, 2004; Maila and Cloete, 2002). Their presence in source waters of the Rietvlei and Roodeplaat Water Treatment Works cannot be attributed to boating activities Rietvlei dam is home to a sailing club and use of motor boats is restricted to rescue operations only. It is suspected that their presence is largely from PAHs in the air from coal burning and from heavy industrial activities from the Kempton Park area.

4.3.4 Carbonyl Compounds

Carbonyl compounds may contribute to taste and odour problems in the water. Up to four carbonyl compounds including 2-octanone and acetophenone (Table 4.1) were identified in the source water samples. Accumulation of these compounds in the treatment train could exercabate the problems caused by the taste and odour compounds such as geosmin and 2-MIB as described earlier in this section. The South African DWAF has threshold concentration of 0.5 mg/L for acetophenone for tainting of organism flesh in water (DWAF 1995). It is classified as a group D compound by the US Environmental Protection Agency (U.S.EPA, 2000). Acetophenone was detected only in the backwash water from the DAFF and GAC filters. This could be due to the retention and concentration of the compound in the filters during the process of filtration.

3,4,5,6,7,8-hexahydro-4a,8a-dimethyl-1-H-naphthalen-2-one is often used as a precursor or an intermediate in the laboratory preparation of geosmin (Saito *et al*., 1996, Hansson *et al*., 1990) and might be a degradation product (intermediate) in the process of natural degradation of geosmin in surface water samples.

4.3.5 Acid Esters

Four acid esters were identified in the water samples. These include three short chain acid esters (C_3 – C_4) and one long chain fatty acid (C_{18}). The short chain acid esters include propanoic acid; 2-methyl-2,2-dimethyl-1-[2-hydroxylmethyl]propylester (MDHP), propanoic acid, 2-methyl-1-[1,1-dimethyl]-2-methyl-3-propanediylester (MDMP) and butanoic acid, methyl ester. The only long chain fatty acid identified in all the water samples is octadecanoic acid, ethenylester.

Esters have distinctive fruit-like odours, and are commonly used in artificial flavourings and fragrances; and widely used as chemical additives in plasticisers. Due to their various applications they have been identified in diverse environmental samples including groundwater, river water, drinking water, open ocean water, soil, lake and marine sediments (Jianlong *et al*., 2004). Though methyl esters in the range of C_8-C_{18} are believed to be non-toxic, their presence in water could contribute to taste and odour in the water. Higher molecular weight acid esters could be health hazards as recent research suggests that women have a unique exposure profile to phthalates, which raises concern about the potential health hazards posed by such exposures (Lovekamp-Swan and Davis, 2003).

4.3.6 s-Triazine-ring herbicide (Atrazine)

GC/MS analysis of SPE extracts of water samples from the Rietvlei Treatment Plant revealed the presence of a very weak atrazine peak only in the raw water and the DAFF backwash water samples. Atrazine was not detected in the GC spectrum of filter backwash water from the GAC filters. This could be due to the adsorption of organic compounds on the surface of activated carbon. Atrazine was not detected in samples analysed on the headspace GC/MS system. This could be due either to its existence at concentrations close to the lower detection limits, or due to the limitation of the use of headspace for the extraction of sufficiently volatilisable compounds with boiling points below 280°C.

Atrazine is an s-triazine-ring herbicide commonly discharged in industrial effluents and as runoff from agriculture land. The U.S.EPA has set a 3 µg/L limit for atrazine. Research has linked abnormal sexual developments in frogs to exposure to atrazine (Sanders, 2002). Though the use of atrazine on heavy clay soils was withdrawn in 1977 in South Africa and the industrial use of atrazine was withdrawn on 31 March 1995, no strong measures have been put in place to enforce the ban. In a study of residual amounts of atrazine, Tshipala (2000) reported levels of 3-20 µg/L in South African surface waters and 0.29-4.36 µg/L in ground waters indicating its continued use. The detection of atrazine in source water samples from the Rietvlei dam indicates that it could be as a result of runoffs from farm lands around the dam.

4.3.7 Alcohols and hydrocarbons

Alcohols identified in the samples include 2-propylcyclohexanol and 2,2,3,3-tetramethylcyclopropanemethanol. A majority (20) of the compounds identified are straight and branched chains hydrocarbons (paraffins) ranging from C_6-C_{10} (Table A1). These are major components of fractionation products of petrol and from burning of coal and are common air pollutants. There is no reported health or environmental hazards associated with alcohols and lower molecular weight hydrocarbons but their presence in water samples going into the water treatment train could result in the formation of DBPs after chlorination.

4.4 Degradation Studies

Photocatalytic and photolytic studies were conducted on compounds chosen to represent classes of organic compounds identified in source waters listed on Table 4.1. Phenol, a very common water pollutant was chosen to represent aromatic compounds and geosmin was chosen to represent volatile, common taste and odour causing compounds. Laboratory scale experiments were conducted using these model compounds and the results obtained are discussed in Chapter 5 for phenol and phenolic compounds and Chapter 6 for geosmin.

Preliminary studies were conducted to test the effect of light intensity on degradation efficiency of geosmin by treating environmentally significant concentration of geosmin (220 ng/L) with both the low pressure 9 W UV lamp and the medium pressure 400 W UV lamp using TiO_2 concentration of 40 mg/L. Under these conditions, geosmin was rapidly degraded by photocatalysis with the medium pressure lamp achieving 95.8% removal in 60 minutes. The low pressure lamp under the same reaction conditions achieved only 49.6% removal after 60 minutes of treatment. Photocatalytic degradation results indicate a direct relationship between the degradation rates and the UV light intensity with improved degradation on increasing the photonic input from 1326 $\mu W/cm^2$ (9 W UV lamp) to 33.65 mW/cm^2 (400 W UV lamp) (Figures 4.1).

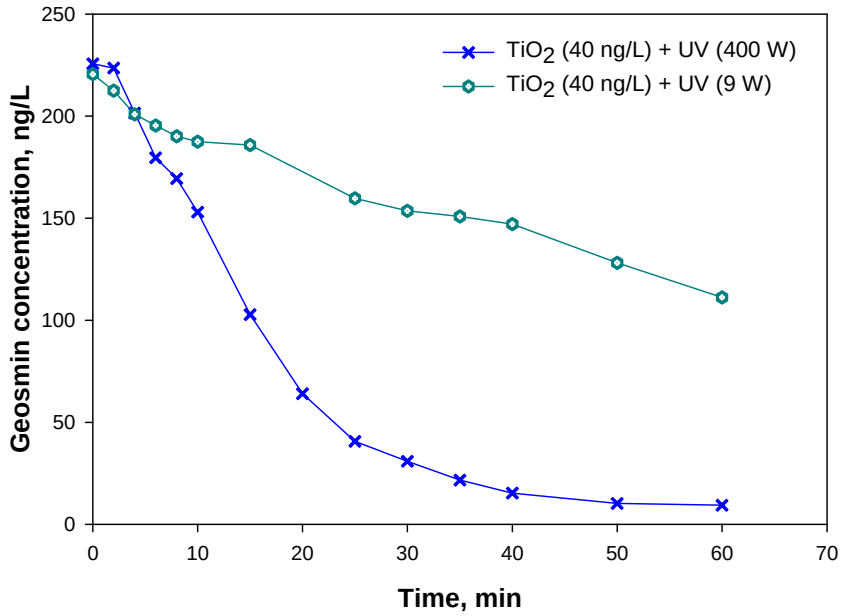

Figure 4.1: Effect of light intensity on the kinetics of geosmin degradation.

The increase in rates from 1.03 to 6.21 ng/(L.min) is however not an adequate reflection of the increase in photonic input. This could be due to higher photonic efficiency of the low pressure lamp with most of its spectral output below 400 nm. For practical purposes a balance between the cost of increased radiation intensity and improvement on degradation rates would be a key factor in the choice of a radiation source.

Geosmin levels below human detection threshold were readily obtained with the medium pressure lamp photocatalytic system. Based on the superior performance of the medium pressure lamp, further experiments to optimise the catalyst concentration were performed with the medium pressure lamp.

CHAPTER FIVE

PHOTOCATALYTIC AND PHOTOLYTIC DEGRADATION OF PHENOLIC COMPOUNDS

5.1 Motivation for Study of Phenolics

Results from analysis of source waters from the treatment plants showed the presence of several aromatic compounds including phenolic compounds and PAHs (Table 4.1). Among the aromatic groups, the congeners of benzene and their oxidised and halogenated forms are widely disposed to natural waters from agricultural and industrial sources (Barakat *et al*., 2005). Due to a wide variety of uses of phenolic compounds, their incidence in source waters is very common especially in areas near human settlements. Additionally, natural organic materials (NOMs) such as humic acid and fulvic acid can degrade partially into phenolic and aliphatic products, which readily form halogenated products such as chlorophenols (CPs), haloacetic acids (HAAs) and trihalomethanes (THMs) during chlorination of the water (Johnstone, 2009). Phenol was chosen as a model organic pollutant to represent the group of aromatic organic compounds identified during chromatographic analysis for photocatalytic study. Photocatalytic degradation of three derivatives of phenol (2-chlorophenol, 4-chlorophenol and nitrophenol) was also studied to ascertain the effect of substituent groups on degradation of aromatic compounds. Geosmin (cyanobacterial metabolite) was chosen as a model compound to represent the taste and odour compounds as the levels of both geosmin and 2-MIB obtained during analysis was higher than the human detection threshold (Table 4.2 and 4.3).

Research has shown the effectiveness of photocatalysis for the degradation (and sometimes the mineralisation) of a variety of organic compounds. The chapter evaluates the effectiveness of the photolytic and photocatalytic systems developed for degrading solutions of phenol and three derivatives of phenol including nitrophenol, 2-chlorophenol and 4-chlorophenol. The structures of the phenol and the chloro- and nitro derivatives of phenol are presented in Figure 2.2.

Photolysis and photocatalysis of phenol was conducted without aeration and the effect of oxygen on the system was evaluated by degradation studies in aerated systems. The fate of major degradation intermediates formed during photocatalysis of phenol was also monitored during the course of the study to give an insight into determining a degradation pathway. Photocatalysis of the three derivatives of phenol as individual pollutants in solution; and as a mixture (of phenol and all three derivatives) was conducted to better understand the degradation behaviour of these compounds when pollutants compete in solution for reactive species. Kinetic models for the various systems were developed to give valuable information necessary for a better understanding of the photocatalytic system.

5.2 Photocatalytic Degradation of Phenol

Solutions of phenol of the desired concentrations were prepared by spiking ultrapure water with the pre-determined and weighed amounts of phenol crystals. Photocatalytic degradation experiments of phenol (10 mg/L) were carried out with the experimental setup configuration A and experiments with phenol (20-30 mg/L) configuration B (Figure 3.1). One litre of the prepared phenol solution was used for each batch of degradation studies and experiments were conducted as described in Sections 3.4 and 3.5. Temperature control in the reactor was not very effective with setup configuration A as temperature in the reactor sometimes varied from 25^{o}C to 40^{o}C. Modification of reactor setup A to B with having a cooling sleeve in the UV lamp jacket improved temperature control within the reactor and temperature were maintained between 25-30^{o}C.

The effect of initial pollutant concentration on the photocatalytic degradation efficiency of phenol solutions was studied across three phenol concentrations (10, 20 and 30 mg/L) with anatase titanium dioxide powder dispersed in solution exposed to UV irradiation (400 W). These experimental batches were conducted without aeration of the batch systems.

Optimum catalyst concentration is a key factor in the performance of a photocatalytic system as excess catalyst leads to decreased efficiencies due to UV photon screening effects (Chirwa and Bamuza-Pemu, 2010; Ahmed *et al.*, 2010; Černigoj *et al.*, 2007; Gogate and Pandit, 2004; Herrmann, 1999). The amount of catalyst available is critical to the efficiency of a photocatalytic system for pollutant degradation in environmental applications as there exists

an optimum catalyst concentration beyond which additional catalyst is detrimental to the system.

Optimum catalyst loading for the system under study was determined by varying catalyst concentration from a 1:1 (pollutant: catalyst) ratio to a maximum where additional catalyst loading resulted in negative effects. The various combinations of phenol and catalyst concentrations studied are presented in Table 5.1.

Table 5.1: Phenol and catalyst concentration combinations.

Phenol Conc. (mg/L)	Titanium Dioxide Concentration (mg/L)									
	10	20	30	40	50	60	70	90	100	150
10	x	x	x	x	x	--	--	--	x	x
20	--	--	x	x	x	--	--	--	x	x
30	--	--	x	x	x	x	x	x	x	x

Effect of the presence of oxygen as an electron acceptor on the degradation kinetics of phenol was studied by conducting photocatalytic degradation experiments with solutions spiked with 30 mg/L of phenol. These batch systems were irradiated with 400 W, UV lamp under constant flow of air varying catalyst concentration from 30-150 mg/L. Aeration of the reactor was achieved by bubbling air through a perforated quartz disc at a constant flow rate of 10 mL/min. Results of this batch of experiments were compared with results obtained for the non-aerated systems.

Progress of degradation was monitored by measuring the concentration of phenol left in solution at regular intervals by HPLC analysis. In all experimental batches, 2 mL aliquots were withdrawn from the reactor at timed intervals, particulate matter was removed by filtration through 0.45 µm syringe filters (Millipore) prior to HPLC analysis. Total reaction time varied for different batches from 40-120 minutes for both photolytic and photocatalytic systems. Detailed HPLC analytical method for determination of phenol concentration is described in Section 3.7.1.

5.3 Photocatalytic Degradation Efficiency of Phenol

Effective treatment and removal of phenol in solution by photocatalysis depended on phenol concentration, catalyst concentration and aeration. The degradation efficiency of phenol is discussed in Section 5.3.1, while effects of initial phenol concentration on degradation efficiency and the effects of catalyst concentration are discussed in Sections 5.3.2 and 5.3.3 respectively.

5.3.1 Degradation efficiency of phenol

Figures 5.1(a) – (c) show the degradation profiles of experiments conducted at initial phenol concentration of 10-30 mg/L, photolysed with UV radiation alone and photocatalysed with UV/TiO_2, varying catalyst concentration from 10-150 mg/L. Degradation of phenol below detection limit was achieved at these concentrations after 15-35 minutes of treatment (for initial phenol concentration of 10 mg/L), 60-100 minutes for initial phenol concentration of 20 mg/L and 120 minutes for solutions with initial phenol concentration of 30 mg/L.

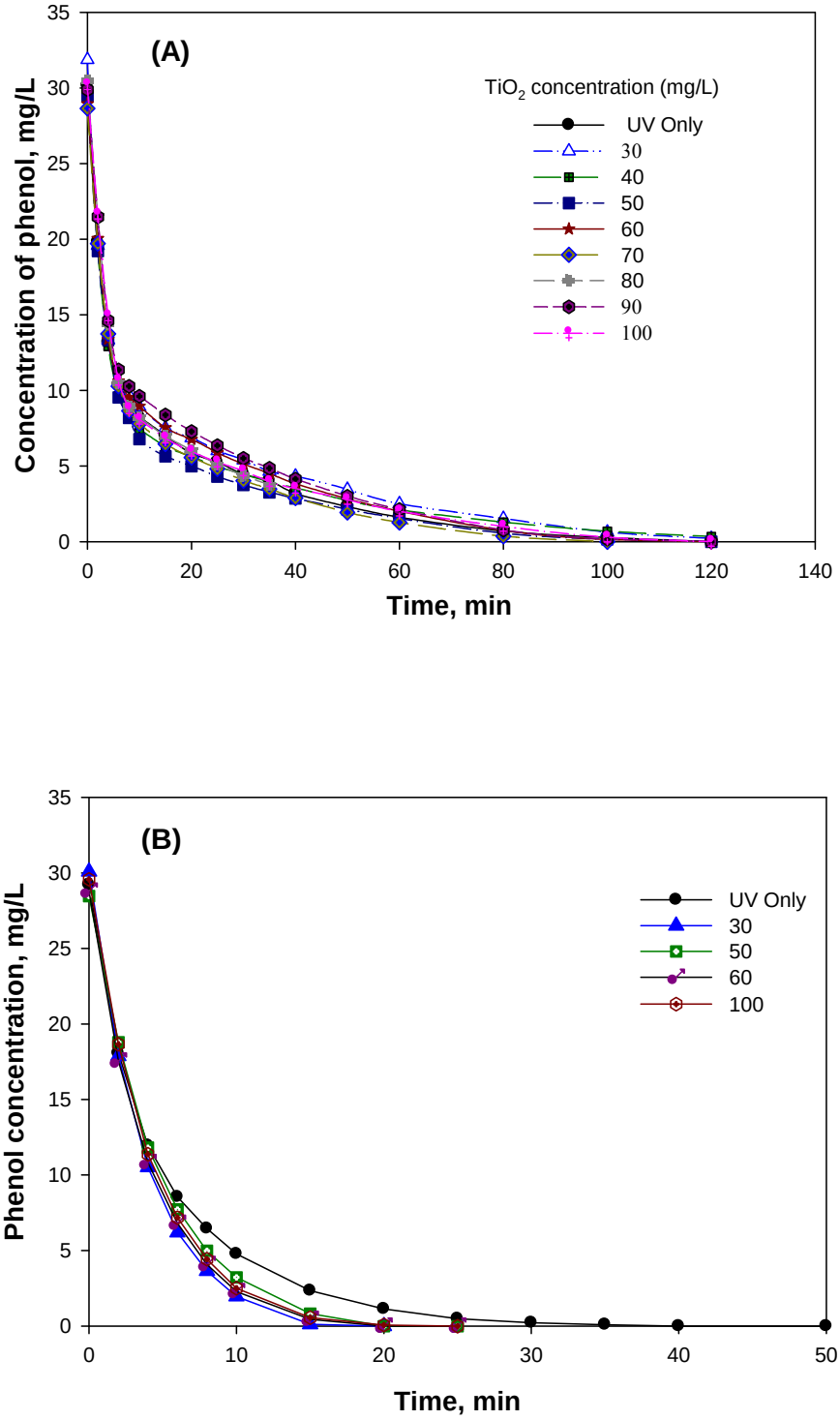

Figure 5.1: Degradation Profile of phenol (30 mg/L), photocatalysis (UV and TiO_2) with catalyst concentration from 30 – 100 mg/L and a batch with UV only as a photolytic control – (A) unaerated, (B) aerated.

5.3.2 Effect of initial pollutant concentration

Degradation efficiency of phenol measured as degradation rates was calculated as the rates of change in concentration of phenol as a function of time of reaction.

$$R = \frac{[C]_o - [C]_t}{t_o - t_t} \tag{5.1}$$

Where:

R = Rate of pollutant degradation (mg/(L. min)),

$[C]_o$ = initial concentration of pollutant (mg/L),

$[C]_t$ = concentration of pollutant at time t (mg/L),

t_o = time at concentration C_o (minutes), and

t_t = time at concentration C_t (minutes).

Degradation efficiency of phenol measured as degradation rates decreased with increasing initial phenol concentration at constant titanium dioxide concentration in solution. Efficiency of the photocatalytic system is measured as the quantum yield which is defined as "the rate at which molecules undergo a given event per photons absorbed per unit time" (Serpone, 1997) or "as the number of events occurring per photon absorbed" (Linsebingler *et al*., 1995).

In this study, highest degradation rates were obtained for solutions of phenol at concentration of 10 mg/L (representing the lowest concentration of phenol studied) for the photolytic and the photocatalytic systems across all TiO_2 concentrations studied (Table 5.2). Increase in initial phenol concentration from 10 mg/L to 20 mg/L resulted in a decrease in degradation rates ranging between 30-51% (from 0.49 mg/(L.min) to 0.39 mg/(L.min)). Impact of a further increase in the initial phenol concentration from 20 mg/L to 30 mg/L on degradation rates ranged from 6% to 29%. However, an increase in phenol concentration from 20 to 30 mg/L at titanium dioxide concentrations of 30 and 100 mg/L resulted in a slight increase in rates from 0.249 to 0.264 mg(L.min).

Degradation rates are governed by the availability and effective contact of reactive species (hydroxyl radicals) in solution and (positive holes) on the catalyst surface with pollutant

species (Equations 2.8 and 2.9). Phenol and its derivatives are relatively soluble in water and the main reaction zone for their destruction during photocatalysis is believed to be the bulk liquid (Ahmed *et al*., 2010). Increasing pollutant concentration without subsequent increase in reactive species in solution would therefore reduce the pollutant/reactive species ratio with a resultant decrease in degradation efficiency.

Decrease in degradation rates with increasing phenol concentration can also be attributed to an increase in the quantity of phenol adsorbed on the TiO_2 catalyst surface thereby reducing available surface sites for the production of hydroxyl radicals (Laoufi *et al*., 2008), especially as formation of the reactive radical species ($^{\bullet}OH$ and $O_2^{-\bullet}$) remain constant at a particular catalyst concentration and light intensity. In addition, pollutant particles also absorb some photons of light and higher concentrations of pollutant in solution would reduce the photons of light available for production of electron hole pairs and reactive radical species.

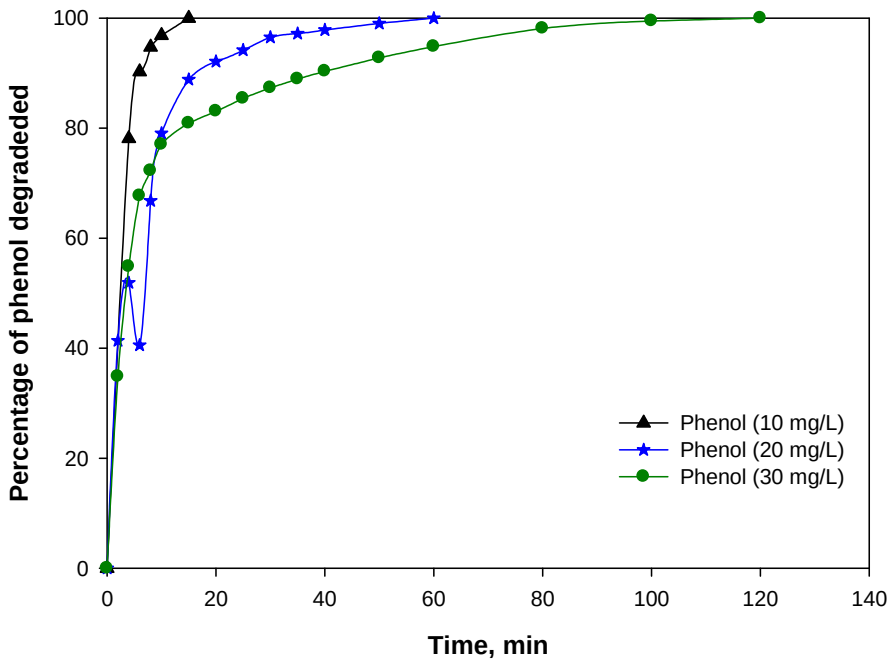

Figure 5.2: Percentages of phenol (10-30 mg/L) degraded by photocatalysis as a function of time with 50 mg/LTiO_2.

A direct relationship between the initial phenol concentration and reaction time for removal of phenol from solution to levels below detection limit was observed. At initial phenol

concentration of 10 mg/L, phenol was degraded to levels below detection limit after 15 minutes of photocatalysis with 50 mg/L TiO_2. Increasing phenol concentration to 20 and 30 mg/L required longer reaction times of 60 and 120 minutes respectively to achieve removal to levels below the detection limits(Figure 5.2).

Parida and Parija (2006) in their studies observed a decrease in degradation efficiency from 100 to 60% (with solar light), and 94 to 52% (under UV irradiation) when phenol concentration was varied from 2 to 25 g/L. Pardeshi and Patil (2008) reported decreases in degradation efficiency of phenol on increasing phenol concentration from 25 to 300 mg/L in a photocatalytic system using ZnO as catalyst irradiated by solar energy. Shukla *et al*., (2010) obtained the highest degradation rates for phenol at the lowest initial phenol concentration of 12.5 mg/L from a study that varied phenol concentrations from 12.5 to 37.5 mg/L with a UV/vis irradiated ZnO/persulfate system. Hong *et al*., (2001), and Maleki *et al*., (2006) also reported similar trends in their study on photocatalytic and photolytic degradation of phenol by TiO_2 respectively. Therefore, the observed degradation rates in this study are consistent with earlier investigations using other UV light sources and other semiconductor types.

5.3.3 Effect of titanium dioxide concentration

The results on degradation efficiency in non-aerated batches showed that increasing the catalyst concentration from 10 to 50 mg/L resulted in a 130% improvement on degradation rates of phenol (10 mg/L) in solution. Further increase in TiO_2 concentration to 100 mg/L resulted in a decrease in the degradation efficiencies by 34%. Further increase of TiO_2 to 150 mg/L resulted in a further decrease by 50% confirming that 50 mg TiO_2/L represents the optimum catalyst dose (Table 5.2, Figure 5.3). The effect of TiO_2 concentration in solution on the photocatalytic degradation efficiencies of phenol solutions (10, 20 and 30 mg/L) are presented in Figures 5.3 to 5.5. After increasing TiO_2 concentration from 10 to 30 mg/L, degradation rates of phenol increased by 74%. A further increase in catalyst concentration from 30 to 50 mg/L resulted in a further 32% increase in degradation rates.

Table 5.2: Phenol degradation efficiency under non-aerated batch conditions tested at a constant initial phenol concentration of 10 mg/L.

TiO_2 concentration	Photocatalytic Degradation Rate	Improvement from Initial Rate	Decreased in Efficiency from Maximum Rate
mg/L	Mg/(L.min)	%	%
10	0.28	0	–
20	0.33	16	–
30	0.49	74	–
40	0.37	31	–
50	0.65	130	–
100	0.49	–	-24
150	0.32	–	-50

The results indicate that increasing TiO_2 concentration above a certain optimum is not beneficial to the overall removal rate. Further increases in TiO_2 concentration beyond this point result in the decrease in degradation rates from 6.50 x 10^{-1} mg/(L.min) to 4.93 and 3.22 mg(L.min). In this study, this occurred with TiO_2 concentrations of 50 mg/L beyond which degradation efficiency decreases by 24 to 34%.

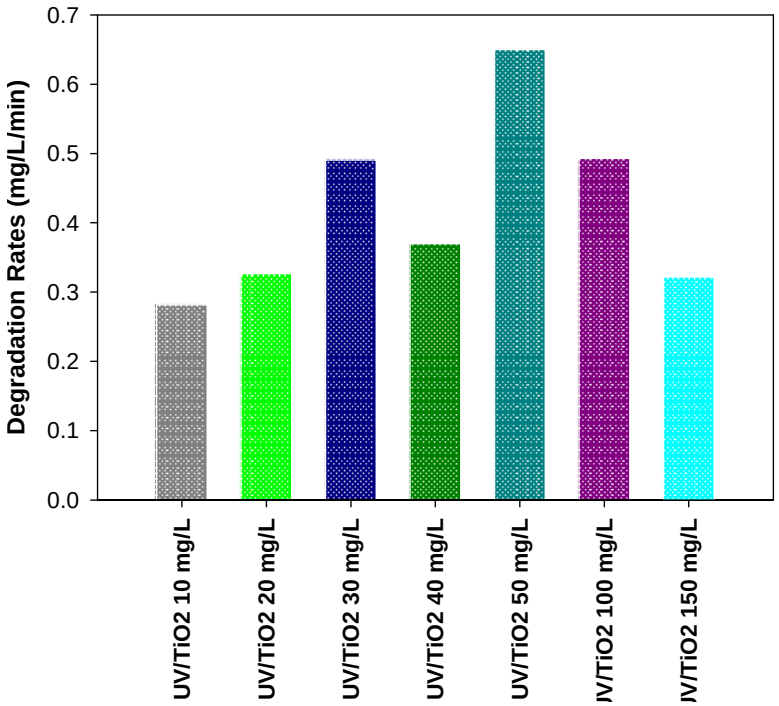

Figure 5.3: Photocatalytic degradation rates for phenol (10 mg/L) with TiO_2 concentrations of 10-150 mg/L in non-aerated system.

Degradation rates for solutions of phenol at concentration of 20 mg/L also increased from 0.25 mg/(L.min) at TiO_2 of 30 mg/L to a maximum of 0.35 mg/(L.min) at catalyst concentration of 50 mg/L representing an increase of 40%, beyond which rates decreased to 0.24 mg/(L.min) (30%) and 0.19 mg/(L.min) (45%); at TiO_2 concentrations of 100 and 150 mg/L respectively (Figure 5.4).

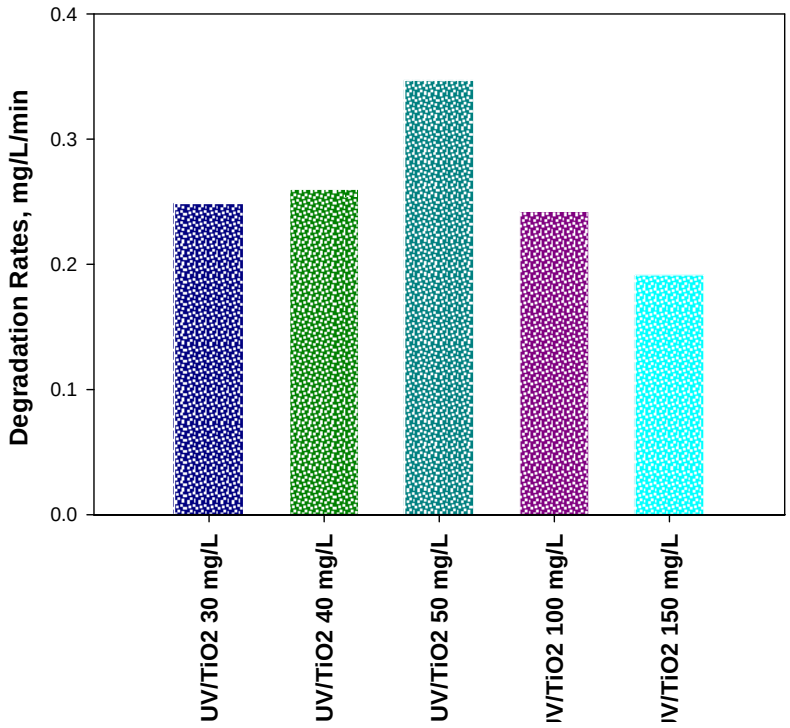

Figure 5.4: Photocatalytic degradation rates for phenol (20 mg/L) with TiO_2 concentrations of 30-150 mg/L.

These results indicate that at catalyst concentrations higher than 50 mg/L, there are reduced active sites due to reduced UV light transmittance in solution. Factors contributing to reduction in light transmittance include light scattering and screening effect of the UV radiance by excess catalyst in solution (Chirwa and Bamuza-Pemu, 2010). Also, excess catalyst particles in solution tend to agglomerate leading to reduced surface area for pollutant adsorption (Ahmed *et al*., 2010). Light scattering and screening of light by excess catalyst particles leads to a reduction in photonic events in the reactor including the reduction in

formation of electron hole pairs and hydroxyl radicals in solution, which ultimately results in reduced oxidative activities under the existing conditions.

The effect of increasing TiO_2 concentrations between 30-100 mg/L on degradation efficiency was less pronounced during photocatalysis of phenol solutions of 30 mg/L. At this concentration comparable degradation rates were obtained for catalyst concentrations 30-100 mg/L; with slightly improved rates at of 70 mg/L (Figure 5.5). Rates increased from 0.26 mg/(L.min) with catalyst concentration of 30 mg/L to 0.28 mg/(L.min) at catalyst concentration of 70 mg/L representing a 9% increase in rates. A further increase in TiO_2 from 70 to 100 mg/L resulted in a 12% decrease in degradation rates. The close degradation rates could be as a result of competing factors of the need for higher surface area for the adsorption of pollutant molecules and the screening, scattering effect of excess particles in solution. The photocatalytic and photolytic degradation rates of phenol for both aerated and non-aerated systems are presented in Table 5.3.

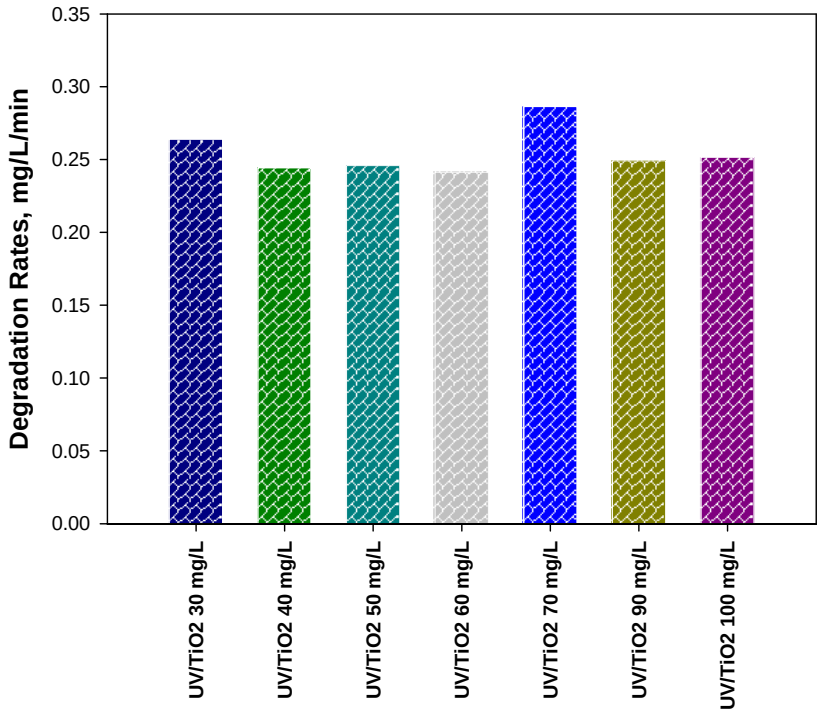

Figure 5.5: Photocatalytic degradation rates for phenol (30 mg/L) with TiO_2 concentrations of 30-100 mg/L.

Table 5.3: Photocatalytic/photolytic degradation rates of phenol (30 mg/L) for aerated and non-aerated systems.

System Catalyst Conc.	Rates -mg/(L.min)					
	Aerated System			Non Aerated Systems		
	2 mins	Final Rate	Rate#	2 mins	Final Rate	Rate#
UV Only	5.17	0.73	0.49	4.57	0.25	**NCD
30	6.03	1.51	0.50	6.14	0.26	**NCD
40	5.57	1.52	0.76	5.18	0.24	**NCD
50	4.71	1.44	0.72	5.14	0.25	**NCD
60	5.63	1.44	0.72	4.45	0.24	**NCD
70	5.10	1.15	0.72	4.47	0.29	**NCD
80	5.38	1.20	0.75	4.46		**NCD
90	4.19	0.87	**NCD	4.21	0.25	**NCD
100	5.33	1.44	0.96	4.28	0.25	**NCD
150	4.00	0.96		--	--	

**NCD – Not completely degraded

Rate# - Rate at the time of complete removal of phenol and all aromatic intermediates formed.

5.4 Photolytic Degradation of Phenol

The extent to which UV irradiation alone degrades aqueous phenol solutions was studied by exposing phenol (10-30 mg/L) to UV radiation in the absence of titanium dioxide powder. Batches of the photolytic experiments were conducted with and without aeration. Photolytic degradation of phenol (10 mg/L) was conducted with experimental setup Configurations A and (2-30 mg/L) with Configuration B (Figure 3.1), keeping reaction conditions the same as in the corresponding photocatalytic experiments with the notable exception of the absence of the titanium dioxide catalyst. Phenol concentrations were analysed by HPLC as described in Section 3.7.1.

Photolysis of 10 mg/L phenol achieved 100% degradation within 15 minutes of treatment. An increase in phenol concentration to 20 mg/L and 30 mg/L required longer reaction time of 80 and 120 minutes respectively to achieve degradation below detection limits (Figure 5.6). The pseudo first order linear transforms are plotted in Figure 5.7.

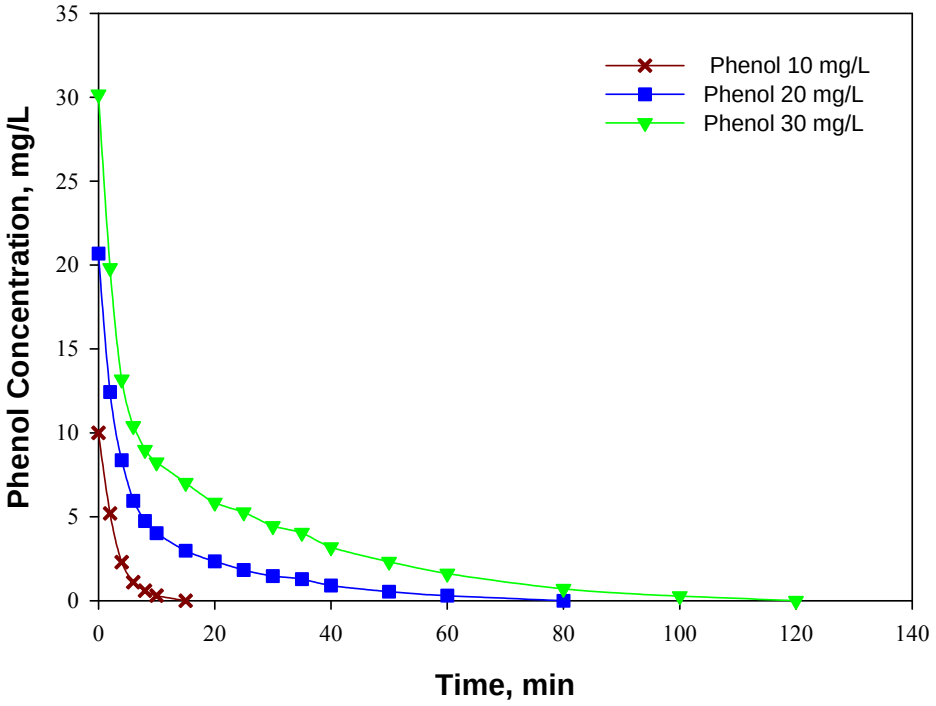

Figure 5.6: Photolytic degradation profile of phenol (10-30 mg/L) without aeration.

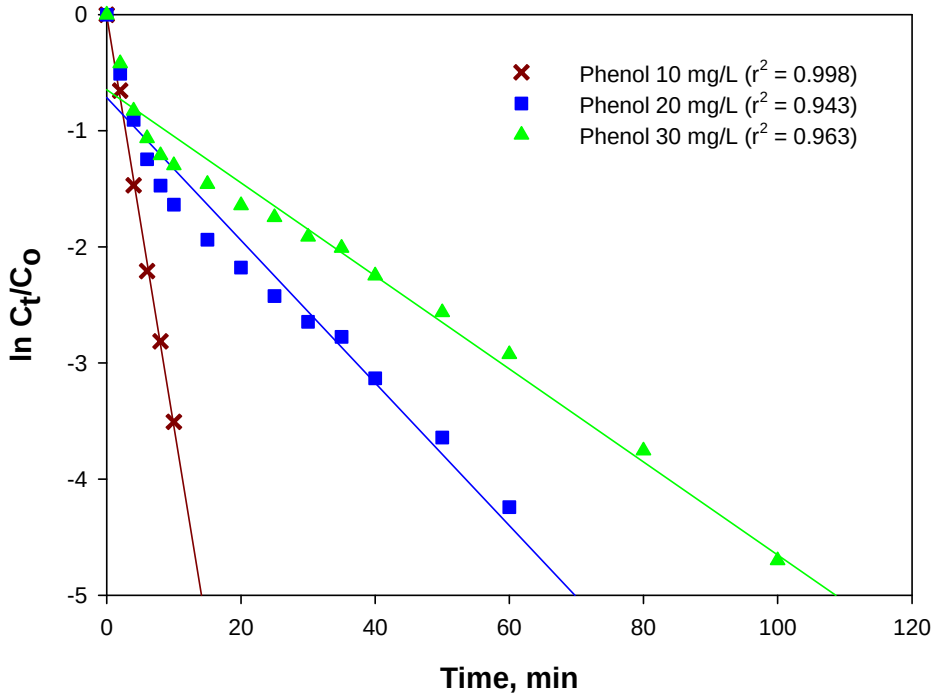

Figure 5.7: First order linear transforms of photolytic degradation profile of phenol (10-30 mg/L) in Figure 5.6.

5.5 Effects of Aeration on Degradation Efficiency

Availability of an electron acceptor is crucial to the efficiency of a photocatalytic system as represented by Equation 2.2 and shown in Figure 2.5. In water purification the electron acceptor is usually oxygen as formation of reactive radical species strongly depends on its presence. The effect of oxygen on the degradation efficiency was studied for both photolytic and photocatalytic systems at phenol solutions of concentration of 30 mg/L. Results were compared with those obtained for the non-aerated system.

Photolytic and photocatalytic degradation rates for phenol (30 mg/L) in aerated and non-aerated systems are presented in Figure 5.8. Aeration of the reactor contents significantly improved degradation rates for both the photolytic and photocatalytic systems across all catalyst concentrations studied resulting in removal of phenol to levels below detection limits for the photocatalytic system at catalyst concentrations between 30-70 mg/L. Improvement in degradation rates due to aeration was very significant with an increase in rates of one order of magnitude. Time required for degradation of phenol to non-detectable levels improved from 100-120 minutes in the non-aerated to 20-35 minutes for the aerated photocatalytic systems; and from 120 minutes to 40 minutes for the photolytic system. Aeration of the system improved photocatalytic degradation rates of phenol by an average of 429% from a maximum of 0.29 mg/(L.min) for the non-aerated photocatalytic systems to a maximum of 1.52 mg/(L.min) for the aerated system.

Degradation rates for photolytic and photocatalytic degradation of phenol for both the aerated and non-aerated systems and the resultant percentage increases in rate are presented in Table B3 in Appendix B. Results obtained for photolysis and photocatalysis of 30 mg/L solutions of phenol show that photolytic degradation rate in the non-aerated system (0.25 mg(L.min)) was comparable to those of the photocatalytic system (0.25 mg/(L.min) to 0.29 mg(L.min)). This is an indication that in limited supply of oxygen, types and quantities of reactive species in solution; predominant degradative pathways in both systems are similar. Degradation under this condition might be due primarily to oxidation by reactive holes formed on the catalyst surface and direct photolysis (Chirwa and Bamuza-Pemu, 2010). Khraisheh and co-workers observed improvement in photocatalytic degradation rates of carbamazepine by a factor of 1.6 by varying dissolved oxygen concentration from 6 mg/L to 24 mg/L (Khraisheh *et al.,* 2013). Higher rates obtained on aeration could be attributed to the synergic effect of

oxidation due to photolysis, oxidation from positive holes on the surface of the catalyst and mainly from hydroxyl radicals formed from the reduction of oxygen by photogenerated electrons on the catalyst surface.

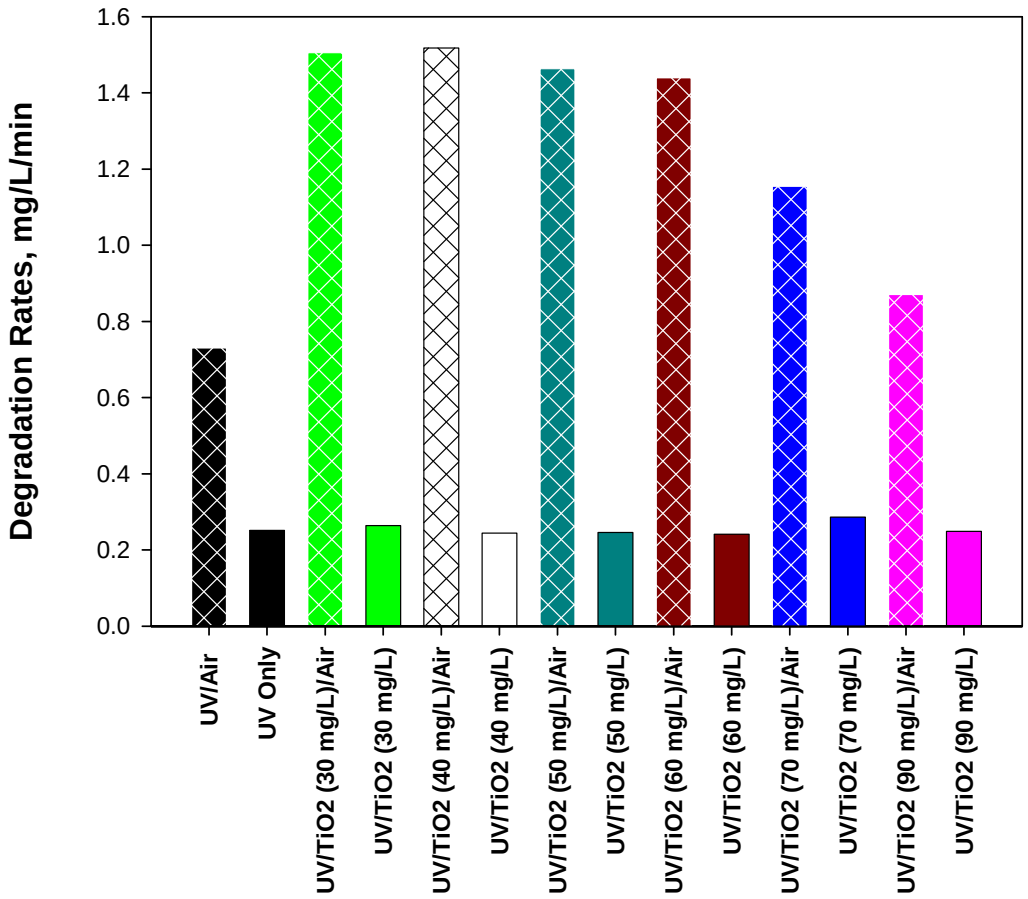

Figure 5.8: Effect of oxygen on the photolytic and photocatalytic degradation rates of phenol (30 mg/L) with TiO_2 concentrations of 30-90 mg/L.

Contribution of hydroxyl radicals to improved degradation rates is supported by the very similar rates obtained for the photolytic and photocatalytic systems in the non-aerated systems. A wider difference in degradation rates was observed between the photolytic system and the photocatalytic systems with aeration (Figure 5.8).

Photolysis of phenol with aeration proceeded at a rate of 0.73 mg/(L.min) and the maximum rate obtained for the aerated photocatalytic systems was 1.52 mg(L.min). Dissolved oxygen in solution plays a further role or inhibiting recombination of $^{\bullet}H$ and $^{\bullet}OH$ radicals thus

increasing the lifespan of the reactive species in solution with a subsequent increase in degradation rates over systems without aeration (Khraisheh *et al.,* 2013)

5.6 Intermediates of Phenol Degradation

Degradation of organic compounds in water is often accompanied by the formation of several intermediates some of which are feared to be more toxic than the original pollutant being treated. Effective treatment is expected to mineralise the primary pollutant and intermediate products formed during the treatment process, or reduce the pollutant/intermediates to environmentally insignificant concentrations.

Phenol has an electron rich aromatic ring which makes it susceptible to both electrophilic aromatic substitution and oxidation reactions. Phenol oxidation is known to produce several aromatic intermediates such as quinones (benzoquinone) (McMurry, 2012), hydroxylated phenols, also referred to as dihydroxylated benzene compounds, notably catechol (benzene-1,2-diol), hydroxyquinone (1,4-Dihydroxybenzene) (Sobczyński *et al.*, 2004; Mokrini *et al*., 1997), resorcinol (benzene-1,3-diol) (Figure 5.9); and some acyclic compounds including oxalic acid, formic acid, maleic acid, glyoxalic acid and fumaric acid. Alapi and Dombi (2006), in their study of UV and UV/VUV photolysis of phenol, intermediate accumulation of 1,2-dihydroxybenzene and 1,4-dihydroxybenzene. Sobczyński *et al*., (2004) identified resorcinol in solution during photocatalysis of phenol in non-quantifiable amounts.

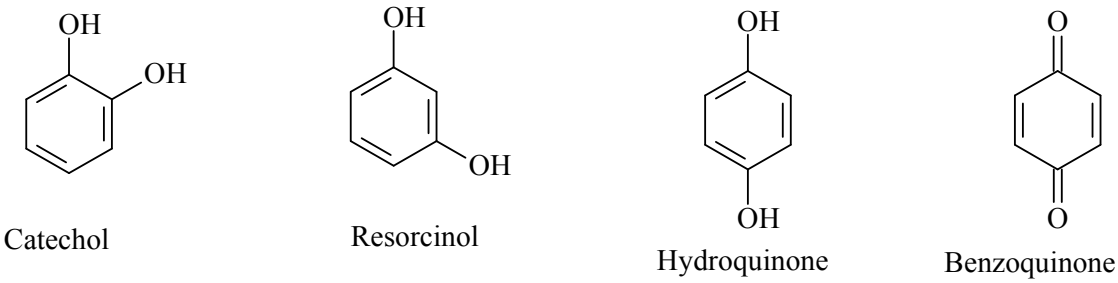

Figure 5.9: Structures of catechol, resorcinol, hydroquinone and benzoquinone.

Aromatic intermediates in solution during the course of photocatalysis of the phenol as initially identified by GC/MS analysis with standards and quantified by HPLC include catechol, hydroxyquinone and resorcinol. Trace amounts of benzoquinone was transiently observed in a few of the systems studied and not identified in solution in most of the systems studied. Concentrations of aromatic intermediates measured show that all three aromatic intermediates are produced within the first two minutes of treatment. Maximum concentrations of intermediates obtained is in the order catechol>resorcinol>hydroquinone (Figure 5.10). Formation rates were calculated as the rates at which the maximum concentrations were obtained and the degradation rates of intermediates were calculated as the rate of disappearance of the intermediate from the maximum concentrations obtained.

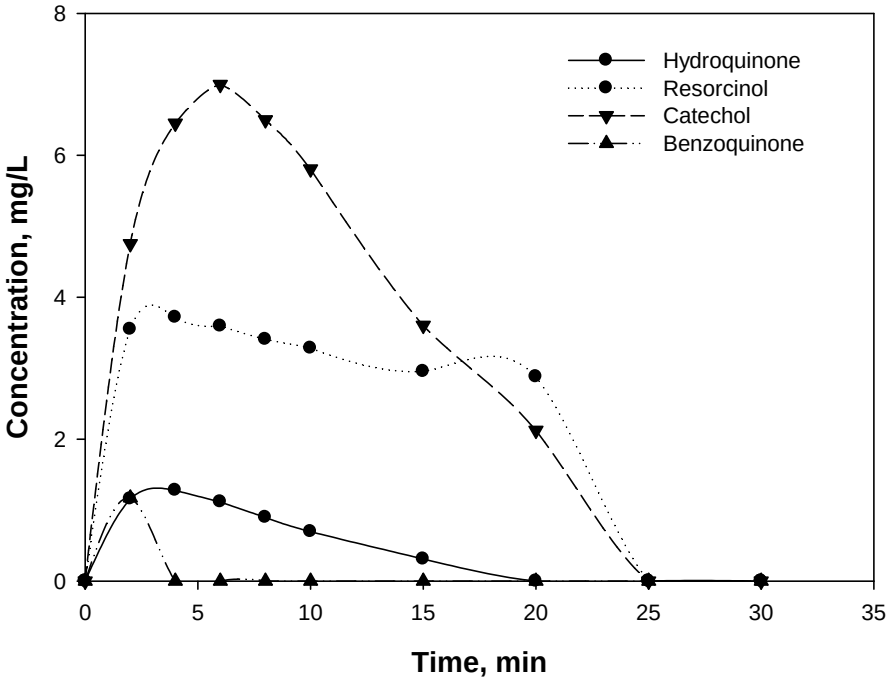

Figure 5.10: Degradation profile of aromatic intermediates of phenol photocatalysis, conditions – TiO_2 50 mg/L, UV 400W, air 10 mL/min.

5.6.1 Catechol

The formation and degradation profiles of catechol obtained during photocatalytic degradation of phenol with different catalyst concentrations are presented in Figure 5.11. Degradation of phenol produced higher concentration of catechol than any other aromatic

intermediate. This could be attributed to the ortho directing properties of the hydroxyl group of phenol. Catechol was formed rapidly within the first 2 minutes of phenol degradation and its concentration in solution increased to a maximum of 7.00-7.11 mg/L; after 6-8 minutes at a rate of 0.76-0.87 mg/(L.min) (Figure 5.11). Detailed list of degradation rates are presented in Table D-4 in Appendix D.

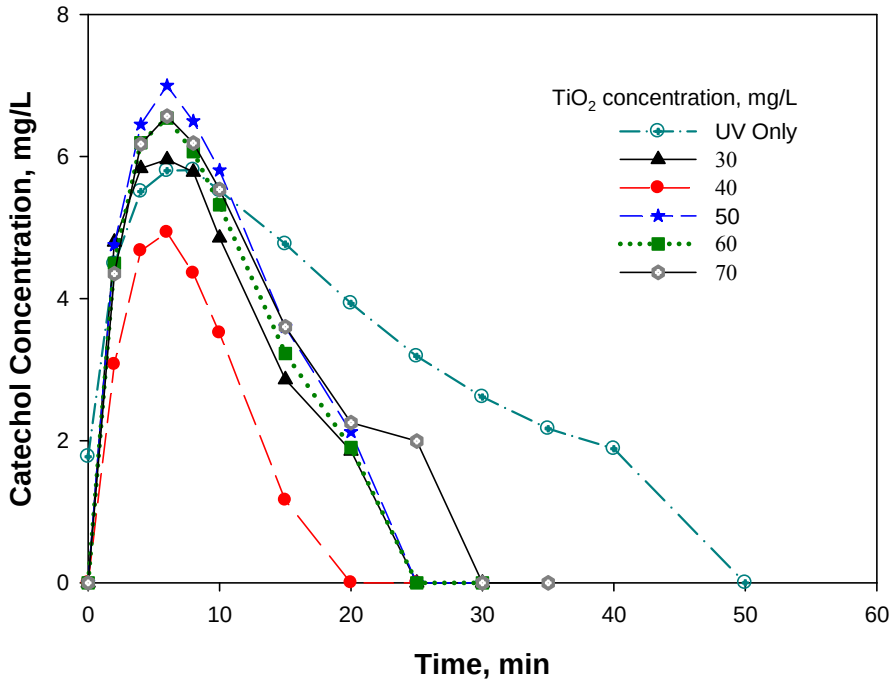

Figure 5.11: Formation and disappearance profile of catechol from photocatalysis of phenol (30 mg/L) with varied TiO_2 concentrations in an aerated system.

Concentration of catechol decreased gradually thereafter at rates of 0.24-0.35 mg(L.min). A study of the degradation profiles of phenol and catechol show that there is a steady increase in catechol concentration as long as the concentration of phenol is higher than that of catechol and a decrease in concentration starts to occur once the concentration of phenol is approximately the same as that of catechol in solution. Catechol is completely removed from solution after the precursor compound is completely degraded (Figure 5.12).

5.6.2 Resorcinol

The formation and disappearance profile for resorcinol is presented in Figure 5.13. Resorcinol is formed from the electrophilic substitution of a meta aromatic hydrogen atom. Maximum concentrations of 3.50±0.15 mg/L of resorcinol were obtained after 2 minutes of

phenol photocatalysis with no appreciable change in its concentrations to the point of disappearance of phenol from solution. The relatively unchanged concentration of resorcinol in solution suggests that production of resorcinol in solution proceeds at approximately the same rate as its removal from solution until all phenol is removed from solution (Figure 5.13). In non-aerated systems, resorcinol formation is transient as it is formed and completely removed from solution within the first 10 minutes of phenol treatment (Figure 5.13b) even though appreciable concentration of phenol is still in solution up to the 120th minute of treatment. This is an indication that formation of dihydroxylated benzene compounds is favoured at the ortho and para carbon positions and not the meta position.

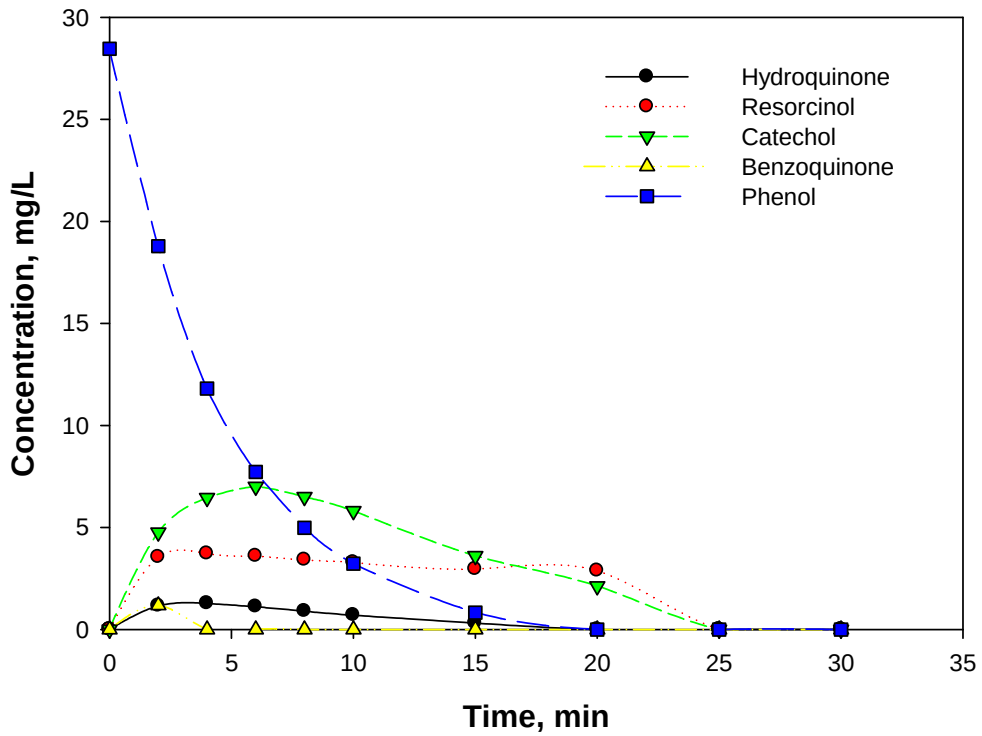

Figure 5.12: Degradation profile of phenol and aromatic intermediates of phenol photocatalysis, condition – TiO_2 50 mg/L, UV 400W, air 10 mL/min.

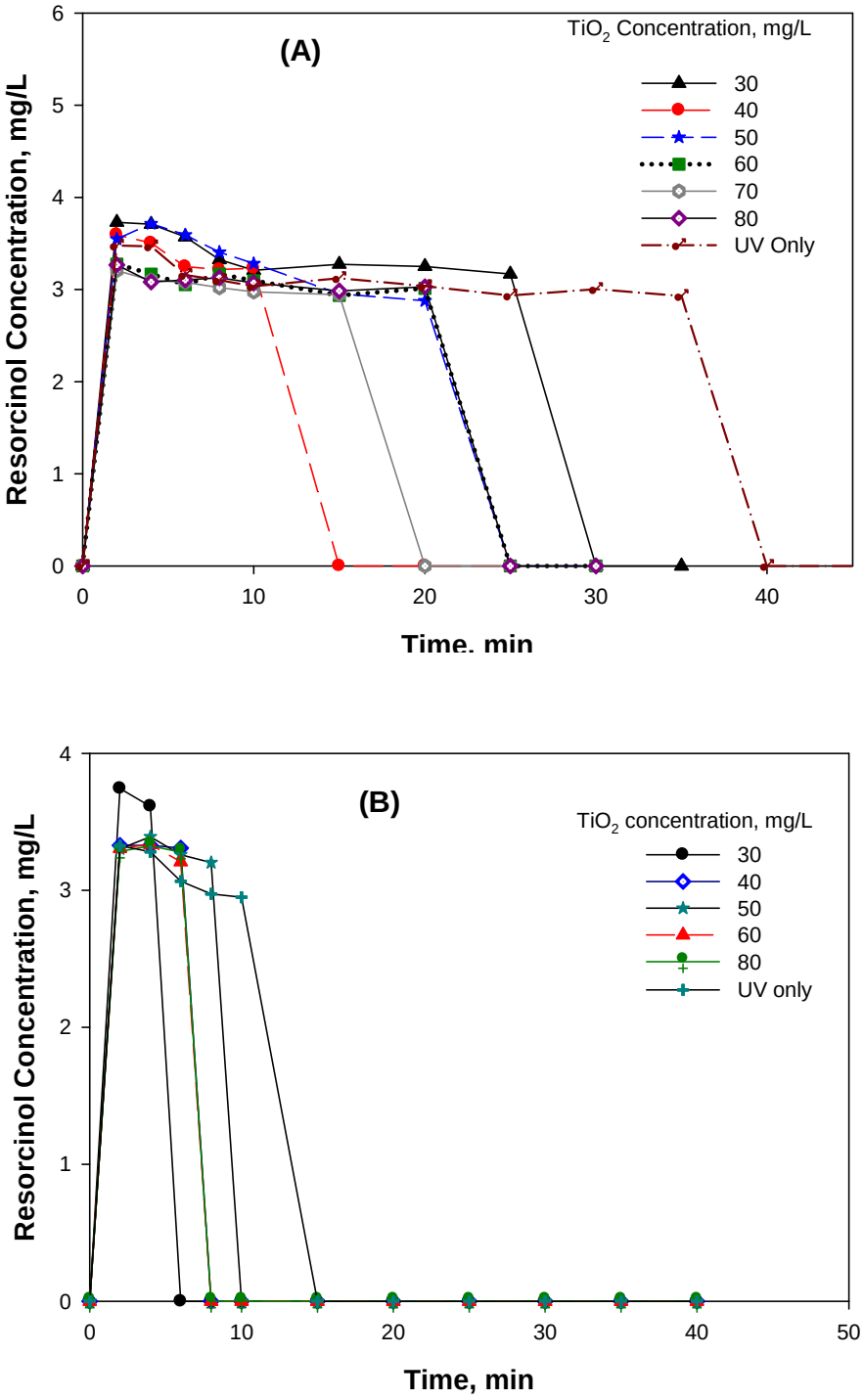

Figure 5.13: Formation and disappearance profile of resorcinol from photocatalysis of phenol (30 mg/L) with varied TiO_2 concentrations in (A) aerated and (B) non-aerated system.

Maximum concentrations of resorcinol obtained were higher than expected as higher concentrations of the para directed product (hydroquinone) were expected. This could be attributed to the non-selective nature of attack of the hydroxyl radical in solution which is a stronger effect than the ortho, para directing effect of the hydroxyl group of phenol. A second contributing factor is the fact that the ortho- and meta- positions present two possible points of attack. Catechol is formed from substitution of an aromatic hydrogen atom on carbon atoms at positions C2 and C6 of the aromatic ring and resorcinol is formed from substitution of an aromatic hydrogen atom on carbon atoms at positions C3 and C5, while hydroquinone formation is possible only from substitution at the para carbon atom at position (C4). The non-selective nature of hydroxyl radical attack is supported by the fact that degradation in non-aerated system produced resorcinol transiently (Figure 5.13b). This school of thought is further strengthened by the fact that resorcinol formation was transient in systems that were not aerated.

5.6.3 Hydroquinone

Hydroquinone formation peaks after 2-4 minutes of phenol degradation at maximum concentrations of 0.96-1.45 mg/L (Figure 5.14) and its concentration decreases steadily and gradually until all phenol is removed from solution. The hydroxyl group of phenol is a strongly activating group which is ortho- and para-directing in aromatic electrophilic substitution reactions, it is expected that higher concentration of ortho- and para-substituted intermediates would be formed. Contrary to expectations concentrations of hydroquinone (para) substituent is remarkably lower than concentrations of both catechol (ortho) and resorcinol (meta) substituents. The highest concentrations of aromatic intermediates obtained is in the order; hydroquinone<resorcinol<catechol. This could be attributed to the non-selective nature of attack of the hydroxyl radical in solution; coupled with the fact that the ortho- and meta-positions present two possible points of attack.

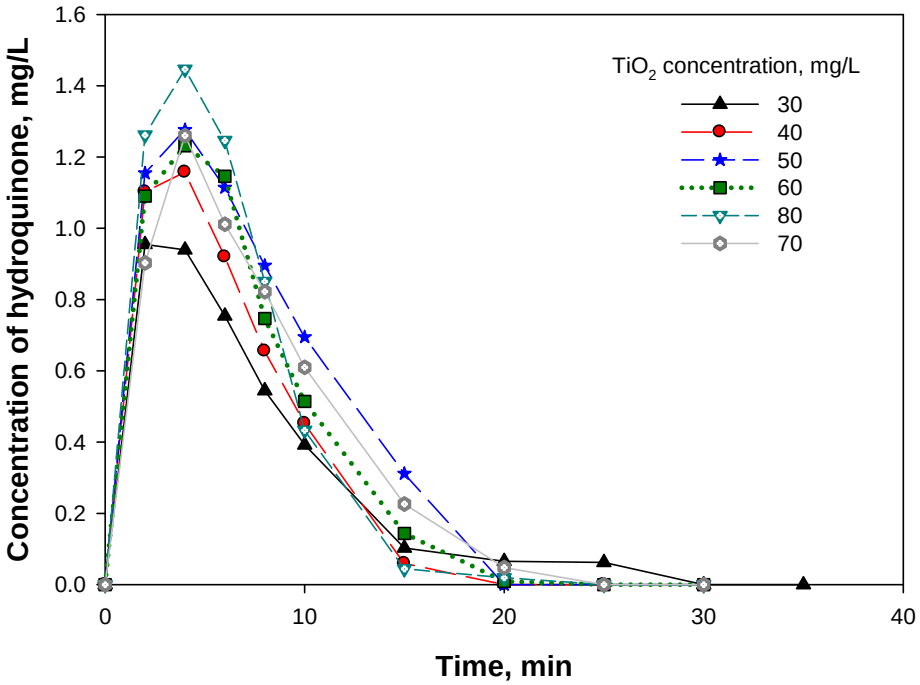

Figure 5.14: Formation and disappearance profile of hydroquinone from photocatalysis of phenol (30 mg/L) with varied TiO_2 concentrations in an aerated system.

Catechol is formed from substitution of an aromatic hydrogen atom on carbon atoms at positions C_2 and C_6 of the aromatic ring and resorcinol is formed from substitution of an aromatic hydrogen atom on carbon atoms at positions C_3 and C_5, while hydroquinone formation is possible only from substitution at the para carbon atom. The non-sustained formation of resorcinol in the non-aerated systems further supports the presence and dominance of hydroxyl radicals as the active specie in solution during photocatalytic degradation of phenol.

5.7 Photocatalytic Degradation of Mono-substituted Derivatives of Phenol

Phenol often is released into the environment along with several of its derivatives, the most common derivative being the chlorophenols and nitrophenol. The effective degradation of derivatives of phenol was simulated by testing the degradation efficiency of chlorophenols and nitrophenols. In this study, 2-chlorophenol (2-CP) and 4-chlorophenol (4-CP) were used to evaluate the effect of halogenation of aromatic compounds on degradation rate. 4-nitrophenol (4-NP) was used to test the effect of nitration on the degradation rate (Figure

5.15). Results show that the mono substituted derivatives (especially the chlorinated derivatives) are more susceptible to photocatalysis than the parent phenol. Very rapid degradation of the chlorophenols (2-chlorophenol and 4-chlorophenol) with 50 mg/L TiO_2 under the reaction conditions was achieved. Degradation rates obtained were in the decreasing order of 4-CP>>>2-CP>>4-NP>≈phenol. Removal of 4-CP from solution to levels below the detection limit was obtained after just 2 minutes of degradation (Figure 5.15) at a rate of 15.2 mg/L min^{-1}, while 2-CP was degraded below detection limits after 8 minutes of photocatalysis at a rate of 3.94 mg/(L.min).

The results in Figure 5.15 show that the dehalogenation of the phenol molecule was inversely correlated to the distance of the halogen group from the hydroxyl group on the benzene ring. The dehalogenation of 4-CP, and therefore its disappearance from solution, was much faster than the rate of disappearance of 2-CP and phenol. This is governed by two opposing electronic effects as 2-chlorophenol and 4-chlorophenol display negative inductive effect (-I) and positive mesomeric effect (+M). The –I effect is more prominent at the ortho than at the para position as it is an effect transmitted through the bonds and gets weaker with distance. It is envisaged that the presence of the highly electronegative chloro group could facilitate the deactivation of the conjugated pi system of the aromatic ring thereby enhancing degradability of the compound. 4-nitrophenol exhibited similar degradability as phenol with degradation below detection limits achieved after 20 minutes of reaction time (Figure 5.15).

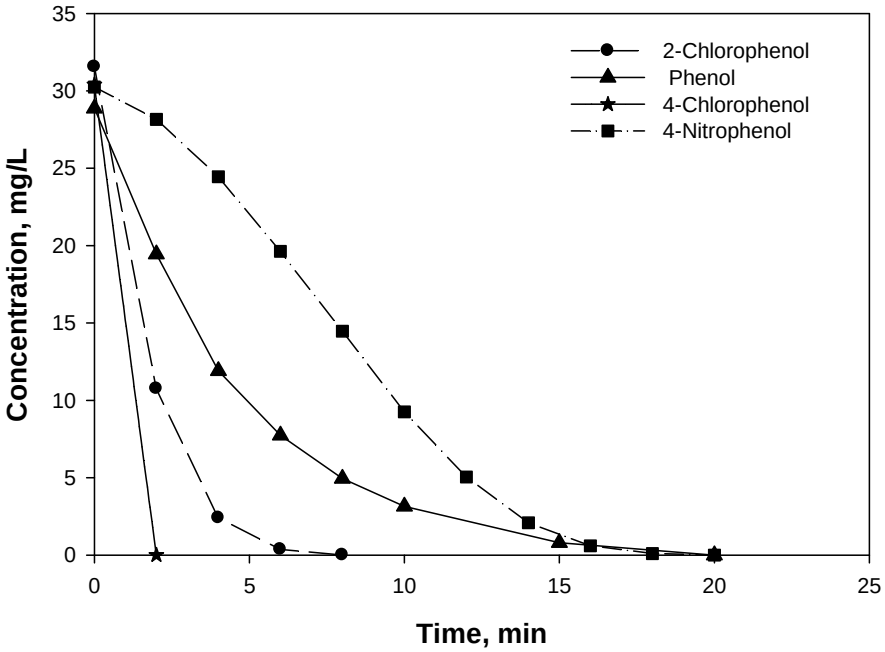

Figure 5.15: Degradation efficiency of individual phenolic compounds (30 mg/L) photocatalysed with 50 mg/LTiO_2.

The much faster degradation rates of 2-chlorophenol and 4-chlorophenol could be attributed to the presence of the highly electronegative chlorine substituent on the aromatic ring, which withdraws to itself part of the electron cloud of the pi electron system of the aromatic ring, this results in weakening of the delocalized pi electron structure. A weakened pi electron structure would result to reduction in bond strengths thereby making it more susceptible to ring cleavage.

5.8 Degradation of Mixed Phenolic Pollutants in Water

The degradation profiles of phenol, 2-CP, 4-CP and 4-NP containing 30 ppm of each phenolic compound photocatlysed in a simulated mixed wastewater using 50 mg/L TiO_2 are presented in Figure 5.15. Amounts degraded as a function of exposure time are presented in Figure 5.16, whereas the degradation rates for the compounds after 6 min.; and at levels below detection limits are presented in Table 5.4. The degradation profiles of the phenolic compounds in the simulated mixed waste are presented in Figure 5.16.

Table 5.4: Photocatalytic degradation rates of phenol, 2-chlorphenol, 4-chlorphenol and 4-nitrophenol.

Compound	Degradation Rates (mg/(L.min))		
	Individual Compounds	Mixture[a]	Mixture[b]
2-Chlorophenol	3.94	4.39	1.52
4-Chlorophenol	15.20	4.73	0.79
4-Nitrophenol	1.51	0.97	0.59[c]
Phenol	1.44	2.12	0.73

[a] Degradation rates after first 6 minutes of photocatalytic treatment

[b] Degradation rates after degradation of pollutant in solution below detection limit

[c] Rate after 50 minutes of irradiation, complete removal was not achieved after 50 minutes

Generally, the degradation efficiency of the individual phenolic compounds decreased significantly in the mixture of phenolic compounds. The relative trend was still in the order of 4-chlorophenol > 2-chlorophenol > 4-nitrophenol > phenol, with 2-chlorphenol and 4-chlorophenol achieving degradation below detection limits after 100 minutes of photocatalysis with 50 ppm TiO_2. Degradation of 2-chlorophenol and 4-chlorophenol occurred in the mixture at the expense of phenol and 4-nitrophenol (Table 5.4 and Figures 5.15 and 5.16).

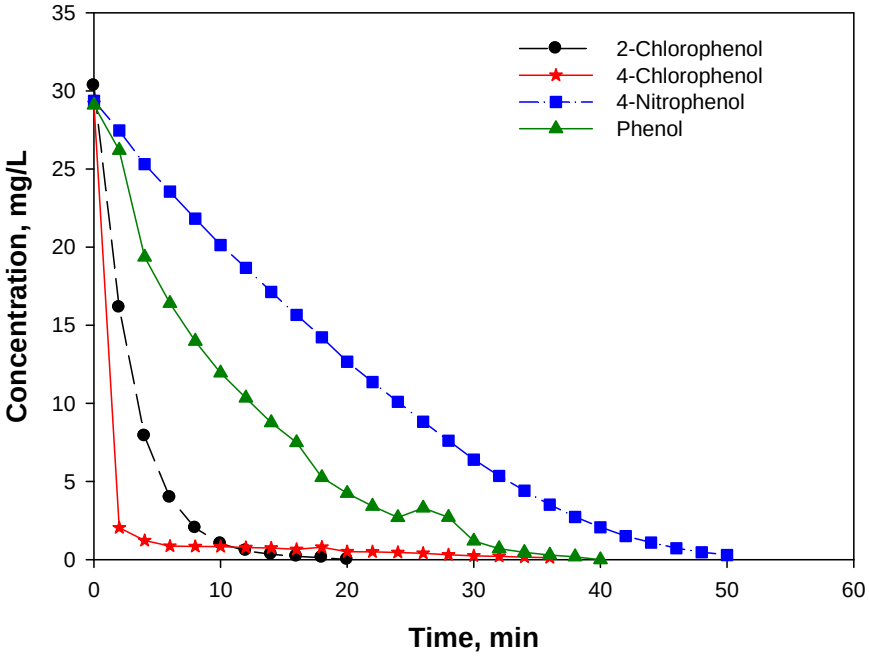

Figure 5.16: Pollutant degradation profile of phenolic compounds in the mixture photocatalysed with 50 ppm TiO_2.

5.9 Kinetics of Phenol Degradation

The initial kinetics of photomineralization of a single general pollutant, *P*, by oxygen, sensitized by TiO_2, upon steady state illumination is often described by Langmuir-Hinshelwood kinetic scheme (Mills and Lee, 2004; Hong *et al*., 2001; Herrmann 1999, Hoffmann *et al*., 1995; Mills *et al*., 1993), represented by Equation 5.2:

$$R = \frac{[C]_o - [C]_t}{t_o - t_t} = \frac{k\mathrm{K}[C]_o}{1 + \mathrm{K}[C]_o} \qquad (5.2)$$

Where:

R = Rate of pollutant degradation (mg/L. min^{-1}),

$[C]_o$ = initial concentration of pollutant (mg/L),

$[C]_t$ = concentration of pollutant at time t (mg/L),

t_o = time at concentration Co (minutes), and

t_t = time at concentration Ct (minutes).

K is equilibrium adsorption constant (mg/L^{-1}), and

k =pseudo first order reaction rate constant (min^{-1}).

Rate constants for degradation of phenol in water was obtained from solutions of the linearized rate equations for all concentrations ranges as presented in Equation 5.3

$$\ln\left(\frac{C_t}{C_o}\right) = k \times t \qquad (5.3)$$

Where:

C_o is the initial concentration of phenol at time t=0; and

C_t is the residual concentration of phenol left in solution at time t.

Plots of $\ln C_t/C_o$ as a function of time for solutions of phenol with varying catalyst concentrations on sigmaplot gave linear curves, typical of pseudo first order kinetics of photocatalytic systems. Pseudo first order rate constants were obtained from linear transforms of the plot of $\ln C_t/C_o$ as a function of time from apparent first order kinetic equation. The linear transform for phenol degradation for the degradation profile in Figure 5.17 (non-aerated) and 5.18 (aerated); and the kinetic parameters are presented in Table 5.5. The good fit of the data to the first order plots at all catalyst concentrations studied, as indicated by the high r^2 is an indication that degradation of phenol can be adequately described with first order kinetics.

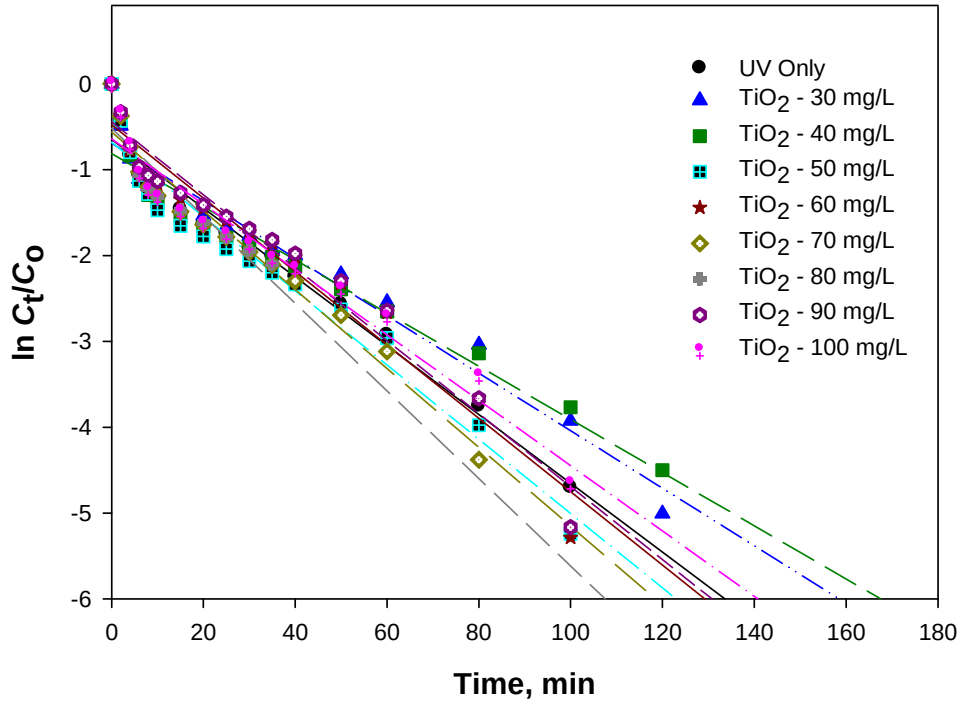

Figure 5.17: First order linear transforms of ln C_t/C_o for phenol (30 mg/L) with TiO_2 concentrations of 0 – 100 mg/L (non – aerated).

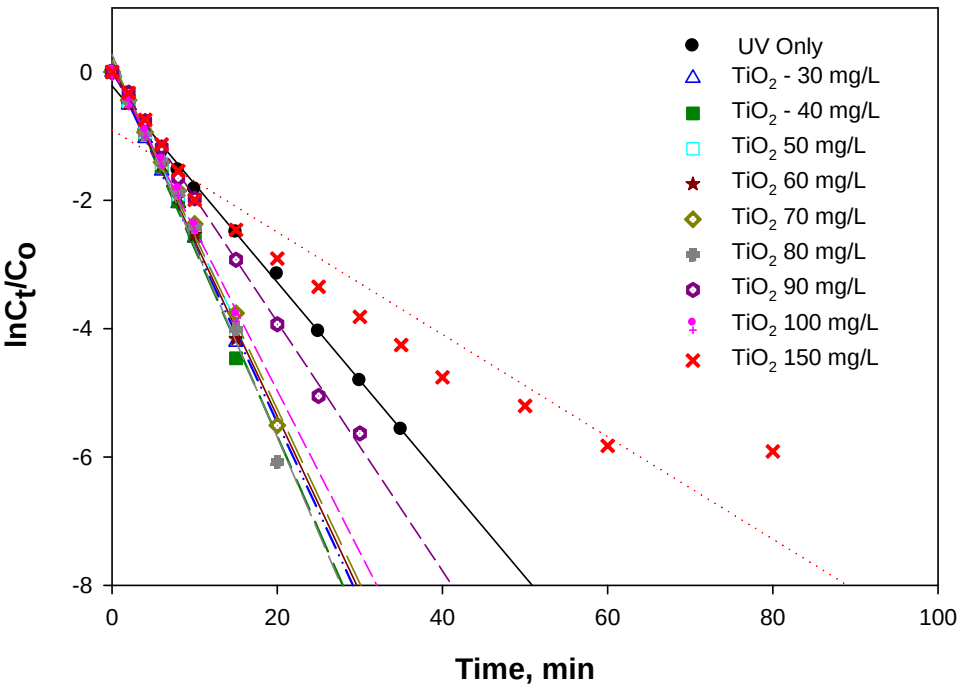

Figure 5.18: First order linear transforms of ln C_t/C_o for phenol (30 mg/L) with TiO_2 concentrations of 0-100 mg/L (aerated).

Table 5.5: First order kinetic parameters for phenol (30 mg/L) degradation with catalyst concentration of 0 – 150 mg/L in aerated and non-aerated system.

$[TiO_2]$ (mg/L)	Aerated			Non Aerated		
	k (min^{-1})	$t_{½}$ (min)	r^2	k (min^{-1})	$t_{½}$ (min)	r^2
UV Only	1.530	4.53	0.997	0. 401	17.29	0.963
30	2.766	2.51	0.996	0. 335	20.69	0.955
40	2.922	2.37	0.988	0. 310	22.36	0.940
50	2.669	2.60	0.993	0. 432	16.05	0.952
60	2.736	2.53	0.994	0. 427	16.23	0.952
70	2.711	2.56	0.993	0.459	15.10	0.955
80	2.979	2.33	0.985	0. 510	13.59	0.846
90	1.939	3.57	0.997	0. 425	16.31	0.959
100	2.516	2.75	0.997	0. 381	18.19	0.944
150	2.253	3.08	0.904	--	--	--

The encouraging results for the degradation of phenol, mono-substituted chloro and the nitro derivatives of phenol to levels below detection limits indicate that photocatalysis is a promising technology for the removal of these compounds from polluted water with careful choice of reaction conditions to ensure the complete mineralisation of not only the pollutant but the intermediates formed during the process of degradation. In a study of comparison of different advanced oxidation methods for phenol degradation, Esplugas and co-workers obtained degradation pseudo first order rate constant of 0.582 h^{-1} and half-life of 1.19 hours with initial phenol concentration in the range of 90 – 100 ppm. (Esplugas *et al*, 2002). Direct comparison of results for both studies will be misleading as the reaction conditions differ greatly.

CHAPTER SIX

DEGRADATION OF TASTE AND ODOUR COMPOUNDS — USING GEOSMIN AS A MODEL

6.1 Rationale of Geosmin Study

The enticing possibility of a greener solution of complete mineralisation of taste and odour causing compounds in water makes photocatalysis a very interesting technology that could be incorporated into the treatment train. The degradation process was studied in batch using geosmin as the model compound. Photocatalytic degradation of geosmin was conducted using reactor configuration B (Figure 3.1). Initial concentration of geosmin in the studies was chosen based on levels detected in the environment. These were determined in source waters at Rietvlei and Roodeplaat Water Treatment and were evaluated over an 11 months period (Table 4.2).

Geosmin solutions were prepared in ultrapure water and geosmin photocatalytic degradation was evaluated using 40 mg/L TiO_2 using two light exposure conditions under a low pressure lamp (9 W UV lamp) and medium pressure lamp (400 W UV lamp). The initial results showed that the catalytic process performed best in the system irradiated using the medium pressure (400 W) UV lamp. Titanium dioxide was then varied over a range of concentrations (40-100 mg/L), irradiated with the medium pressure UV lamp; and with titanium dioxide only in the absence of UV radiation – used as control.

6.2 Methodology of Geosmin Study

To obtain parameters for system optimization, studies were conducted to test the effects of geosmin concentration, concentration of titanium dioxide catalyst, and the presence of ionic species on the performance of photocatalytic degradation. Results of analysis of intermediates formed during degradation gave an insight to the mode of fragmentation of the cyclic compound in water which will form a framework for understanding of degradation pathways in similar and more complex organic pollutants. The extent of contribution of reactive

hydroxyl radical specie (˙OH) to degradation was examined by conducting photocatalytic experiments in the presence of radical scavenger, tertiary butanol (t-BuOH).

Slight modifications were made to the reactor configuration for more effective cooling of the heat generated by the UV lamp. Photocatalytic degradation of geosmin was conducted in a slightly modified reactor configuration. The setup consisted of 2 L glass reactor (Pyrex® glass (Corning, NY); with the UV lamp enclosed in a double walled quartz sleeve. Temperature in the reactor was controlled by circulating the cooling water through the outer jacket of the double walled quartz sleeve. The schematic of the modified reactor is presented in Figure 3.1 as configuration B. The reactor contents were continually aerated at a flow rate of 10 mL/min using an air Flow Meter and a perforated quartz disc or a quartz rod. Dissolved oxygen (DO) was measured with an HQ30d DO Meter.

Aliquots (12 mL) were withdrawn from the reactor at predetermined intervals and filtered through 0.22 µm syringe filters (Millipore). 10 mL of the filtered solution was analysed in the GC/MS after the addition of 3 g of salt; and 0.5 mL of t-butanol. Tertiary butanol was added as a radical scavenger to prevent further degradation by hydroxyl radicals in solution during analysis. Total reaction time in all instances was 60 minutes. GC/MS conditions used to monitor the progress of degradation of geosmin are listed in Table 3.4. The SIR scan parameters used for this set of analysis are as presented in Table 3.6b.

6.3 Efficiency of Photocatalysis Degradation Geosmin

For practical application purposes, maximization of the photonic efficiency of a photocatalytic system depends on optimized conditions in the photoreactor. One of the key parameters is the catalyst concentration, since concentration strongly influences the photonic efficiency of the lamp and subsequently the destruction rates (Lawton *et al*., 2003; Herrmann, 1999).

6.3.1 Effect of catalyst concentration on degradation efficiency

Rapid degradation was obtained at all catalyst concentrations studied after 40-60 minutes of treatment. Degradation rates of geosmin increased with an increasing catalyst concentration to an optimum of 60 ppm above which a reduction in rates was observed as shown in Table

6.1. Degradation to below lowest detectible concentration was achieved at catalyst concentration of 60 ppm after 40 min of treatment (Figures 6.1).

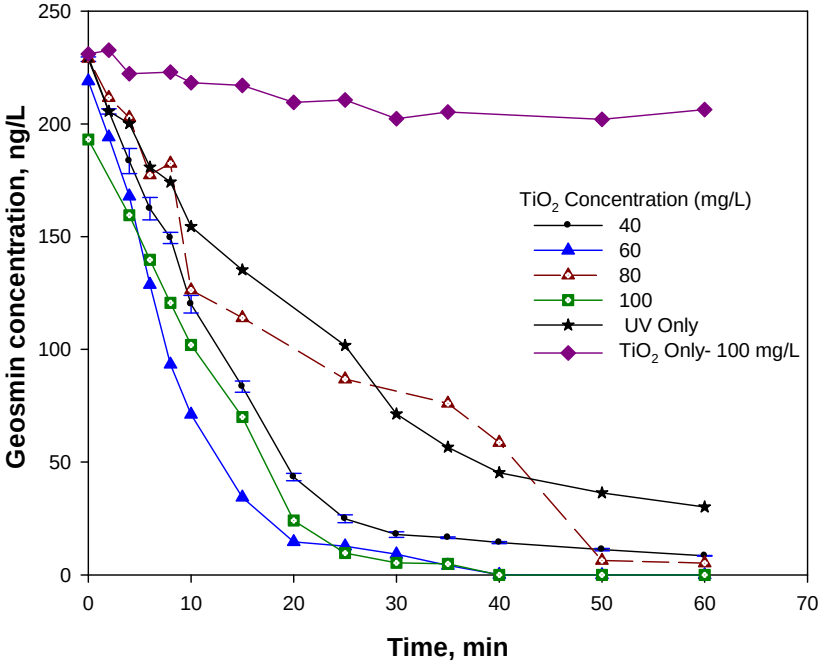

Figure 6.1: Photolytic and photocatalytic degradation profiles of geosmin (220 ng/L) with TiO_2 concentrations of 0 – 100 mg/L in an aerated system.

Though literature showing the effect of catalyst loading for geosmin photocatalytic degradation is lacking, the general observed trend reflects an increase in organic degradation rate with an increasing catalyst concentration to a maximum beyond which a negative effect is observed due to screening of light by the catalyst particles dispersed in water (Serpone, 1997; Herrmann, 1999). Similar trends have been reported from other studies on photocatalytic degradation of phenolics (Barakat, Tseng and Huang 2005; Hong *et al*., 2001; Serpone, 1997) and for the degradation of phenol in the present study as shown in Figures 5.3 and 5.4.

Table 6.1: Initial rates, rate constants, adsorption constant and photonic efficiencies of the various systems for geosmin degradation.

Reaction Conditions	R_i (ng/L min^{-1})	k x 10^{-2} (ng/L min^{-1})	R^2	K x 10^{-3} (ng/L $^{-1}$)	δ x 10^{-3}
TiO_2 40 mg/L /UV – 9W	3.31	1.03	0.98	4.58	7.77 x10^{-3}
TiO_2 40 mg/L /UV - 400W	7.26	6.21	0.97	4.47	1.85 x10^{-3}
TiO_2 60 mg/L /UV - 400W	14.78	15.50	0.87	4.61	4.61 x10^{-3}
TiO_2 80 mg/L /UV - 400W	10.27	5.80	0.84	4.39	1.72 x10^{-3}

Treating geosmin with the catalyst alone (100 mg/L) in the dark achieved less than 8% removal from solution (Figure 6.1) which gives a strong indication that the success of degradation of the organic pollutants is dependent on the availability of reactive radical species in solution and on the catalyst surface. Overall removal in the range of 92-100% was observed in the batches spiked with 220 and 440 ng/L and 10 µg/L (Figure 6.1, 6.2) with photocatalysis. Treating geosmin at the same concentrations (220, 500 ng/L and 10 µg/L) with photolysis alone achieved 86% removal. Residual geosmin from solutions spiked with 220 ng/L after 60 min of treatment of 30 ng/L, was still significantly above the human detection threshold. This implies that UV photolysis would not be an effective stand-alone method for the degradation of geosmin.

6.3.2 Effect of Pollutant Concentration of Degradation Rates

Increasing geosmin concentration from 220 ng/L to 440 ng/L resulted in a decrease in the efficiency of the photocatalytic system as degradation of geosmin below detection limit was not achieved after 60 minutes of treatment (Figure 6.2) even with catalyst concentration of 60 mg/L which was determined to as an optimum catalyst concentration for geosmin degradation with 220 ng/L. It is interesting to note that UV photolysis on geosmin with initial geosmin concentration of 440 ng/L achieved 86% degradation as that with the initial geosmin

concentration of 220 ng/L. This might suggest that for geosmin photolytic degradation could proceed at rates that are independent of initial geosmin concentration with the UV radiation conditions used in the study.

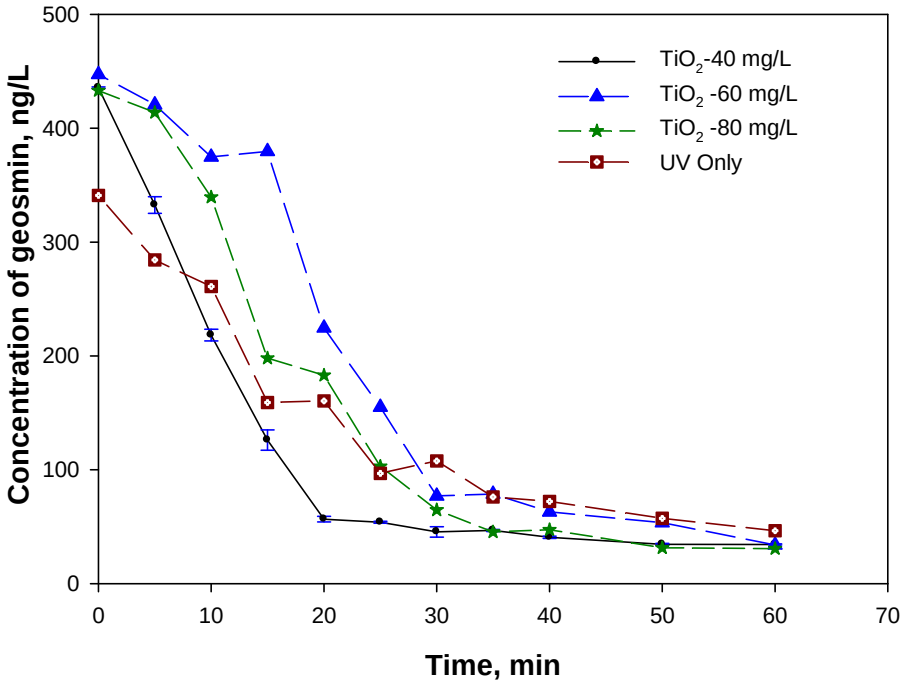

Figure 6.2: Degradation profiles of geosmin (440 ng/L) with TiO_2 concentrations of 0 – 80 mg/L.

Though photocatalysis achieved degradation for solutions of geosmin (220 ng/L) in 40 minutes of treatment with catalyst concentration of 60 mg/L to levels below the lowest detectable concentrations, degradation of geosmin in solutions containing initial concentration of 440 ng/L of geosmin achieved about 92% after 60 minutes of treatment.

6.3.3 Effect of Ionic Species on Degradation Kinetics of Geosmin

The presence of ionic species in water can affect the degradation efficiency of a photocatalytic system positively or negatively depending on the type of ionic species present and the type of interaction that occurs between the ionic species and reactive species in solution, particularly their interaction with hydroxyl radicals in solution. Common ionic species in water include CO_3^{2-}, HCO_3^-, Cl^- and SO_4^{2-}. The effect of bicarbonate and sulphate ions in solution on the degradation efficiency of geosmin was examined at geosmin

concentrations of 220 ng/L and 500 ng/L with the optimum TiO_2 concentration of 60 mg/L. The degradation profile of geosmin (220 ng/L) in the presence of a range of bicarbonate (0.001- 0.1M) and sulphate (0.1M) ions is presented in Figure 6.3.

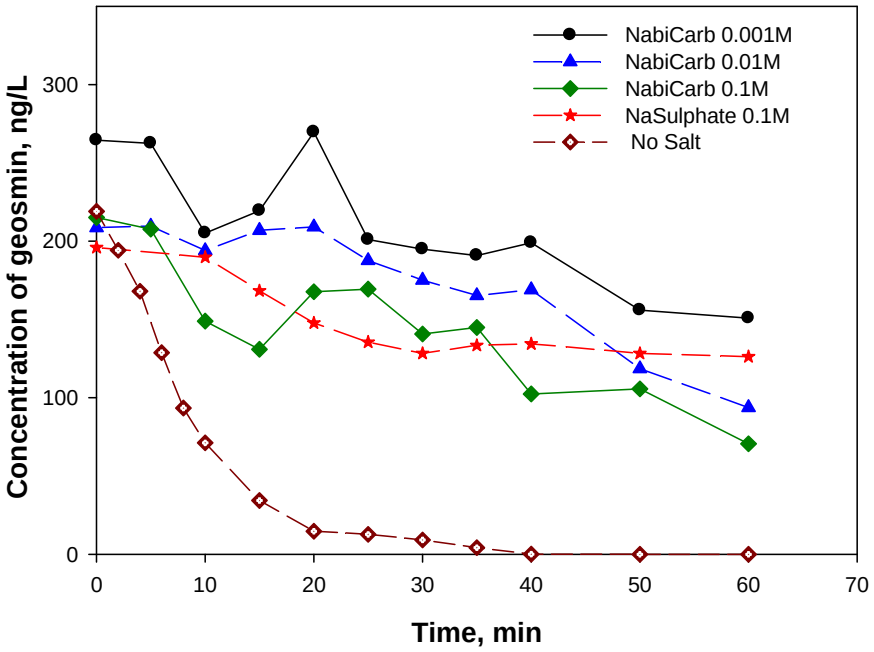

Figure 6.3: Degradation profile of geosmin in the presence of ionic species. Conditions – geosmin 220 ng/L, TiO_2 60 mg/L, UV 400 W, air – 10 mL/min.

Degradation profile of geosmin at an initial concentration of 220 ng/L in the absence of ionic species is also presented in Figure 6.3 for comparison. Degradation rates calculated for, and percentages degraded after 60 minutes of reaction are presented in Table 6.2. The presence of bicarbonate in solution had a negative impact on the degradation efficiency of geosmin with the effect more prominent at lower initial geosmin concentration of 220 ng/L than at 500 ng/L. Degradation rates of geosmin (220 ng/L) decreased from 5.47 ng/(L.min) in the absence of bicarbonate to 1.90 mg/(L.min) when degradation was carried out in the presence of 0.001M HCO_3^- in solution typical of bicarbonate concentrations in natural surface waters. Percentages degraded decreased from 100% to 43% for geosmin at initial concentration of 220 ng/L; and 92% to 77% for initial geosmin concentrations of 500 ng/L.

Table 6.2: Impact of ionic species on degradation efficiency of geosmin.

Ionic Species	Geosmin 220 ng/L		Geosmin 500 ng/L	
	Final Rates	% Removed	Final Rates	% Removed
HCO_3^{2-} 0.001M	1.90	43	6.60	75
HCO_3^- 0.01M	1.92	55	4.86	77
HCO_3^- 0.1M	2.41	67	1.90	56
SO_4^{2-} 0.1M	1.16	36	-	-
None	5.47	100	6.89	92

Degradation rates could be affected by contributions from intermediates formed in-situ in solution that would naturally compete for reactive species in solution, a factor that was not considered in the calculation of the rates for the determination of effects of ionic species. Trans *et al.*, (2009) in their study on the effect of bicarbonate reported a small negative effect of bicarbonate to degradation efficiency of geosmin at an initial concentration of 250 ng/L from degradation rates calculated for the first 30 minutes. Ionic effects impacted rates more significantly at lower pollutant concentrations, as the effects were less prominent when geosmin concentration was increased from 220 to 500 ng/L. This can be attributed to the lower ionic specie/pollutant ratio at higher pollutant concentrations.

6.4 Intermediates of Geosmin Degradation

The intermediates formed during photocatalytic degradation of geosmin are yet to be established though studies on intermediates from the microbial degradation of geosmin have been reported (Saito *et al.*, 2005). Geosmin is a bicyclic` tertiary alcohol (Figure 6.4) with mainly single covalently bonded sp^3—sp^3 (C—C) bonds with bond energies of 83-85 kcal mol^{-1}; sp^3—O (C—O) bond with bond energies of 85-91 kcal mol^{-1}; sp^3—H (C—H) bond with bond energies of 96-99 kcal $mol^{-1}$and an O—H bond with energies 110-111 kcal mol^{-1} (Smith and March, 2006). UV light with λ_{max} at 365 nm has energy of 78.28 kcal mol^{-1}, which is of the same order of magnitude and comparable with bond energies in geosmin structure. There is a possibility of photolytic bond cleavage when exposed to hydroxyl radicals in solution and to photons at 365 nm, with the most susceptible bonds been the C—O and the C—C bonds. Cleavage of the C—O bond would lead to a more stable tertiary carbocation making it the

most susceptible point of attack followed by an adjacent hydrogen abstraction which would lead to two possible dehydration products - (1*S*,4a*R*)-1,4a-dimethyl-1,2,3,4,4a,5,6,7-octahydronaphthalene (product II) and (R)-4a,8-dimethyl-1,2,3,4,4a,5,6,7-octahydronaphthalene (product III); with the elimination of water (Figure 6.4).

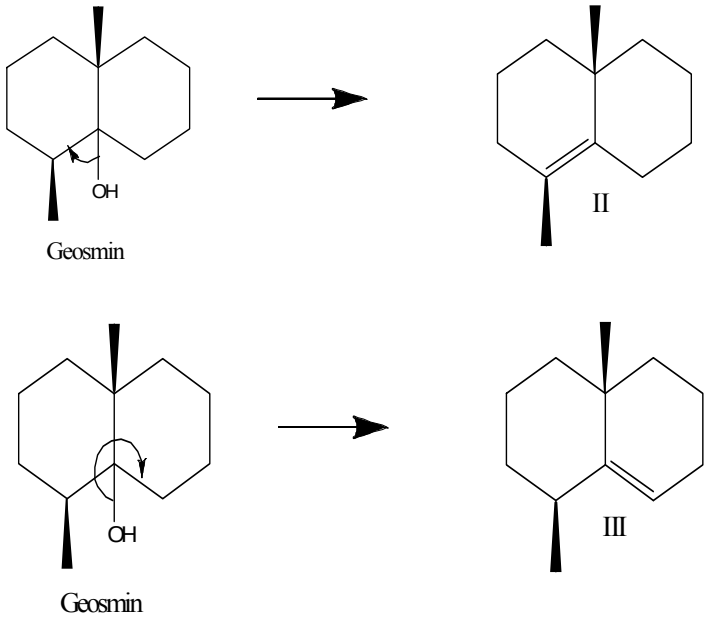

Figure 6.4: Structures of geosmin and dehydration Products II and III.

During the process of photocatalytic degradation of geosmin in solution, bond fission is possible at all C─C bond cites with subsequent decyclization of the ring structure of both geosmin and the dehydration products II and III, and skeletal rearrangement leading to the formation of a collection of acyclic saturated and unsaturated compounds. GC/MS data obtained for solutions of geosmin halfway through the degradation process revealed the possible identity of some intermediate compounds formed form photocatalytic decyclization and C─C. These tentatively identified intermediate compounds are presented in Table 6.3.

Table 6.3: GC/MS data of geosmin and some tentatively identified intermediate compounds from photocatalytic degradation of geosmin.

Chemical formula	Compound No. in Figure 6.5	Retention Time (Min)	Match Probability	Major Ions for Identification
$C_{12}H_{22}O$(geosmin)		24.98	Standard	112,41,55,111,125,43,97
C_8H_{16}	V	15.64	824	41,31,55,57,70,83
$C_7H_{14}O$	VI	24.06	759	43,71,56,55,41,39
$C_6H_{12}O_2$	VII	24.06	766	43,71,55,41,39
$C_7H_{12}O$	VIII	15.64	751	41,31,55,57,70,83

Degradation intermediates suggested from GC/MS analysis include 3,5-dimethlyhex-1-ene(V), which would most likely be a product of ring fission at positions indicated in Figure 6.5 (IV). Other intermediate products suggested include 2,4-dimethlypentan-3-one (VI), 2-methylethylpropanoate (VII), 2-heptanal (VIII) (Figure 6.5).

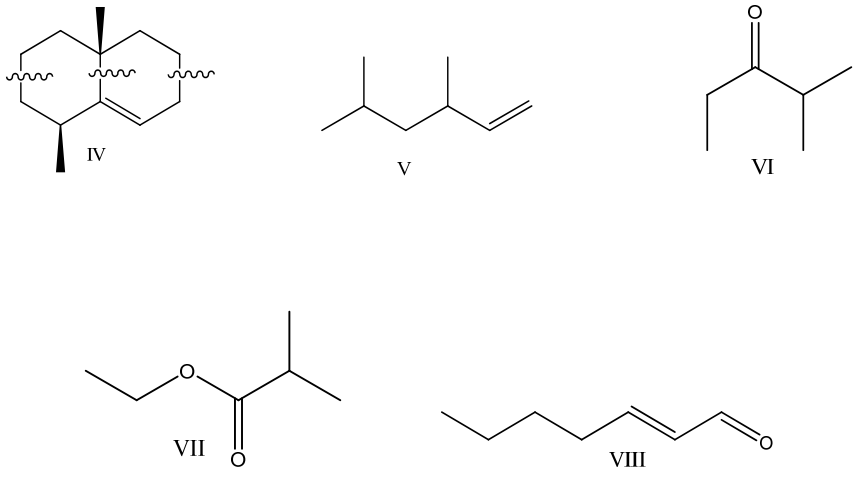

Figure 6.5: Structures of some GC/MS tentatively identified intermediates from the degradation of geosmin.

Cleavage of the C─C bonds of the terminal methyl group (bond a) with the elimination of methane would produce a transient intermediate product (X), further cleavage of methyl group (b) from product X yields intermediate products XII and XIII and XII) (Figure 6.6).

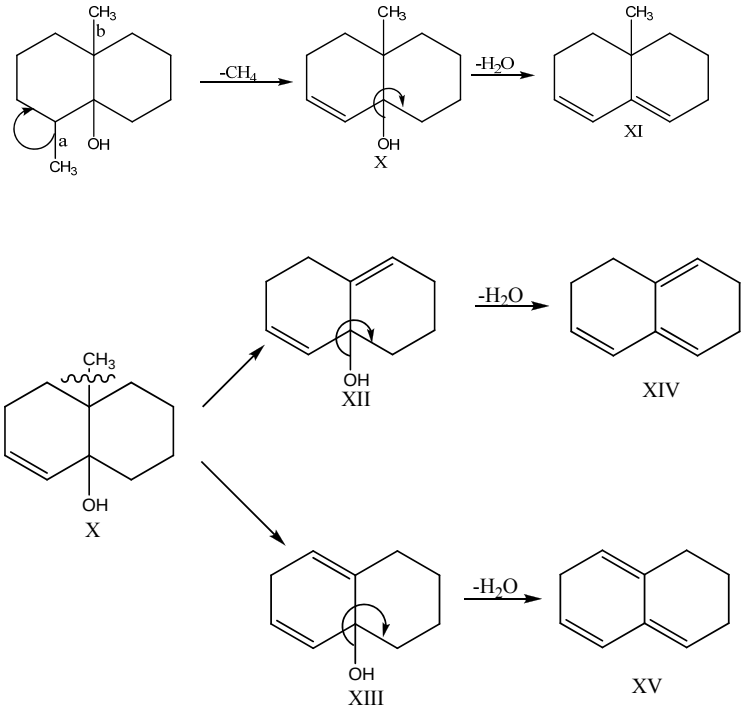

Figure 6.6: Structure of geosmin and possible products from the elimination of methane.

Elimination of water from intermediate products X, XII and XIII which on decyclization from C─C bonds cleavage would account for the acyclic hydrocarbons listed in Figure 6.5.

Though under the reaction conditions for the analysis of intermediates, total mineralisation was not obtained, the intermediate products tentatively identified are not known priority pollutants and are not listed in the U.S.EPA list of priority pollutants (U.S.EPA, 2011). The presence of the intermediates compounds is of no serious concern as degradation to non-detectible concentrations of geosmin and intermediate products, formed during photocatalysis of environmentally significant levels of geosmin was achieved under optimum conditions (Chirwa and Bamuza-Pemu. 2010). Higher than environmentally significant concentrations of Geosmin of 10 µg/L used for this component of the study was chosen to avoid the total mineralisation zone to allow the study of transitional compounds before complete mineralisation to CO_2 and H_2O. Also less than optimal catalyst concentrations were used in

the current study, reaction conditions were chosen to attempt the identification of intermediates formed during degradation rather than achieving mineralisation during degradation.

6.5 Degradation Pathway Analysis

Degradation of organic pollutants during photocatalysis is often attributed to the hydroxyl radical oxidation. However, UV photolysis is also used as a stand-alone method for water treatment and from the theory of photocatalysis, the positive holes generated are capable of oxidation of organic compounds in water. The dominant of these degradation pathways is not fully established. To obtain better understanding of the degradation pathway for geosmin, degradation studies were conducted under three experimental conditions:

- Photolysis – with UV irradiation with 400W UV lamp
- Photocatalysis with 400W UV lamp and anatase TiO_2 (40 mg/L); and
- Photocatalysis with 400W UV lamp and anatase TiO_2 (40 mg/L) in the presence of t-butanol (a radical scavenger).

Degradation of organic compounds by photocatalysis is often attributed to reaction with highly reactive hydroxyl radicals generated in solution (Lawton *et al*., 2003), the current study indicates that there is synergic contribution of the three possible reactive paths leading to the rapid degradation of geosmin in solution. This can be attributed to the significant level of degradation achieved with UV radiation alone in the absence of the catalyst. However, reaction rate constants obtained for the reactions where hydroxyl radicals in solution were quenched by the introduction of tertiary butanol indicate that the dominant reactive pathway is via oxidation by hydroxyl radicals in solution. This is consistent with findings by Trans *et al*., (2009) in their study on the effect of ionic species on the photocatalytic degradation efficiency of geosmin. This is due to the very high oxidative potential of hydroxyl radicals (2.8 V), which is higher than most other oxidants with the exception of fluorine. The presence of oxygenated degradation products (VI-VII) – Figure 6.5; rather than only products from bond cleavage is also an indication of the presence of oxidative species in solution.

Control experiments with the catalyst only (100 mg/L) in the absence of UV radiation gave no appreciable reduction in geosmin concentration (Figure 6.1), indicating that reduction in

geosmin concentration is due to the suggested reactive pathways and no significant losses from evaporation and other unidentified sources occurred.

6.6 Photolytic Degradation Kinetics

The reactive component in the presence of UV light was earlier determined to be the hydroxyl radicals ($^{\bullet}OH$) generated from the splitting of water by electromagnetic waves (Schwarzenbach *et al*., 2003). The rate of reaction of any compound will therefore be dependent on the availability of reactive sites, i.e., a concentration will be reached when the amount of reactant in the system exceeds the amount of hydroxyl radicals ($^{\bullet}OH$) produced at which point the amount of reactant supplied is at equilibrium with the amount of oxidant. The saturation kinetics can thus be applied in a system with increasing reactant concentration as follows:

$$v = \frac{kC \cdot C_{\bullet OH}}{K_C + C} \tag{6.1}$$

where C = concentration of geosmin (ML^{-3}) at time t, $C_{\bullet OH}$ = concentration of hydroxyl radicals (ML^{-3}) generated at the given UV light intensity, v = geosmin oxidation rate ($ML^{-3}T^{-1}$), k = reaction rate coefficient (T^{-1}), and K_C = half velocity concentration of geosmin (ML^{-3}). In the above equation, the multiple of the degradation rate coefficient (k) and the maximum achievable hydroxyl radical concentration ($C_{\bullet OH}$) yields the maximum reaction rate coefficient, $v_{max} = k \cdot C_{\bullet OH}$ ($ML^{-3}T^{-1}$).

In this study, a much lower concentration of geosmin was evaluated in the ngL^{-1} range. Under these conditions, geosmin concentration could be much lower than the half velocity concentration, $K_C >> C$, such that the group $k \cdot C_{\bullet OH}/K_C$ becomes constant and Equation 6.1 is reduced to the first order form:

$$v = \left(\frac{k \cdot C_{\bullet OH}}{K_C} \right) \cdot C \tag{6.2}$$

Equation 6.2 is evaluated using the experimental data by plotting $\ln(C/C_o)$ versus t and the slope is a constant $k \cdot C_{\bullet OH}/K_C$ represented by the pseudo constant k' (T^{-1}).

The data from three sets of experiments at initial concentrations 220 ng/L, 500 ng/L and 10 µg/L was evaluated and the closeness of fit was demonstrated by the high values of regression coefficient (r^2) (Figure 6.8, Table 6.4). The model fitness confirms that indeed the driving factor of photolytic degradation for geosmin is the hydroxyl radical. The results show that the degradation rate coefficient *k'* was relatively constant regardless of the initial concentration of geosmin used in this range which further confirms the relevance of the photolytic reaction via hydroxyl radical oxidation as represented by Equations 6.1 and 6.2 above.

6.7 Photolytic Reaction with Particle Surface Catalysis

Particles contribute to light attenuation in a water sample, both by light absorption and scattering. Depending on which effect is predominant, the rate of direct photolysis of a dissolved species in a given system may be decreased or enhanced (Schwarzenbach *et al*., 2003). Experimental observations in the case of titanium dioxide (TiO_2) showed a marked increase in degradation of geosmin. The enhanced degradation in the presence of TiO_2 particles was attributed to the possibility of extra oxidation reactions occurring near or at the solid semiconductor surfaces. Preliminary inspection of degradation rate kinetics in the presence of TiO_2 showed that phenol degradation complied with and can be adequately described by the first order reaction rate kinetics as shown by the linear plots of ln C_t/C_o (Figure 5.17 and 5.18) for the aerated and non-aerated systems. On the other hand, it is apparent that geosmin degradation in the presence of the TiO_2 particles did not comply completely with the first-order reaction rate kinetics (data not shown) as indicated by low r^2 values of 0.77-0.89. At the moment, the uncertainty on the amount of $^{\bullet}OH$ generated affects the reliability of the model. However, the stability in the parameter *k'* could serve as an indirect indicator of the stability in this parameter.

Since the observed increase in geosmin degradation was at best minimal, we assume reaction rate limitation of the overall removal of geosmin associated with the particles. In other words, the rate at which geosmin molecules reach the reaction sites superseded the rate of conversion at the sites. A concurrent reaction analogous to the Langmuir equation (Equation 5.2) must then occur at the particles as follows:

$$v_s = \frac{k_q \cdot K_q C_s}{1 + K_q C_s} \cdot M_s \qquad (6.3)$$

where k_q = maximum specific surface degradation rate coefficient (T^{-1}), K_q = surface affinity coefficient (L^3M^{-1}), C_S = concentration at the particle surface (ML^{-3}), M_S = concentration of catalysis in the system (ML^{-3}). If the mass of the catalysis is not changing, then the group of terms $k_qK_qM_S$ will be constant and can be replaced by the pseudo constant value $k_q' = k_qK_qM_S$ (T^{-1}). The concentration at the surface Cs is a function of the bulk liquid concentration C and is influenced by the diffusion rate coefficient and amount of catalysis in the system. If the two reactions, photolytic degradation and catalytic degradation, occur simultaneously, the system cannot be solved algebraically, thus a numerical solution is achieved using the Computer Program for the Identification and Simulation of Aquatic Systems AQUASIM 2.01 (AQUASIM™, EAWAG, Dübendorf, Switzerland). The fitness of the model is demonstrated by the reasonably good fit (Figure 6.7) with non-linear regression coefficients ranging from 0.95-0.99 (Table 6.4). The optimum surface affinity coefficient K_q for all batches tested was near constant at K_q = 4.55±0.03 L/mg.

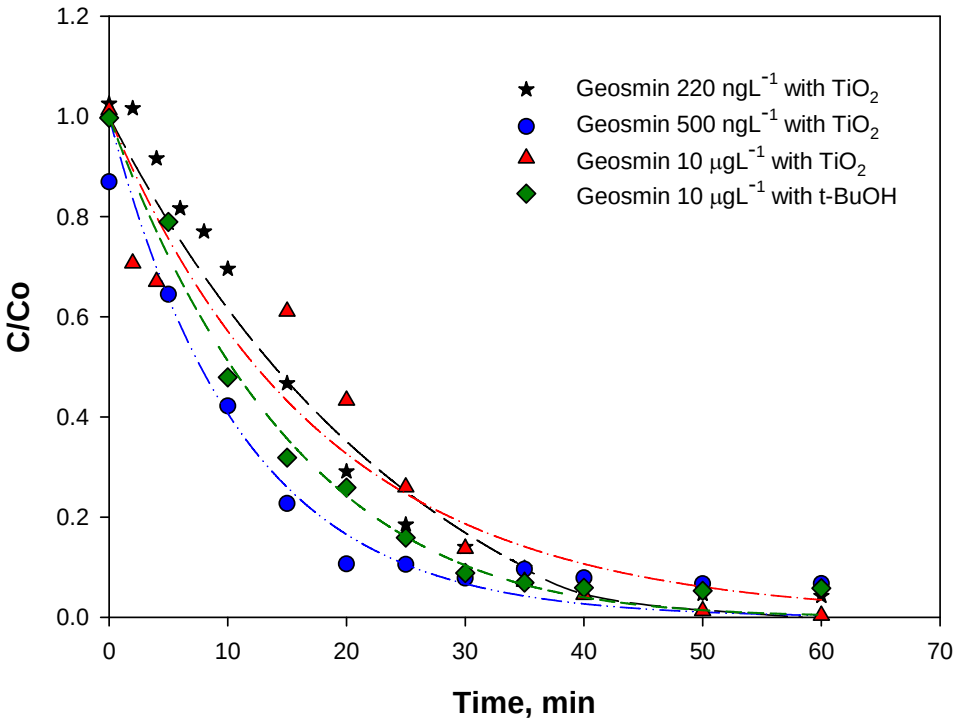

Figure 6.7: Photocatalytic model for geosmin.

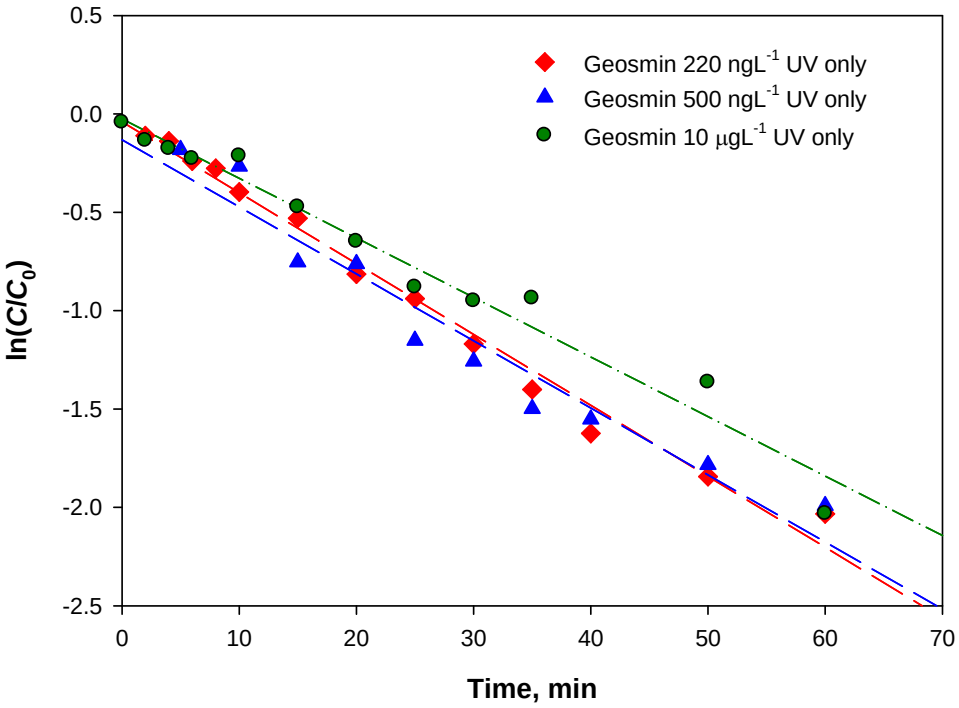

Figure 6.8: Photolytic model for geosmin.

Table 6.4: Geosmin degradation kinetics fitting the photolytic and surface reaction model.

Initial Concentration ngL^{-1}	Experimental Conditions	Degradation Rate Coefficient k' (min^{-1})	Surface Reaction Coeff. k_q' (min^{-1})	Extinction Factor - •OH F_x (ng/ng)	Regression Coefficient r^2
220	UV Only	0.036	--	--	0.987
500	UV Only	0.034	--	--	0.947
10,000	UV Only	0.030	--	--	0.970
220	TiO_2/UV	0.021	0.099	--	0.892
500	TiO_2/UV	0.036	0.090	--	0.964
10,000	TiO_2/UV	0.055	0.027	--	0.937
10,000	TiO_2/ UV/t-BuOH[a]	0.038	0.055	2.554	0.982

[a] Experiment with the •OH scavenger t-BuOH.

The system was also tested on the phenol degradation systems as shown in Figure 6.9 for the phenolic system, the parameters for the disappearance of the parent compound were affected by the shielding effect of –OH group on the activity on the nearest functional group in the benzene ring structure.

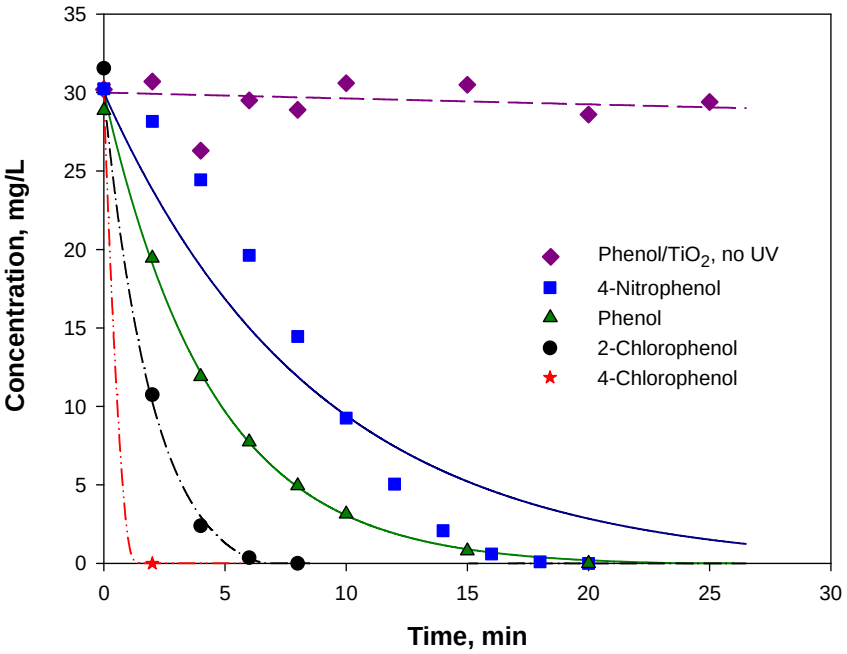

Figure 6.9: Photocatalytic model for phenol and derivatives of phenol.

The results show generally an increase in the reaction rate coefficients with increasing relative distance of the –Cl group from the –OH group (Table 6.5), this could be due to positive mesomeric effect of the chloro subsequent attached to the aromatic ring.

Table 6.5: Kinetics of degradation of phenolic compounds fitting the photolytic and surface reaction model.

Name of Compound	Photo-Degradation Rate Coeff. k' (min^{-1})	Surface Reaction Coeff. k_q' (min^{-1})	Surface Affinity Coeff. (L/mg)	χ^2
Phenol (Control)	0.00014	3.12	n.d.	57.57
Phenol	0.224	6.35	199.60	1.48
2-Chlorophenol	0.493	6.75	9.78	2.93
4-Chlorophenol	0.787	9.91	0.43	18.93
4-Nitrophenol	0.114	5.75	219.50	127.90

n.d. – non-determinable

However, the negative inductive effect is more prominent with the ortho than the para chloro subsequent as the impact of inductive effect decreases with the increasing distance. Environmentally significant concentration of geosmin (220 ng/L) was completely mineralised from solution by photocatalysis, while photolysis alone achieved about 86% degradation of

geosmin regardless of initial concentration of geosmin. Degradation in solution is attributed to the synergic contribution from hydroxyl radicals (•OH), photolysis and reactive positive holes though results from kinetic analysis suggest that hydroxyl radical (•OH) as the critical reactant in the system. Thus engineering of the photolytic/photocatalytic system could focus on maximising oxidative potential by enhancing the processes responsible for generating •OH. Presence of ionic species reduces photocatalytic degradation efficiency of geosmin.

Kinetic parameters obtained from the photolytic and photocatalytic model for geosmin obtained in this study could not be compared with other values in literature as no studies on photolytic modelling on particle surface for geosmin were found in literature as at the time of reporting these results.

CHAPTER SEVEN

CONCLUSION AND RECOMMENDATIONS

7.1 Conclusion

A study of the results from laboratory experiments obtained from both degradation studies of phenol, mono substituted phenols and geosmin has led to the following conclusions and recommendations.

1. The study shows that the degradation of phenol, chlorophenol and nitrophenol in the photo-reactor followed first-order kinetics for photolytic reaction (UV only) and mixed-order kinetics for the reaction catalysed by TiO_2 semiconductor particles.
2. The trend of dehalogenation and its effects on degradation of phenol and its substituted derivatives was determined. Presence of the highly electronegative chloro-group on phenol greatly improves degradation rates of phenol.
3. Results from degradation of phenol suggest that catechol, resorcinol and hydroquinone are the three main aromatic intermediates formed. Catechol, resorcinol and hydroquinone are the aromatic intermediates formed from phenol degradation but are completely removed from solution minutes after phenol is completely degraded in solution.
4. Degradation of geosmin in the photo-reactor also followed first-order kinetics for photolytic reaction (UV only) and mixed-order kinetics for the reaction catalysed by TiO_2 semiconductor particles.
5. Intermediate products obtained from rapid photolytic/photocatalytic degradation of geosmin in solution were also tentatively identified.
6. The results show that geosmin undergoes rapid ring opening and subsequent bond cleavage at multiple sites to produce acyclic saturated and unsaturated compounds including some alkanones and esters.
7. Degradation below lowest detectible concentrations was achieved in batches operated at low geosmin and phenol concentrations. Complete degradation of intermediates accumulated at higher initial geosmin concentration could require longer reaction times or additional stages if used in a continuous flow process.

8. The kinetic analysis results suggest the hydroxyl radical (•OH) as the critical reactant in the system. Thus engineering of the photolytic/photocatalytic system could focus on maximising oxidative potential by enhancing the processes responsible for generating •OH. Degradation in solution is attributed to the synergic contribution from hydroxyl radicals (•OH), photolysis and reactive positive holes.
9. Kinetic parameters obtained from the photolytic and photocatalytic model for geosmin obtained in this study could not be compared with other values in literature as no studies on photolytic modelling on particle surface for geosmin degradation were found in literature as at the time of reporting these results.
10. Lessons learnt can be applied to the degradation of similar organic compounds of environmental concern.

7.2 Recommendations

For practical purposes, the cost related to power input using electricity powered radiation sources could be lowered by using solar energy (UV radiation from the sun) and engineering effective plates to harness this readily available power source. Some configurations of solar plates are now available commercially and can be tested for in replacement of the artificial UV light sources.

The catalyst in the dispersed form presents the problems of separation of the catalyst from solution and reduction in efficiency at high catalyst concentrations due to turbidity as a result of screening effect of the photons of light by excess catalyst particles. Further research is necessary to test the performance of the system with fixed phase catalyst, by exploring a variety of substrates that can be used as support for the fixed phase. The catalyst in the fixed phase has the additional advantage of the possibility of reuse of the fixed film. Focus in the effort to obtain suitable fixed film configurations should be geared towards maximising surface area of the catalyst available to photons of light and contact with pollutants in solution.

Geosmin degradation intermediates formed in solution could be quantified for better understanding of the formation and degradation pattern of the suggested intermediates in solution. Verification and quantification of intermediates can be achieved by analysing varied

concentrations of standard solutions by GC/MS. Corresponding individual calibration graphs can be obtained for each intermediate from which concentrations of intermediates formed in solution can be obtained by analysing aliquots withdrawn from the reactor at regular time intervals. This information can be pooled together to give a formation/ degradation profile for each intermediate in solution.

Further studies could be conducted with the pollutants from actual polluted waste water streams or source water to determine the effect of presence of other pollutant matrix on the degradation efficiencies of the compounds under study

Total Organic Carbon (TOC), Chemical Oxygen Demand (COD) and Dissolved Organic Compound (DOC) measurements during degradation studies will give conclusive information as to the total mineralisation of parent pollutants and intermediate compounds formed during degradation.

Profiling of the degradation intermediates of 2-chlorophenol, 4-chlorophenol and nitrophenol should give vital information as to the effect of the presence of substituent groups on the degradation rates of phenol. Information on the cleavage pattern of the chloro, nitro and hydroxyl substituents on the benzene aromatic ring could provide relevant information that can be used to predict degradation patterns of substituted aromatic compounds and the relative effects of the presence of such substituents on the system.
Testing the system with a continuous flow configuration would be a step forward to bridging the gap from the laboratory to the possibility of incorporation in the water treatment train as it would give necessary kinetic parameters needed for s system scale-up.

REFERENCES

Abe K. and Tanaka K. (1997) Fe^{3+} and UV-enhanced ozonation of chlorophenolic compounds in aqueous medium. *Chemosphere* **35** 2837-2847.

Ahmed S. Rasul M.G, Martens W.N., Brown R., Hashib M.A. (2010) Heterogeneous photocatalytic degradation of phenols in wastewater: A review on current status and developments. *Desalination* **261** 3-18.

Alapi T. and Dombi A. (2006) *Comparative study of the UV and UV/VUV photolysis of phenol in aqueous solution by using different types of low-pressure mercury lamps. International Conferenceon Ozone and UV, Berlin, Germany*.

Alnuaimi M.A., Rauf M.A. and Ashraf S.S. (2007) Comparative decolouration study of Neutral Red by different oxidative processes. *Dyes and Pigment* **72** (3) 367-371.

Alvarez D.A., Stackelberg P.E., Petty J.D., Huckins E.T., Furlong E.T., Zaugg S.D. and Meyer M.T. (2005) Comparison of a novel passive sampler to standard water-column sampling for organic contaminants associated with wastewater effluents entering a New Jersey stream. *Chemosphere* **61**, 610-622.

Andreozzi R., Caprio V. and Insola A. (1996) Kinetics and Mechanisms of polyethyleneglycol fragmentation by ozone in aqueous solution. *Water Research* **30** 2955 -2960.

Andreozzi R., Caprio V., Insola A. and Marotta R. (1999) Advanced oxidation processes (AOP) for water purification and recovery. *Catalysis Today* **53** 51-59.

Andreozzi R., Caprio V., Insola A., Marotta R. and Sanchirico R. (2000) Advanced oxidation processes for the treatment of mineral oil-contaminated wastewaters. *Water Research* **34** (2) 620-628.

Ashok B.T., Saxena S., Singh K.P. and Musarrat J. (1995) Biodegradation of polycyclic aromatic hydrocarbons in soil around Mathura oil refinery, India. *World Journal of Microbiology and Biotechnology* **11** (6) 691-692.

Apha (1995) *Standard methods for the examination of water and wastewater*. 18th ed. Washington D.C. American Public Health Association 1995.

Auguglisto V., Litter M., Palmisano l. and Soria J. (2006) The combination of heterogenous photocatalysis with chemical and physical operations: A tool for improving the photoprocess performance. *Journal of Photochemistry and Photobiology C*: **7** 127-144.

Bacaloni A., Cafaro C., De Giorgi L., Ruocco R. and Zoccolillo L. (2004) Improved analysis of polycylic aromatic hydrocarbons in atmospheric particulate matter by HPLC-fluorescence. *Annali di Chimica* **94** (9-10) 751-759

Bahnemann D. (2004) Photocatalytic water treatment: solar energy applications. *Solar Energy* **77** 445-459.

Baird, C. (2000) *Environmental Chemistry*. W.H. Freeman & Co., New York.

Bamuza-Pemu E.E. and Chirwa E.M.N. (2012) Photocatalytic degradation of geosmin: degradation pathway analysis. *Water SA* **38** (5) 689-696.

Bamuza-Pemu E.E. and Chirwa E.M.N. (2011) Photocatalytic degradation of geosmin: intermediates and degradation pathway analysis. *10th International Conference on Chemical and Process Engineering),* 8-11May 2011, Florence, Italy.

Bamuza-Pemu E.E. and Chirwa E.M.N. (2010) Photocatalytic degradation of taste and odour causing compounds in natural water sources. *Chemical Engineering Transaction* 23 387-392.

Banerjee A.N., Joo S.W., and Min B-K (2012) Photocatalytic degradation of organic dye by sol-gel-derived gallium-doped anatase titanium oxide nanoparticles for environmental remediation. *Journal of Nanomaterials, Volume 2012, Article ID 201492, 14 pages. doi:10.1155/2012/201492*

Bao M-L, Barbieri K., Burrini D., Griffini O. and Pantani F. (1997) Determination of trace levels of taste and odour compounds in water by microextraction and gas chromatography-ion-trap detection-mass spectrometry. *Water Research* **31** (7) 1719-1727.

Barakat M.A., Tseng J.M. and Huang C.P. (2005) Hydrogen peroxide-assisted photocatalytic oxidation of phenolic compounds. *Applied Catalysis B: Environmental* **59** 99-104.

Basson M.S., Van Niekerk P.H. and Van Rooyen J.A. (1997) *Overview of water resources availability and utilisation in South Africa*. Department of Water Affairs and Forestry, Pretoria.

Bauer R., Waldner G., Fallmann H., Hager S., Klare M., Krutzler T., Malato S. and Maletzk P. (1999) The photo-Fenton reaction and the TiO2/UV process for wastewater treatment-novel developments. *Catalysis Today* **53** 131-144.

Beltrán F.J., Rivas FJ and Montero-De-Espinosa R. ((2002) Catalytic ozonation of oxalic acid in an aqueous TiO_2 slurry reactor. *Applied Catalysis B: Environmental* **39** 221-231.

Bourgeois J.C., Walsh M.E. and Gagnon G.A. (2004) Treatment of drinking water residuals: comparing sedimentation and dissolved air flotation performance with optimal cation ratios. *Water Research* **38** (5) 1173-1182.

Brugger A. (2000) Reuse of Filter backwash water using ultrafiltration technology. *Filtration Separation* **37** (1) 22-26.

Buchanan W., Roddick F. and Porter N. (2004) Enhanced biodegradability of UV and VUV pre-treated natural organic matter. *Water Science and Technology: Water Supply* **4** (4) 103-111.

Buchanan W., Roddick .F and Porter N. (2006) Formation of hazardous by-products resulting from the irradiation of natural organic matter: Comparison between UV and VUV irradiation. *Chemosphere* **63** 1130-1141.

Busca G., Berardinelli S., Resini C., Arrighib L. (2008) Technologies for the removal of phenol from fluid streams: A short review of recent developments. *Journal of Hazardous Materials* **160** 265–288.

Carmichael W.W. (2001) Human fatalities from cyanobacteria: Chemical and Biological cyanotoxins. *Environmental Health Perspectives* **109** 663-668.

Černigoj U., Štangar U.L. and Trebše P. (2007) Evaluation of a novel carberry type photoreactor for the degradation of organic pollutants in water. *Journal of Photochemistry and Photobiology A: Chemistry* **118** 169-176.

Ceronio A.D., Basson N.D., Kruger M., Taljaard C., Bauman C.M. and Haarhoff J. (2002) The in-depth evaluation of three filtration facilities. *Water SA Special Edition: WISA Proceedings* 6-9.

Chang S.M., Hou C.Y., Lo P.H., Chang C.T. (2009) Preparation of phosphated Zr-doped TiO_2 exhibiting high photocatalytic activity through calcination of ligand-capped nanocrystals. *Applied Catalysis B: Environmental* **90** 233–241.

Chemspider *http://www.chemspider.com/Chemical-Structure.20474023.html* - Last accessed 10 May 2012.

Chen D., Weavers L.K. and Walker H.W. (2006) Ultrasonic control of ceramic membrane fouling by particles: Effect of ultrasonic factors. *Ultrasonics Sonochemistry* **13** 379–387.

Chen D., Weavers L.K. and Walker H.W. (2006) Ultrasonic control of ceramic membrane fouling by particles: Effect of particle characteristics. *Water Research* **40** 840-850.

Chen Y. and Dionysiou D.D. (2006) Correlation of structural properties and film thickness to photocatalytic activity of thick TiO_2 films coated on stainless steel. *Applied Catalysis B: Environmental* **69** 25-34.

Chirwa E.M.N. and Bamuza-Pemu E.E. (2010). *Investigation of photocatalysis as an alternative to other advanced oxidation processes for the treatment of filter backwash water*. WRC Report No 1717/1/10, Water Research Commission, Gezina, South Africa. Available online at *http://www.wrc.org.za/Pages/KnowledgeHub.aspx*. Last accessed 29/12/2012, 19:00.

Collivignarelli C., Sorlini S. and Riganti V. (2002) *Proceedings of VI Simpósio Ítalo Brasileiro de Engenharia Sanitária e Ambiental*. 1-10.

Colón G., Maicu M., Hidalgo M.C. and Navío J.A. (2006) Cu-doped TiO_2 systems with improved photocatalytic activity. *Applied Catalysis B: Environmental* **67** 41–51.

Comninellis C., Kapalka A., Malato S., Parsons S.A., Poulios I. and Mantzavinos D. (2008) Perspective – Advanced oxidation processes for water treatment: advances and trends for R&D. *Journal of Chemical Technology and Biotechnology* **83** 769-776.

Contreras S., Rodriguez M., A.L. Momani F., Sans C. and Esplugas S. (2003) Contribution of the ozonation pre-treatment to the biodegradation of aqueous solutions of 2,4-dichlorophenol. *Water Research* **37** 3164-3171.

Daniel J.W., Green T. and Phillips P.J. (1973) Metabolism of the phenolic antioxidant 3,5-di-tert-butyl-4-hydroxanisole (Topanol 354). III. The metabolism in rats of the major autooxidation product, 2,5-di-tert-butyl-1,4-benzoquinone. *Food and Cosmetic Toxicology* **11** (5) 793-796.

Devilliers D. (2006) Semiconductor Photocatalysis: Still an active research area despite barriers to commercialization. *Energeia* **17** (3), 1-6.

Devries S.E., NamikoshI M., Galey F.D., Merrit J.E., Rinehart K.L. and Beasley V.R. (1993) Chemical study of the hepatotoxins from microcystis aeruginosa collected in California. *Journal of Veterinary Diagnostic Investigation* **5** 409-412.

Dijkstra M.F.J., Buwalda H., De Jong A.W.F., Michorius A., Winkelman J.G.M. and Beenackers A.A.C.M. (2001) Experimental comparison of three reactor designs for photocatalytic water purification. *Chemical Engineering Science* **56** 547-562.

Doan H.D., Weli A. and Wu J. (2009) A combined photocatalytic and electrochemical treatment of wastewater containing propylene glycol methyl ether and metal ions. *Chemical Engineering Journal* 151 51–58.

Doll T.E. and Frimmel F.H. (2005) Removal of selected persistent organic pollutants by heterogeneous photocatalysis in water. *Catalysis Today* **101** 195-202.

DWAF (1996) *South African water quality guidelines. Volume 1: Domestic water use*. Pretoria, South Africa.

DWAF (1999) Gazette 20615 of 12th November of 1999, Pretoria, South Africa

El-Bahy Z.M., Ismail A.A. and Mohamed R.M. (2009) Enhancement of titania by doping rare earth for photodegradation of organic dye (Direct Blue). *Journal of Hazardous Materials* **166** 138–143.

EPA (1999), *Drinking Water Treatment*, EPA 810-F-99-013

Eriksson E., Auffarth K., Eilersen A-M, Henze M. and Ledin A. (2003) Household chemicals and personal care products as sources for xenobiotic organic compounds in grey water. *Water SA* **29** (2) 135-146.

Esplugas S., Marco A. and Saum G.L. (1997) How and why combine chemical and biological processes for wastewater treatment. *Water Science and Technology* **35** 321-327.

Esplugas S., Gimenez J., Contretras S., Pascual E. and Rodriguez M. (2002) Comparison of different advanced oxidation processes for phenol degradation. *Water Research* **36** 1034-1042.

European Communities (1980*) Drinking Water Directive 80/778/EEC, Commission of the European Communities*.

Fane J., Macintosh P. and Leslie G. (2006) Chapter 11: *Water reclamation, remediation and cleaner production with nanofiltration*: in *Nanofiltration- principles and application*. Elsevier Limited, Oxford UK.

Fang H.H.P., Chen T., Li Y.Y. and Chui H.K. (1996) Degradation of phenol in wastewater in an up flow anaerobic sludge blanket reactor. *Water Research* **30** 1353-1360.

Fiorentino G., Spaccini R. and Piccolo A. (2005) Separation of molecular constituents from a humic acid by solid-phase extraction following a transesterification reaction. *Talanta* 68 (4) 1135–1142.

Freshour A.R., Mawhinney S. and Bhattacharyya D. (1996) Two-phase ozonation of hazardous organics in single and multicomponent systems. *Water Research* **30** 1949-1958.

Giokas D.L. and Vlessidis A.G. (2007) Application of a novel chemometric approach to the determination of aqueous photolysis rates of organic compounds in natural waters. *Talanta* **71** 288-295.

Gogate P.R., Mujumdar S., Pandit A.B. (2003) Sonochemical reactors for waste water treatment: comparison using formic acid degradation as a model reaction. *Advances in Environmental Research* **7** 283-299.

Gogate P.R. and Pandit A.B. (2004) A review of imperative technologies for wastewater treatment I: Oxidation technologies at ambient conditions. *Advances in Environmental Research* **8** 501-551.

Guidechem - Chemical properties- *http://www.guidechem.com/reference/dic-21115.html#id2* – Last accessed 10 May 2012.

Halmann M.M. (1996) *Photodegradation of water pollutants*. CRC Press Inc, New York, 254-255.

Hamoda M.F., Al-Ghusain I. and Al-Mutairi N.Z. (2004) Sand filtration of wastewater for tertiary treatment and water reuse. *Desalination* **16** 203-211.

Han W., Zhu W., Zhang P., Zhang Y and Li L. (2004) Photocatalytic degradation of phenols in aqueous solution under irradiation of 254 and 185 nm UV light. *Catalysis Today* **90** 319-324.

Harding W.R. and Praxton B.R. (2001) *Cyanobacteria in South Africa*. Water Research Commission WRC report noTT 153/01. Pretoria.

Hassoon S., Bulatov V., Yasman Y. and Schechter I. (2004) Fluorescence monitoring pf ultrasound degradation processes. *Analytica Chimica Acta* **512** 125-132.

Hansson L., Carlson R., and Sjöberg A-L (1990) Synthesis of (±)-geosmin. Part 1. On the synthesis and epoxidation of 1,4a-dimethyl-4,4a,5,6,7,8-hexahydronaphthalen-2(3H)-one. *Acta Chemica Scandinavica* **44** 1036-1041.

Health Canada (2004) *Blue-Green algae (cyanobacteria) and their toxins*. http://hc-sc.gc.ca/ewh-semt/water-eau/drink-potable/cyanobateries-e.html Last accessed 15th September 2007.

Hernandez R., Zappi M., Colucci J. and Jones R. (2002) Comparing the performance of various advanced oxidation processes for treatment of acetone contaminated water." *Journal of Hazardous Materials* **92** 33-50.

Herrmann J. (1999) Heterogeneous photocatalysis: fundamentals and applications to the removal of various types of aqueous pollutants. *Catalysis Today* **53** 115-129.

Hidalgo M.C., Maicu M., Navío J.A. and Colón G. (2008) Study of the synergic effect of sulphate pre-treatment and platinisation on the highly improved photocatalytic activity of TiO_2. *Applied Catalysis B: Environmental* **81** 49–55.

Ho L., Newcombe G. and Croue´ J-P, (2002) Influence of the character of NOM on the ozonation of MIB and geosmin. *Water Research* **36** 511–518.

Hoefel D., Ho L., Monis P.T., Newcombe G. and Saint C.P. (2009) Biodegradation of geosmin by a novel Gram-negative bacterium; isolation, phylogenetic characterisation and degradation rate determination. *Water Research* **43** 2927-2935

Ho L., Hoefel D., Bock F., Saint C.P. and Newcombe G. (2007) Biodegradation rates of 2-methylisoborneol (MIB) and geosmin through sand filters and in bioreactors. *Chemosphere* **66** (11) 2210-2218.

Hoffmann M.R., Martin S.T., Choi W., and Bahnemann D.W. (1995) Environmental applications of semiconductor photocatalysis. *Chemical Reviews* **95** 69-96.

Hong S.S., Ju C.S., Lim C.G., Ahn B.H., Lim K.T. and Lee G.D. (2001) Photocatalytic degradation of phenol over TiO_2 prepared by sol-gel method. *Journal of Industrial and Engineering Chemistry* **7** (2) 99-104.

Huang W-J, Cheng B-L, Hu S-K and Chu C. (2006) Ozonation of algae and odour causing substances in eutrophic waters. *Journal of Environmental Science and Health Part A*, **41**1587-1605.

Hynning P.A. (1996) Separation, Identification and quantification of components of industrial effluents with bioconcentration potential. *Water Research* **30** 1103 – 1108.

Jianlong W., Xuan Z. and Weizhong W. (2004) Biodegradation of phthalic acid esters (PAEs) in soil bioaugmented with acclimated activated sludge. *Process Biochemistry* **39** 1837–1841.

Jüttner F. and Watson S.B. (2007) Biochemical and ecological control of geosmin and 2-methylisoborneol in source waters. *Applied and Environmental Microbiology* **73** (14) 4395–4406.

Jyoti KK and Pandit AB (2001) Water disinfection by acoustic and hydrodynamic cavitation. *Biochemical Engineering Journal* **7** 201-212.

Kasprzyk-Hordern B., Ziółek M. and Nawrocki J. (2003) Catalytic ozonation and methods of enhancing molecular ozone reactions in water treatment. *Applied Catalysis B: Environmental* **46** 639-669.

Khraisheh M., Kim J., Campos L., Al-Muhtaseb A.H., Al-Hawari A., Ghouti M.A. and Walker G.M. (2013) Removal of pharmaceutical and personal care products (PPCPs) pollutants from water by novel TiO2–Coconut Shell Powder (TCNSP) composite. *J. Ind. Eng. Chem.* http://dx.doi.org/10.1016/j.jiec.2013.06.032.

Kitis M. and Kaplan S.S. (2007) Advanced oxidation of natural organic matter using hydrogen peroxide and iron-coated pumice particles. *Chemosphere* **68** 1846-1853.

Klán P. and Vavrik M. (2006) Non-catalytic remediation of aqueous solutions by microwave-assisted photolysis in the presence of H_2O_2. *Journal of Photochemistry and Photobiology A*: *Chemistry* **177** 24-33.

Kluson P., Luskova H., Cerveny L., Klisakova J. and Catjthaml T. (2005) Partial photocatalytic oxidation of cyclopentene over titanium (IV) oxide. *Journal of Molecular Catalysis A: Chemical* **242** 62-67.

Kolb B. and Ettre L.S (2006) *Static headspace-gas chromatography: Theory and practice.* John Wiley publishing, New Jersy, U.S.A.

Kondarides D. (2005) *Encyclopaedia of Life Support Systems* (EOLSS). *www.eolss.net/Sample-Chapters/C06/E6-190-16-00.pdf* Last accessed July, 18th 2012.

Laoufi N.A., Tassalit D. and Bentahar F. (2008) The degradation of phenol in water solution by TiO_2 photocatalysis in a helical reactor. *Global NEST Journal* **10 (**3) 404-418.

Lawton L.A., Robertson P.K.J, Robertson R.F. and Bruce F.G. (2003) The destruction of 2-methylisoborneol and geosmin using titanium dioxide photocatalysis. *Applied Catalysis B: Environmental* **44** 9-13.

Lee C., Yoon J. and von Gunten U. (2007) Oxidative degradation of N-nitrosodimethylamine by conventional ozonation and the advanced oxidation process ozone/hydrogen peroxide. *Water Research* **41** 581-590.

Li S., MA Z., Zhang J., Wu Y. and Gong Y. (2008) A comparative study of photocatalytic degradation of phenol of TiO_2 and ZnO in the presence of manganese dioxides. *Catalysis Today* **139** 109-112.

Liang Z., Zhou G., Lin S., Zhang Y. and Yang H. (2006) Study of low-frequency ultrasonic cavitation fields based on spectral analysis technique. *Ultrasonics* **44** 115-120.

Linde J.J., Freese S.D. and Pieterse (2003) *Evaluation of powdered activated carbon (PAC) for the removal of taste and odour causing compounds from water and the relationship between this phenomenon and the physic-chemical properties of the PAC and the role of water quality*. *A Report for the Water Research Commission (WRC) of South Africa* – 2003.

Linsebigler A.L., Lu G., and Yates J.T., Jr. (1995). Photocatalysis on TiO_2 surfaces: Principles, mechanisms, and selected results. *Chemical Reviews* **95** 735-758.

Liu Y., Chen G., Zhou C., Hu Y., Fu D., Liu J. and Wang Q. (2011) Higher visible photocatalytic activities of nitrogen doped In_2TiO_5 sensitized by carbon nitride. *Journal of Hazardous Materials* **190** 75–80.

Liu G., Wang X., Chen Z., Cheng H.M. and Lu G.Q. (2009) The role of crystal phase in determining photocatalytic activity of nitrogen doped TiO_2. *Journal of Colloid and Interface Science* **329** 331–338.

Liu L., Liu H., Zhao Y-P, Wang Y., Duan Y., Gao G., Ge M. and Chen W. (2008) Directed synthesis of hierarchical nanostructured TiO_2 catalysts and their morphology-dependent photocalysis for phenol degradation. *Environmental Science and Technology* **42** 2342-2348.

Ljubas D. (2005) Solar photocatalysis – a possible step in drinking water treatment. *Energy* **30** 1699-1710.

Lovekamp-Swan T. and Davis B.J. (2003) Mechanisms of phthalate ester toxicity in the female reproductive system. *Environmental Health Perspectives* **111** (2) 139-145.

Maciel R and Sant'anna GL (Jr) and Dezotti M (2004) Phenol removal from high salinity effluents using Fenton's reagent and photo-Fenton reactions. *Chemosphere* **54** 711-719.

Maleki A., Mahvi A.H., Alimohamadi M. and Ghasri A. (2006) Advanced oxidation of phenol by ultraviolet irradiation in aqueous system. *Pakistan Journal of Biological Sciences* **9** (12) 2338-2341.

Maila M.P. and Cloete T.E. (2002) Germination of Lepidium sativum as a method to evaluate polycyclic aromatic hydrocarbons (PAHs) removal from contaminated soil. *International Biodeterioration and Biodegradation* **50** 107-113.

Malato S., Fernández-Ibáñez P., Maldonado M.I., Blanco J. and Gernjak W. (2009) Decontamination and disinfection of waterby solar photocatalytic: Recent overview and trends. Catalysis Today 147 1-59.

Malato S., Blanco J., Alarcón D.C., Maldonado M.I., Fernández-Ibáñez P. and Gernjak W. (2007) Photocatalytic decontamination and disinfection of water with solar collectors. *Catalysis Today* **122** 137-149.

Martens D.A. and Frankenberger Jr. W.T. (1995) Enhanced degradation of polycylic aromatic hydrocarbons in soil treated with an advanced oxidation process – Fentons Reagent. *Journal of Soil Contamination* **4** (2) 175-190.

Matos J., Laine J., Herrmann J.-M., Uzcategui D. and Brito J.L. (2007) Influence of activated carbon upon titania on aqueous photocatalytic consecutive runs of phenol photodegradation. *Applied Catalysis B: Environmental* **70** 461–469.

Matsui, Y. Yoshida T., Nakao S., Knappe D.R.U and Matsushita T. (2012) Characteristics of competitive adsorption between 2-methylisoborneol and natural organic matter on superfine and conventionally sized powdered activated carbons. *Water Research* **46** 4741-4749.

McMurry J. (2012) *Organic chemistry*. Brooks/Cole Publishing Company, California, USA. 8th Ed.

Meepagala K.M., Schrader K.K., Wedge D.E. and Duke S.O. (2005) Algicidal and antifungal compounds from the roots of *Ruta graveolens* and synthesis of their analogs. *Phytochemistry* **66** 2689–2695.

Metcalf and Eddy (2003) *Wastewater Engineering. Treatment and reuse*. McGraw Hill, 4th Ed.

Michalski R. (2003) Toxicity of bromate ions in drinking water and its determination using ion chromatography with post column derivatisation. *Polish Journal of Environmental Studies* **12** (6) 727-734.

Mills A., Morris S. and Davies R. (1993) Photomineralisation of 4-chlorophenol sensitised by titanium dioxide: a study of intermediates. *Journal of Photochemistry and Photobiology A*: Chemistry **70** 183-191.

Mills A. and Lee S. (2004) Semiconductor photocatalysis. In: *Advanced Oxidation Processes for Water and Wastewater Treatment*, Parsons S (ed) IWA Publishing, UK, pp 137-180.

Ministry of Health and Welfare Ordinance No.15 (2000) Ministry of Health and Welfare, Tokyo, Japan. http://www.jicwels.or.jp/water_supply/suido_kankyo_kanren/MHW_no15_020301.pdf

Misra V., Pandey S.D. and Viswanathan P.N. (1998) Chemical approach to study the environmental implications interaction of humic acid and gamma-HCH. *Chemistry and Ecology* **14** 97-106.

Modrzejewska B., Guwy A.J., Dinsdale R. and Hawkes D.L. (2007) Measurement of hydrogen peroxide in an advanced oxidation process using an automated biosensor. *Water Research* **41** 260-268.

Momani F., Sans C. and Esplugas S. (2004) A comparative study of the advanced oxidation of 2,4-dichlorophenol. *Journal of Hazardous Material* **B107** 123-129.

Montgomery D.C. and Runger G.C. (1999) *Applied statistics and probability for engineers*. Wiley, New York. 2nd Ed.

Morais J.L. and Zamora P.P. (2005) Use of advanced oxidation processes to improve the biodegradability of mature landfill leachates. *Journal of Hazardous Material* 181-186.

Mokrini A., Oussi D. and Esplugas S. (1997) Oxidation of aromatic compounds with UV radiation/ozone/hydrogen peroxide. *Water Science and Technology* **35** (4) 95-102.

Morrison A. (1995) Recovery and reuse of filter backwash water. *http://www.environment.gov.au/net/environet.html* Last accessed 2nd October, 2006.

Munter R (2001) Advanced oxidation processes – current status and prospects. *Proceedings of Estonian Academy Sciences: Chemistry* **50** 59-80.

Nadezhdin AD (1988) Mechanism of ozone decomposition in water. The role of termination. *Indian Engineering Chemistry Research* **27** 548-550.

Naude Y. (2002) The extraction of persistent organic pollutants from samples from selected sites in South Africa. Poster Presentation at *Analitika* 2002, Stellenbosch, South Africa, December 2002.

Pan Pesticides Database - *http://www.pesticideinfo.org/Detail_Chemical* Last accessed 10th Dec 2009.

Pardeshi S.K. and Patil A.B. (2008) A simple route for photocatalytic degradation of phenol in aqueous zinc oxide suspension using solar energy. *Solar Energy* **82** 700-705.

Parida KM and Parija S (2006) Photocatalytic degradation of phenol under solar radiation using microwave irradiation zinc oxide. *Solar Energy* **80** 1048-1054.

Parsons S.A. and Williams M. (2004) *Advanced oxidation processes for water and wastewater treatment*. IWA Publishing, UK.

Perkin Elmer (2008) Turbomatrix headspace sampler and HS 40/110 trap – User's guide, Shelton, U.S.A.

Piccolo A., Conte P. and Tagliatesta P. (2005) Increased conformational rigidity of humic substances by oxidative biomimetic catalysis. *Biomacromolecules* **6** 351-358.

Piccolo A., Conte P., Spaccini R. and Chiarella M. (2003) Effects of some dicarboxylic acids on the association of dissolved humic substances. *Biology and Fertility of Soils* **37** 255-259.

Plummer J.D. and Edzwald J.K. (1998) Effect of ozone on disinfection by-product formation of algae. *Water Science and Technology* **37** (2) 49-55.

Raj C.B.C. and Quen H.L. (2005) Advanced oxidation processes for wastewater treatment: Optimization of UV/H_2O_2 process through a statistical technique. *Chemical Engineering Science* **60** 5305-5311.

Rampaul A., Parkin I.P., O'Neill S.A., DeSouza J., Mills A. and Elliott N. (2003) Titania and tungsten doped titania thin films on glass; active photocatalysts. *Polyhedron* **22** 35-44.

Rand Water – Consumption Patterns. http://www.randwater.co.za/WaterAndInfastructureManagement/Pages/ConsumptionPatterns.aspx

Reddy J.K., Durgakumari V., Subrahmanyam M. and Sreedhar B. (2009) Structure and photocatalytic activity studies of TiO_2-supported over Ce-modified Al-MCM-41. *Materials Research Bulletin* **44** 1540–1546.

Reynolds T.D. and Richards P.A. (1996) *Unit operations and processes in environmental engineering*. PWS. 2nd Ed.

Robertson P.K.J., Lawton L.A., Münch and Rouzade J. (1997) Destruction of cyanobacterial toxins by semiconductor photocatalysis. *Chemical Communications* **3** 393-394.

Rosal R., Rodríguez A., Perdigón-Melón J.A., Petre A. and García-Calvo E. (2009) Oxidation of dissolved organic matter in the effluent of a sewage treatment plant using ozone combined with hydrogen peroxide (O_3/H_2O_2). *Chemical Engineering Journal* **149** 311-318.

Saito A., Tanaka A. and Oritani T. (1996) A practical synthesis of enantiomerically pure (-)-geosmin via highly diastereoselective reduction of (4aS, 8S)-4,4a,5,6,7,8-hexahydro-4a,8-dimethyl-2(3H)-naphthalenone. *Tetrahedron: Assymmetry* **7**(10) 2923-2928.

Sanders R. (2002) University of California, Berkeley, Campus News, Media Relations, Press Release, Popular weed killer demasculinizes frogs, disrupts their sexual development, UC Berkeley study shows, *www.berkeley.edu/news/media/releases/2002/04/15_frogs*.

Serpone N. (1997) Relative photonic efficiencies and quantum yield in heterogenous photocatalysis. *Journal of Photochemistry and Photobiology A: Chemistry* **104** 1-12.

Shin W-T, Mirmiran A., Tiacoumi S. and Tsouris C. (1999) Ozonation using microbubbles formed by electric fields. *Separation and Purification Technology* **15** 217-282.

Shukla P.R., Wang S, Ang H.M. and Tade M.O. (2010) Photocatalytic oxidation of phenolic compounds using zinc oxide and sulphate radicals under artificial solar light. *Separation and Purification Technology* **70** 338–344.

Silva A.M.T., Silva C.G., Joaquim G.D. and Faria L. (2009) Ce-doped TiO_2 for photocatalytic degradation of chlorophenol. *Catalysis Today* **144** 13–18.

Simonsen M.E., Jensen H., Li Z. and Søgaard, E.G. (2008) Surface properties and photocatalytic activity of nanocrystalline titania films. *Journal of Photochemistry and Photobiology A: Che*mistry **200** (2-3) 192-200.

Smejkalova D. and Piccolo A. (2006) Rates of Oxidative Coupling of humic phenolic conomers catalyzed by a ciomimetic iron-porphyrin. *Environmental Science and Technology* **40** 1644-1649.

Smejkalova D. and Piccolo A. (2005) Enhanced molecular dimension of a humic acid induced by photooxidation catalyzed by biomimetic metalporphyrins. *Biomacromolecules* **6** 2120-2125.

Smith M.B. and March J. (2006) *March's Advanced Organic Chemistry: Reactions, Mechanisms, and Structure.* Wiley, New York. 2357 pp.

Sobczyński A., Duczmal Ł. and Zmudziński W. (2004) Phenol destruction by photocatalysis on TiO_2: an attempt to solve the reaction mechanism. *J of Molecular Catalysis A: Chemical* **213** 225–230.

Son S., Ko G. and Zoh K-D. (2009) Kinetics and mechanism of photolysis and TiO_2 photocatalysis of triclosan. *Journal of Hazardous Materials* **166** 954-960.

Song W. and O'Shea K.E. (2007) Ultrasonically induced degradation of 2-methylisoborneol and geosmin. *Water Research* **41** (12) 2672-2678.

Staehelin J. and Hoigné J. (1985) Decomposition of ozone in water in presence of organic solutes acting as promotors and inhibitors of radical chain reactions. *Environmental Science and Technology* **19** 120-126.

Stasinakis A.S. (2008) Use of selected advanced oxidation processes (AOPs) for wastewater treatment – a mini review. *GlobalNEST Journal* **10 (**3) 376-385.

Steiner F., Mcleod F., Rohrer J., Fabel S., Lang L., Qun X. and Jing C. (2008) Determination of phenols in drinking and bottled mineral waters Uusing online solid-phase extraction followed by HPLC with UV detection. *Dionex Product Notes*.

Stocchi E. (1990) *Industrial Chemistry* Vol. I, Ellis Horwood (ed), New York, USA.

Stockinger H., Kut O.M. and Heizle E. (1996) Ozonation of wastewater containing N-methylmorpholine-N-Oxide. *Water Research* **30** 1745-1748.

Sumita T., Yamaki T., Yamamoto S. and Miyashita A. (2001) A new characterization method for photocatalytic activity in semiconductor photocatalysis. *Japanese Journal of Applied Physics* **40** 4007-4008.

Summerfelt, S.T., Sharrer, M.J., Tsukuda, S.M. and Gearheart, M., (2009) Process requirements for achieving full-flow disinfection of recirculating water using ozonation and UV irradiation. *Aquacultural Engineering* 40 (1) 17-27.

Sung Yu-H, Li T.Y. and Huang S.D. (2005) Analysis of earthy and musty odours in water samples by solid-phase micro-extraction coupled with gas chromatography/ion trap mass spectrometry. *Talanta* 65 518-524.

Swanepoel A. and D D Preez H. (2006). An Incident of High Cyanobacteria Concentrations, Causing Large-Scale Problems in Water Purification. *Proceedings Of the 2nd Water Research Showcase,* University of Pretoria, Pretoria, October 2006.

Thoma G.J., Bowen M.L. and Hollensworth D. (1999) Dissolved air precipitation/solvent sublation for oil-field produced water. *Separation and Purification Technology* **16** 101-107.

Tran H., Evans G.M., Yan Y., and Nguyen A.V. (2009) Photocatalytic removal of taste and odour compounds for drinking water treatment. *Water Science and Technology: Water Supply* **9** (5) 477-483.

Tran H., Evans G.M., Yan Y. and Nguyen, A.V. (2008) Photocatalytic removal of geosmin and MIB and its potential applications for drinking water treatment. *Proceedings of the Environment* 08, 5-7 May, Melbourne, Australia.

Tshipala K.E. (2000) *Implications of residual atrazine for wheat*. Master's Thesis submitted to the University of Pretoria.

UN (2005) *Health, Dignity and Development: What will it Take? UN Millenium Project Task Force on Water and Sanitation*, Final Report, Abridged Edition. Stockholm International Water Institute (SIWI) and United Nations Millenium Project, New York, New York.

U.S.EPA (2009) *National Drinking Water Regulations Handbook*. EPA 816-F-09-004

U.S.EPA (2006) Disinfectant Byproducts: A Reference Resource. *http://www.epa.gov/environ/html/icr/gloss_dbp.html* Last accessed 15th September 2007.

U.S.EPA (2006) Polluted Runoff (Non point source pollution)". *http://www.epa.gov/owow/nps/facts/point1.html. Last accessed 05/04/2006*

U.S.EPA (2001) Parameters of water quality – Interpretation and Standards.

U.S.EPA (2000) Hazard Summary – Created in April 1992. *http://www.epa.gov/ttn/atw/hlthef/acetophe.htm* . Last accessed 9th December 2009.

U.S.EPA (1997) Pollution Prevention as Defined Under the Pollution Prevention Act of 1990.

Von Gunten U. (2003) Ozonation of drinking water: Part I. Oxidation kinetics and product formation. *Water Research* **37** 1443-1467.

Vu A.T., Nguyen Q.T., Bui T.H.L, Tran M.C., Dang T.P. and Tran T.K.H. (2010) Synthesis and characterization of TiO_2 photocatalyst doped by transition metal ions (Fe^{3+}, Cr^{3+} and V^{5+}). *Advances in Natural Sciences: Nanoscience and Nanotechnology* **1** 015009 (4pp)

Wadley S. and Waite T.D. (2004) Fenton Processes: In: *Advanced Oxidation Processes for Water and Wastewater Treatment*, Parsons S (ed) IWA Publishing, UK, pp 111-132.

Watkinson A.J., Murby E.J. and Costanzo S.D. (2007) Removal of antibiotics in conventional and advanced wastewater treatment: Implications for environmental discharge and wastewater recycling. *Water Research* **41** 4164-4176.

Watson S.B., Brownlee B., Satchwill T. and Hargesheimer E.E. (2000) Quantitative analysis of trace levels of geosmin and MIB in source and drinking water using headspace SPME. *Water Research* **34**1 (0) 2818-2828.

WHO (1971) *International Standards for drinking water* 3rd ed. Geneva.

WHO (1999) *Toxic Cyanobacteria in Water*: A guide to their public health consequences, monitoring and management.

Wnorowski A.U. (1992) *Taste and odour forming micro-organisms in South African Surface waters.* WRC Report No. 320/1/93

Young W.F., Horth H., Crane R., Ogden T. and Arnott M. (1996) Taste and odour threshold concentrations of potential potable water contaminants. *Water Research* **30** (2) 331-340.

Zaitlin B. and Watson S.B. (2006) Actinomycetes in relation to taste and odour in drinking water: Myths, tenets and truths. *Water Research* **40** 1741-1753.

Zala S.M. and Penn D.J. (2004) Abnormal behaviours induced by chemical pollution: a review of the evidence and new challenges. *Animal Behaviour* **68** 649-664.

Zaleska A., Grabowska E., Sobczak J.W., Gazda M. and Hupka J. (2009) Photocatalytic activity of boron-modified TiO_2 under visible light: The effect of boron content, calcination temperature and TiO_2 matrix. *Applied Catalysis B: Environmental* **89** 469–475.

Zhou H. and Smith D.W. (2002) Advanced technologies in water and wastewater treatment. *Journal of Environmental and Engineering Sciences* **1** 247-264.

Zhou J.L. and Rowland S.J. (1997) Evaluation of the interactions between hydrophobic organic pollutants and suspended particles in estuarine Waters. *Water Research* **31** 1708-1718.

Zoschke K. Engel C., Börnick H. and Worch E. (2011) Adsorption of geosmin and 2-methylisoborneol onto powdered activated carbon at non-equilibrium conditions: Influence of NOM and process modelling. *Water Research* **45** 4544-4550.

APPENDICES

Appendix A:

Table A1: List of organic compounds identified in water samples from Rietvlei and Roodeplaat dams.

S / No.	t_R (min)	Name of Compound (Formula)	Fit	Reverse Fit
		Acid Esters		
1	8.140	Butanoic acid, methylester ($C_5H_{10}O_2$)	844	896
2	14.828	Octadecanoic acid, ethenylester ($C_{20}H_{38}O_2$)	617	654
3	20.087	Propanoic acid, 2-methyl-2,2-dimethyl-1-[2-hydroxylmethyl]propylester($C_{12}H_{24}O_3$)	562	679
4	21.778	2-Methyl-3-hydroxy-2,4,4-trimethylpentylester, propanioc acid	788	820
5	24.834	Propanoic acid, 2-methyl-1-[1,1-dimethyl]-2-methyl-3-propanediylester ($C_{16}H_{30}O_4$)	866	885
		Indenes		
1	17.496	1-Methylene -1H -indene	663	828
1	10.136	[1,3]Diazepan-2,4-dione ($C_5H_8N_2O_2$)	551	656
		Alcohols		
1	16.935	2-Propylcyclohexanol ($C_9H_{18}O$)	556	602
2	18.202	2,2,3,3-Tetramethylcyclopropanemethanol ($C_8H_{16}O$)	688	736

Table A1 continued

S / No.	t_R (min)	Name of Compound (Formula)	Fit	Reverse Fit
		Hydrocarbons		
1	7.645	Octane (C_8H_{18})	897	904
2	8.290	2,5-Dimethylheptane (C_9H_{20})	783	865
3	8.900	4-Methyloctane (C_9H_{20})	874	893
4	9.055	3-Methyloctane (C_9H_{20})	889	891
5	9.706	Nonane (C_9H_{20})	906	908
6	10.076	2,4,6-Trimethylheptane ($C_{10}H_{22}$)	785	903
7	10.281	3,5-Dimethyloctane ($C_{10}H_{22}$)	800	882
8	10.526	Decane ($C_{10}H_{22}$)	786	873
9	11.041	4-Mthyloctane ($C_{10}H_{22}$)	712	917
10	11.206	4-Methylnonane ($C_{10}H_{22}$)	867	872
11	11.291	2-Methylnonane ($C_{10}H_{22}$)	887	888
12	11.461	3-Methylnonane ($C_{10}H_{22}$)	879	889
13	12.222	Decane ($C_{10}H_{22}$)	928	934
14	12.622	2,4,6-Trimethylheptane ($C_{10}H_{22}$)	732	863
15	12.697	4-Ethylheptane (C_9H_{20})	515	746
16	12.697	2,6,7-Trimethyldecane ($C_{13}H_{28}$)	781	874
17	13.692	5-Methyldecane ($C_{11}H_{24}$)	844	844
18	13.787	4-Methyldecane ($C_{11}H_{24}$)	835	845
19	13.902	2-Methyldecane ($C_{11}H_{24}$)	904	908
20	14.066	3-Methyldecane ($C_{11}H_{24}$)	923	932

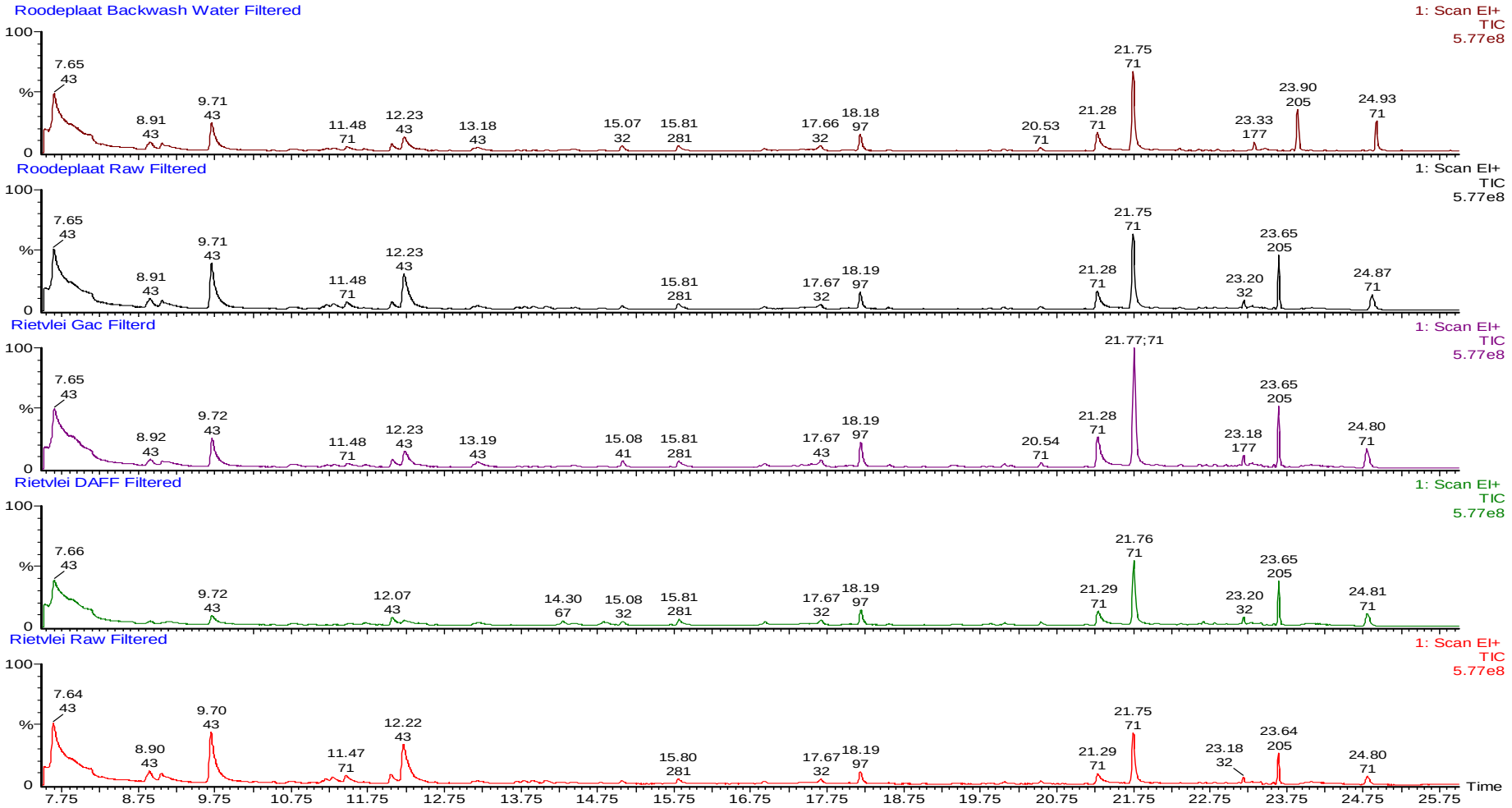

Figure A-1: Chromatogram of water samples from Rietvlei and Roodeplaat.

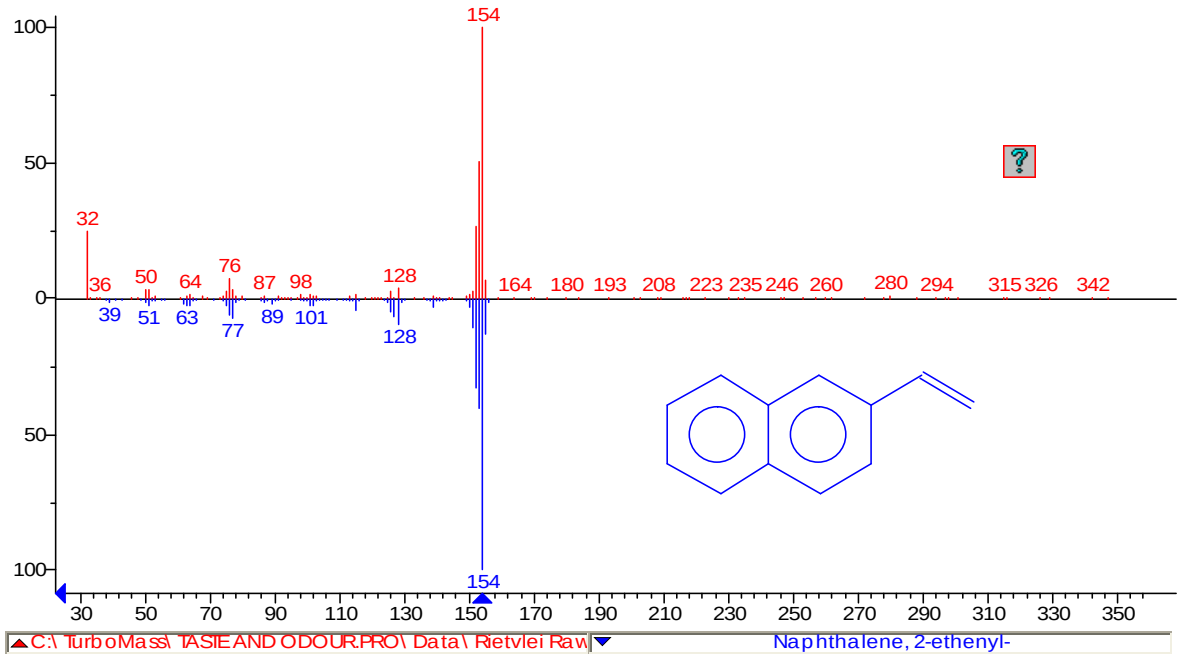

Figure A-2: Spectrum of 2-ethhenylnaphthalene from water samples and the corresponding library match.

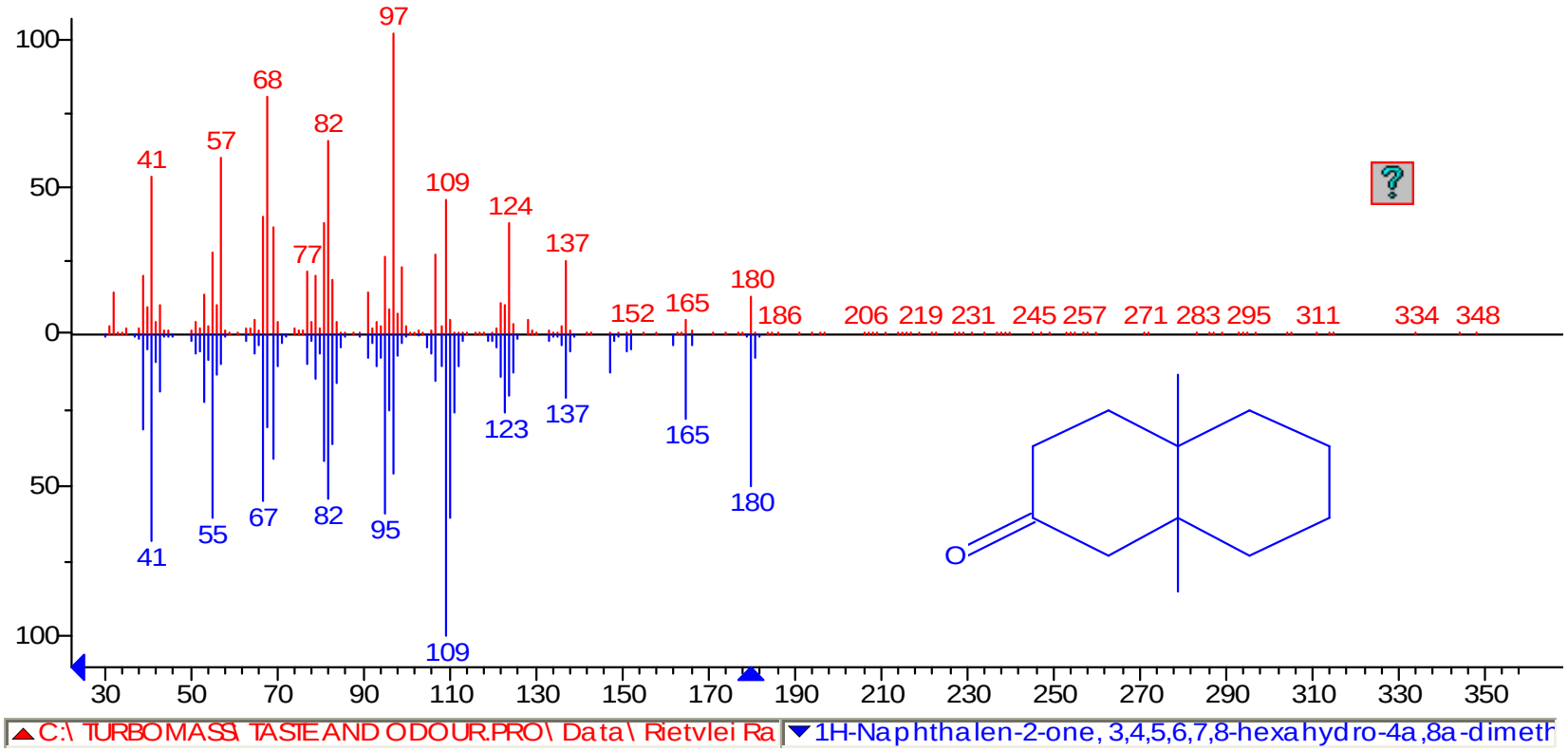

Figure A-3: Spectrum of 3,4,5,6,7,8-hexahydro-4a,8a-dimethyl-1H-naphthalen-2-one from water samples and the corresponding library match.

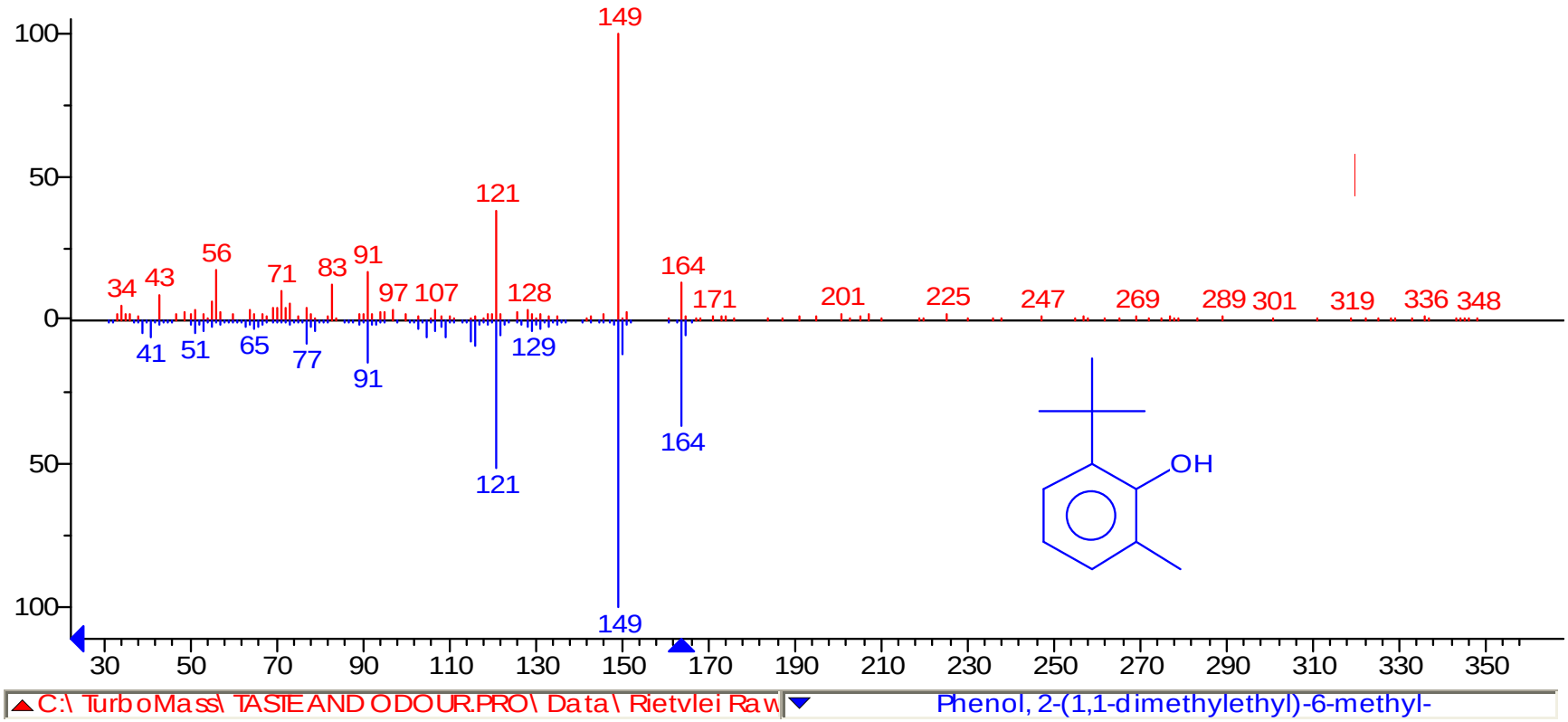

Figure A-4: Spectrum of 2,6-bis[1,1-dimethylethyl]-4-methylphenol (butylated hydroxytoluene) from water samples and the corresponding library match.

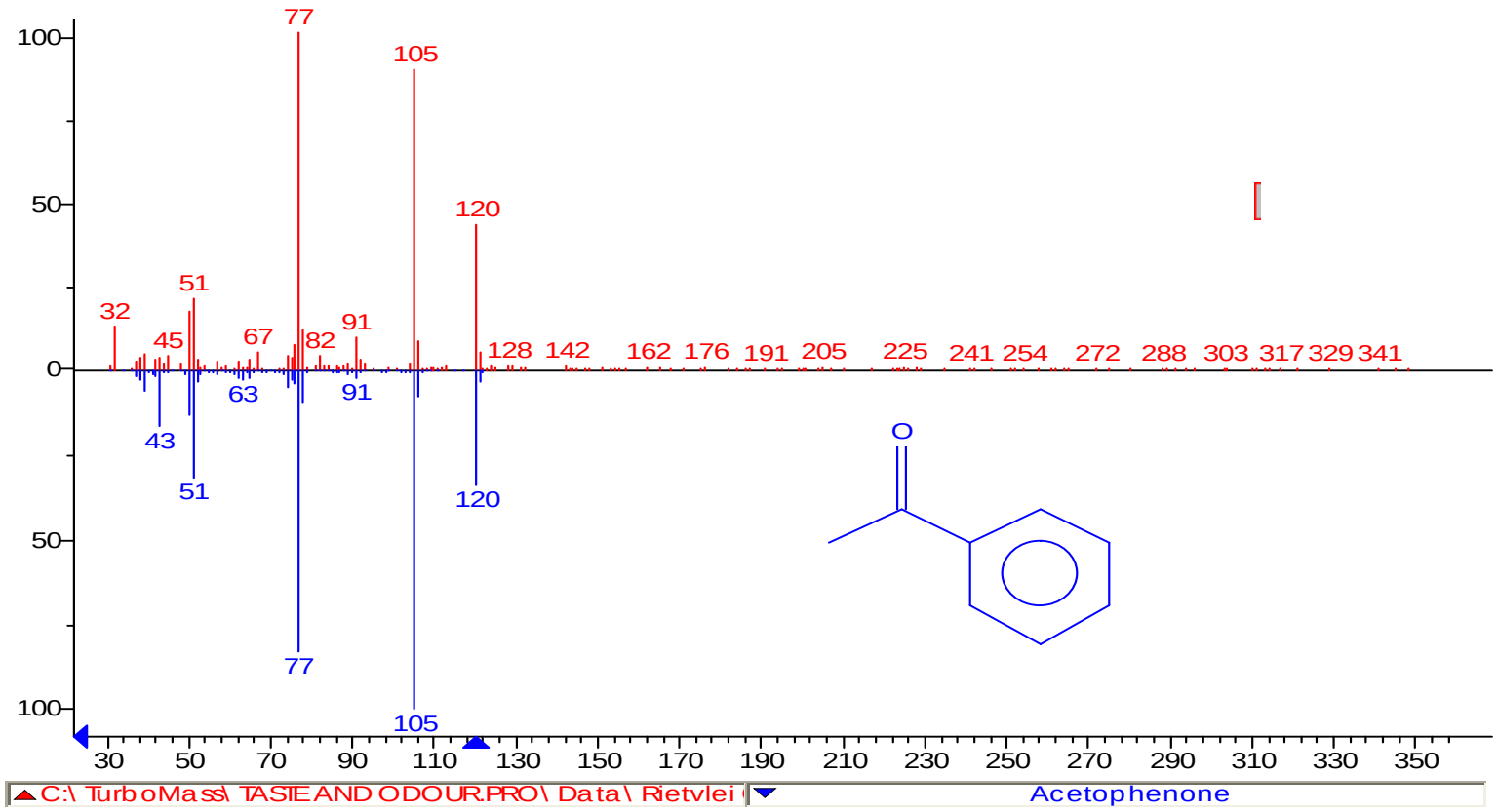

Figure A-5: Spectrum of acetophenone from water samples and the corresponding library match.

Appendix B:

Table B-1: Percentages removed for photolytic; and photocatalytic degradation of 10 mg/L phenol with 400 W, UV lamp and catalyst concentrations of 10-150 mg/L.

	Photolysis		Photocatalysis Degradation of 10 mg/L Phenol with TiO_2 concentrations of 10 – 150 mg/L												
			Catalyst Concentrations and Percentage Removal												
Time (mins)	UV Only	% Removal	10 mg/L	% Removal	20 mg/L	% Removal	30 mg/L	% Removal	40 mg/L	% Removal	50 mg/L	% Removal	100 mg/L	150 mg/L	% Removal
0.00	10.00	0.00	9.90	0.00	9.80	0.00	9.80	0.00	9.25	0.00	9.75	0.00	9.86	9.65	0.00
2.00	5.20	48.00	5.10	48.48	4.50	54.08	5.10	47.96	5.19	43.87			6.14	6.47	32.97
4.00	2.30	77.00	2.40	75.76	2.40	75.51	1.90	80.61	2.36	74.51	2.13	78.11	3.11	4.04	58.20
6.00	1.10	89.00	1.40	85.86	1.20	87.76	1.00	89.80	1.36	85.27	0.95	90.24	1.69	2.32	75.99
8.00	0.60	94.00	0.80	91.92	0.60	93.88	0.53	94.64	0.70	92.41	0.51	94.72	0.85	1.24	87.15
10.00	0.30	97.00	0.50	94.95	0.40	95.92	0.37	96.27	0.51	94.53	0.31	96.85	0.39	0.93	90.33
15.00	**ND	100.00	0.30	96.97	0.30	96.94	0.17	98.26	0.23	97.51	ND	100.00	0.18	0.33	96.60
20.00			0.20	97.98	0.20	97.96	ND	100.00	0.13	98.58			ND	0.35	96.34
25.00			0.30	96.97	0.20	97.96			ND	100.00				0.14	98.55
30.00			0.10	98.99	ND	100.00								ND	100.00
35.00			ND	100.00											

**ND – Not Detected

Table B-2: Percentages removed for photolytic and photocatalytic degradation of 20 mg/L phenol with 400 W, UV lamp and catalyst concentrations of 30-150 mg/L.

Time (mins)	Photolysis		Photocatalysis Degradation of 20 mg/L Phenol with TiO2 concentrations of 30 – 150 mg/L Catalyst Concentrations and Percentage Removal									
	UV Only	% Removal	30 mg/L	% Removal	40 mg/L	% Removal	50 mg/L	% Removal	100 mg/L	% Removal	150 mg/L	% Removal
0.00	20.68	0.00	19.88	0.00	20.79	0.00	20.82	0.00	19.38	0.00	19.16	0.00
2.00	12.43	39.89	11.27	43.34	13.56	34.79	12.21	41.36	12.58	35.10	13.77	28.13
4.00	8.37	59.54	6.63	66.64	8.55	58.90	10.02	51.90	7.95	59.00	9.04	52.81
6.00	5.95	71.22	4.77	75.99	5.80	72.09			5.31	72.59	6.22	67.54
8.00	4.74	77.06	4.01	79.85	4.21	79.77	6.92	66.78	4.06	79.04	4.72	75.35
10.00	4.03	80.53	3.76	81.10	3.47	83.32	4.36	79.04	3.61	81.36	4.16	78.29
15.00	2.98	85.60	2.75	86.19	2.50	87.99	2.32	88.85	2.62	86.47	3.27	82.93
20.00	2.34	88.68	2.17	89.07	2.00	90.38	1.64	92.13	2.00	89.68	2.78	85.50
25.00	1.83	91.15	1.68	91.55	1.56	92.48	1.21	94.17	1.46	92.49	2.22	88.43
30.00	1.47	92.90	1.20	93.96	1.32	93.64	0.73	96.51	1.26	93.49	1.79	90.66
35.00	1.29	93.77	0.89	95.50	1.03	95.04	0.58	97.20	1.00	94.86	1.44	92.48
40.00	0.90	95.64	0.68	96.56	1.04	95.01	0.45	97.84	0.72	96.26	1.16	93.93
50.00	0.54	97.38	0.37	98.12	0.79	96.20	0.20	99.04	0.42	97.82	0.73	96.21
60.00	0.30	98.56	0.18	99.07	0.30	98.56	ND	100.00	0.24	98.78	0.51	97.33
80.00	ND	100.00	ND	100.00	ND	100.00			ND	100.00	0.16	99.16
100.00											0.00	100.00

Appendix C

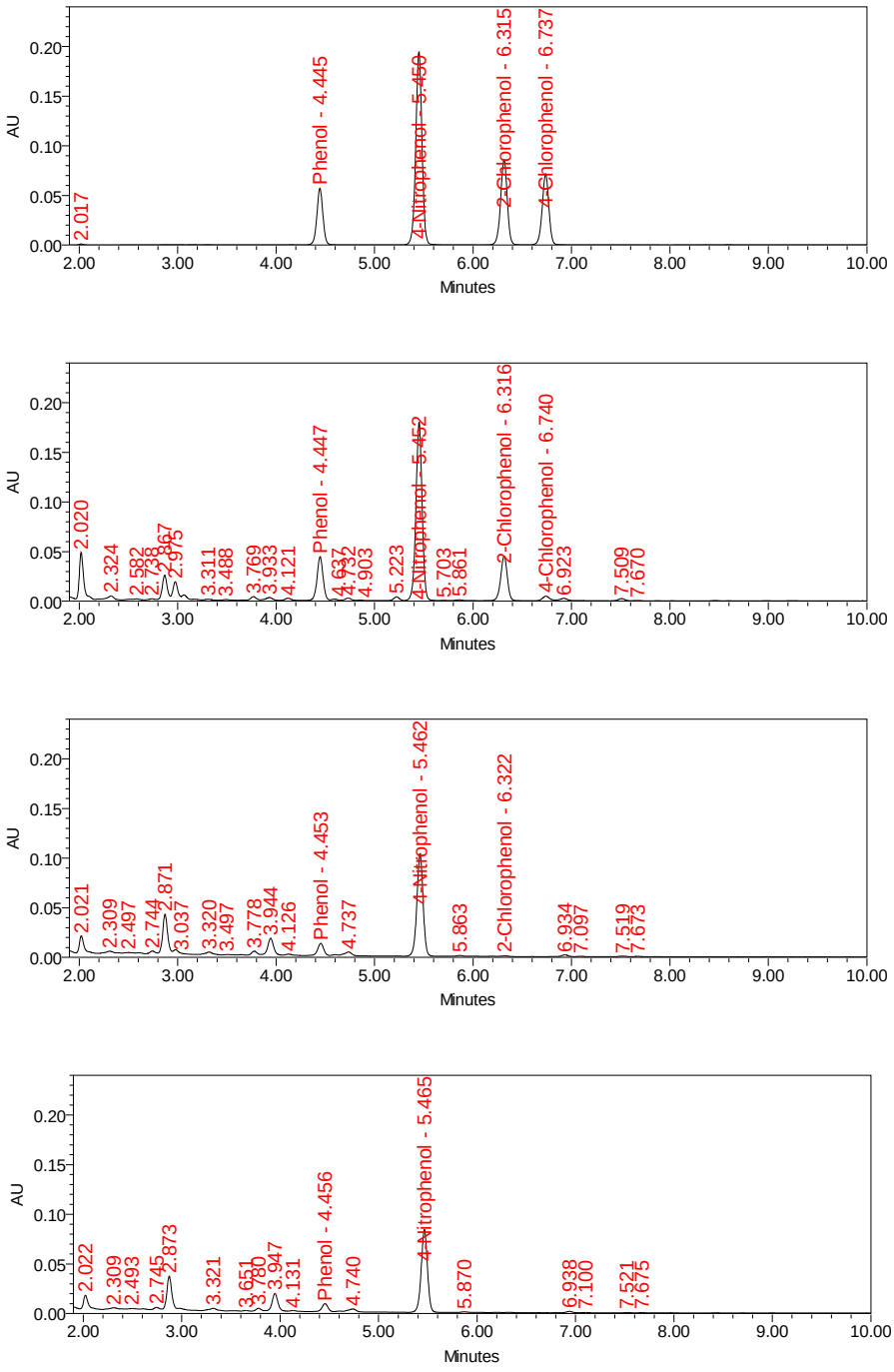

Figure C1: Chromatograms displaying phenol and its derivatives in the course of photocatalysis in a Mixture containing 30 mg/L of each pollutant. Conditions: TiO_2 50 mg/L – UV/Air after 0, 2, 16, and 20 minutes of treatment.

Appendix D

Table D-1: Intermediate formation profile during photocatalysis of phenol (phenol 30 mg/L, UV 400W, TiO_2 30 mg/L, Aerated).

TIME (MINS)	HYDROQUINONE (mg/L)	RESORCINOL (mg/L)	CATECOL (mg/L)	PHENOL (mg/L)
0	0	0	0	30.012
2	0.956	3.716	3.144	17.783
4	0.925	3.668	4.311	10.384
6	0.704	3.433	4.585	6.108
8	0.546	3.456	4.235	3.523
10	0.317	3.338	3.330	1.880
15	0	3.100	1.321	0.049
20	0.059	3.181	0.34	0
25	0.116	0	0	0
30	0	0	0	0

Table D-2: Intermediate formation profile during photocatalysis of phenol (phenol 30 mg/L, UV 400W, TiO_2 40 mg/L, Aerated).

TIME (MINS)	HYDROQUINONE (mg/L)	RESORCINOL (mg/L)	CATECOL (mg/L)	PHENOL (mg/L)
0	0	0	0	30.281
2	1.102	3.578	2.933	18.938
4	1.157	3.475	4.356	11.205
6	0.919	3.416	4.866	6.542
8	0.655	3.295	4.356	3.656
10	0.452	3.108	3.517	1.986
15	0.127	3.216	1.158	0
20	0	0	0	0

Table D-3: Intermediate formation profile during photocatalysis of phenol (phenol 30 mg/L, UV 400W, TiO_2 80 mg/L, Aerated).

TIME (MINS)	HYDROQUINONE (mg/L)	RESORCINOL (mg/L)	CATECOL (mg/L)	PHENOL (mg/L)
0	0	0	0	30.204
2	1.262	3.506	2.953	19.959
4	1.447	3.642	4.707	12.058
6	1.247	3.489	5.208	7.318
8	0.935	3.506	4.838	4.291
10	0.645	3.442	3.935	2.341
15	0.178	3.347	1.397	0.215
20	0.111	0	0.32	0
25	0	0	0	

Table D-4: Catechol formation/degradation rates during photocatalysis of phenol at phenol/TiO_2 concentrations.

Phenol Conc/TiO_2 Conc (mg/L)	Max. Conc Obtained (mg/L)	Time (Mins)#	Formation Rate (mg(L.min))	Rate of Disappearance (mg(L.min))*
Phenol 10/ TiO_2 40	3.197	6	0.5331	0.133
Phenol 10/ TiO_2 50	3.280	4	0.8199	0.126
Phenol 10/ TiO_2 100	4.580	4	1.1449	0.176
Phenol 10/ TiO_2 150	3.422	6	0.2673	0.078
Phenol 20/ TiO_2 30	4.794	4	1.1986	0.063
Phenol 20/ TiO_2 40	4.969	6	0.8282	0.053
Phenol 20/ TiO_2 50	4.553	4	0.7170	0.060
Phenol 20/ TiO_2 100	5.050	6	0.4988	0.054
Phenol 20/ TiO_2 150	5.297	8	0.6621	0.058
Phenol 30/ TiO_2 30	6.946	8	1.1680	0.043
Phenol 30/ TiO_2 40	7.109	6	1.1849	0.044
Phenol 30/ TiO_2 50	6.890	8	0.8612	0.046
Phenol 30/ TiO_2 60	6.251	6	1.0418	0.055
Phenol 30/ TiO_2 70	6.140	8	0.7675	0.055
Phenol 30/ TiO_2 80	6.472	8	0.8090	0.058
Phenol 30/ TiO_2 90	6.395	8	0.7993	0.089
Phenol 30/ TiO_2 100	4.216	8	0.5269	0.046

* - Disappearance rates calculated from time of maximum concentration in solution
# -Time at which maximum concentrations were observed

Table D-5: Resorcinol formation and degradation rates during photocatalysis of phenol.

System Phenol Conc/TiO_2 Conc	Max. Conc (mg)	Time (min)#	Formation Rate (mg(L.min))	Rate of Disappearance (mg(L.min))*
Phenol 20/ TiO_2 30	3.348	2	1.674	0.837
Phenol 20/ TiO_2 40	3.401	8	0.425	0.309
Phenol 20/ TiO_2 50	3.414	10	0.341	0.683
Phenol 30/ TiO_2 30	3.743	2	1.872	0.936
Phenol 30/ TiO_2 40	3.328	4	0.832	0.832
Phenol 30/ TiO_2 50	3.391	4	1.872	

* - Disappearance rates calculated from time of maximum concentration in solution
# -Time at which maximum concentrations were observed